Università degli Studi di Ferrara

DOTTORATO DI RICERCA IN
"SCIENZE DELL'INGEGNERIA"

CICLO XXIV

COORDINATORE Prof. Trillo Stefano

A NUMERICAL AND EXPERIMENTAL VALIDATION OF THE DIFFUSION EQUATION APPLIED TO ROOM ACOUSTICS

Settore Scientifico Disciplinare ING/IND 11

Dottoranda

Dott.ssa Visentin Chiara

Tutore

Prof. Prodi Nicola

Anni 2009/2011

Abstract

The recently developed room-acoustics diffusion model relies on the basic assumptions of the Fick's law of diffusion, relating the acoustic intensity and the energy density inside a room, through a constant diffusion coefficient. This study investigates the relationship between these two acoustic quantities in the stationary state, for the particular case of long rooms with different amounts of boundary scattering, by means of numerical simulations and experimental measurements. The numerical study was performed with a sound particle-tracing code. The experiments consist in measurements inside the scale model of a long room, where a three-dimensional Microflown® probe (calibrated and equalized with digital filters) was employed to collect data in terms of pressure and axial velocity components. Then, for each receiver position, the intensity and the energy density gradient were derived. Both numerical and experimental results show that inside long rooms the diffusion coefficient is not a constant but increases with the distance from the source, with a slope depending on the scattering coefficient of the walls. This result implies that, for such long enclosures, the diffusion model should consider a space-varying diffusion coefficient to be more consistent with real phenomena.

Riassunto

La teoria della diffusione applicata all'acustica architettonica deriva dalla legge di Fick sulla diffusione e mette in relazione intensità e densità di energia sonora all'interno di un ambiente attraverso il valore costante del coefficiente di diffusione. In questo lavoro viene analizzata l'effettiva relazione che intercorre tra le due grandezze in condizioni stazionarie, nel caso particolare di ambienti lunghi caratterizzati da differenti valori del coefficiente di scattering superficiale. L'analisi è condotta sia attraverso simulazioni numeriche che impiegando misure sperimentali. Le simulazioni numeriche sono state effettuate impiegando un software di *particle-tracing*. La parte sperimentale è invece basata su misure all'interno di un modello in scala: una sonda Microflown® tridimensionale (calibrata ed equalizzata mediante l'impiego di filtri digitali) è stata utilizzata per acquisire i valori di pressione sonora e delle tre componenti assiali di velocità delle particelle all'interno dell'ambiente. Le grandezze misurate sono poi state impiegate per calcolare intensità e gradiente della densità di energia sonora. Sia i risultati numerici che quelli sperimentali evidenziano come, in ambienti lunghi, il coefficiente di diffusione non sia costante ma aumenti al'aumentare della distanza dalla sorgente, con una pendenza che dipende dal coefficiente di scattering delle pareti. I risultati ottenuti portano a concludere che, per simulare correttamente la propagazione del suono all'interno di questo tipo di ambienti, il modello di diffusione dovrebbe basarsi su un coefficiente di diffusione variabile nello spazio.

Contents

List of symbols

$\hat{a}$	estimate for the intercept of the distance-D_{est} curve
$\hat{b}$	estimate for the slope of the distance-D_{est} curve
B	statistical bandwidth
c	speed of sound [m/s]
d	accomodation coefficient
D	measured diffusion coefficient (only propagating energy [m^2/s]
D_{emp}	empirical diffusion coefficient [m^2/s]
D_{est}	numerical estimate of the diffusion coefficient [m^2/s]
D_{meas}	measured diffusion coefficient [m^2/s]
D_{th}	theoretical value of the diffusion coefficient [m^2/s]
e	mass of the particles [kg]
e_{init}	initial energy of the particles (particle-tracing code)
$e_{kin}(\boldsymbol{r}, t)$	kinetic energy density [J/m^3]
$e_p(\boldsymbol{r}, t)$	propagating part of the energy density [J/m^3]
$e_{pot}(\boldsymbol{r}, t)$	potential energy density [J/m^3]
$e_{np}(\boldsymbol{r}, t)$	non propagating part of the energy density [J/m^3]
$E(\hat{a}, \hat{b}$	quadratic error
EDT	early decay time [s]
E_0	energy at $t = t_0$ [J/m^3]
$E_{rec}(n)$	sound energy inside the receiver volume [J]
$f(\boldsymbol{r}, \boldsymbol{v}, t)$	particles distribution function
$G(\boldsymbol{r}, \boldsymbol{r_s})$	Green function in an unbounded medium
h	exchange coefficient [m/s]
h_E	exchange coefficient based on the Eyring absorption coefficient [m/s]
h_M	modified exchange coefficient [m/s]
$H_{p\hat{p}}(\omega)$	transfer function between pressure signals
$H_{\hat{p}\hat{u}}(\omega)$	measured impedance
$H_{th}(\omega)$	theoretical admittance
$H_{u\hat{u}}(\omega)$	transfer function between velocity signals
i	imaginary number
$\boldsymbol{I}(\boldsymbol{r}, t)$	active sound intensity [W/m^2]
$\boldsymbol{I}(\omega, \Delta\omega)$	active sound intensity in a given frequency band [W/m^2]
$\boldsymbol{I}_{dir}(\boldsymbol{r}, t)$	direct sound intensity [W/m^2]
$\boldsymbol{I}_{rec}(n)$	sound intensity inside the receiver volume [W/m^2]
$\boldsymbol{I}_{rev}(\boldsymbol{r}, t)$	reverberant sound intensity [W/m^2]

I_{ref}	reference sound intensity [W/m^2]
I_x	intensity component along the x-axis [W/m^2]
I_y	intensity component along the y-axis [W/m^2]
I_z	intensity component along the z-axis [W/m^2]
$\boldsymbol{J}(\boldsymbol{r}, t)$	reactive sound intensity [W/m^2]
$\boldsymbol{J}(\omega, \Delta\omega)$	reactive sound intensity in a given frequency band [W/m^2]
k	wave number [1/m]
K	correction factor (empirical diffusion coefficient)
$\mathcal{K}$	diffusion coefficient (transport equation)
l_i	distance covered inside a receiver volume [m] (particle-tracing code)
L	length of the room [m]
L_e	sound energy density level (dB)
L_{Ix}	sound intensity level along the x-axis (dB)
L_{Iy}	sound intensity level along the x-axis (dB)
L_{Iz}	sound intensity level along the x-axis (dB)
L_W	sound power level (dB)
m	coefficient of atmospheric absorption [1/m]
$\boldsymbol{n}$	normal vector of the surface
n_t	spatial density of the scattering elements [1/m^3]
N	total number of particles (particle-tracing code)
N_0	number of particles crossing the receiver (particle-tracing code)
$p(\omega)$	raw pressure signal
$p_{corr}(\omega)$	corrected pressure signal
$p_{ref}(\omega)$	pressure signal of the reference microphone
$\hat{p}(\omega)$	pressure signal of the built-in microphone during the calibration
$p(\boldsymbol{r}, t)$	sound pressure [Pa]
$p(\boldsymbol{r}, \boldsymbol{v}, t)$	sound source function (transport equation)
$P(x)$	collision probability of the sound particles
$P(\boldsymbol{r}, t)$	source function (diffusion equation)
q	number of particles emitted from a source per second [1/s]
Q_a	absorption cross section of the scattering elements [m^2]
Q_s	scattering cross section of the scattering elements [m^2]
Q_t	total cross section of the scattering elements [m^2]
$\boldsymbol{r}$	receiver position [m]
$\boldsymbol{r_s}$	source position [m]
r	source-receiver distance [m]
r_r	reverberant radius [m]
R	radius of the scattering elements [m]
$RT30$	reverberation time [s]
s	scattering coefficient
s_e	surface of the scattering elements [m^2]
S	room surface [m^2]
SPL	sound pressure level (dB)
SIL	sound intensity level (dB)
$S_{pp}(\omega)$	auto-spectra between pressure signals
$S_{pu}(\omega)$	cross-spectrum between pressure and velocity signals

$S_{u_r u_r}(\omega)$	auto-spectra between velocity signals along a given direction
t	time [s]
t_0	initial time [s]
T	spatial average of the reverberation time [s]
T_s	total simulation time [s] (particle-tracing code)
$u(\omega)$	raw velocity signal
$\hat{u}(\omega)$	velocity signal acquired during the calibration
$\boldsymbol{v}$	particle velocity [m/s]
v	volume of the source sub-domain [m^3]
V	room volume [m^3]
V_r	position space
V_s	source sub-domain [m^3]
V_v	velocity space
V_{rec}	receiver volume [m^3] (particle-tracing code)
$w(\boldsymbol{r}, t)$	sound energy density [J/m^3]
$w_d(\boldsymbol{r}, t)$	direct component of the sound energy density [J/m^3]
$w_{diff}(\boldsymbol{r}, t)$	energy density solution of the diffusion equation [J/m^3]
$w_r(\boldsymbol{r})$	corrected energy density [J/m^3]
$w_{rec}(n)$	energy density inside the receiver volume [J/m^3]
$w_{rev}(\boldsymbol{r})$	reverberant energy density [J/m^3]
W	constant power of the sound source [W]
α	surface absorption coefficient
α_E	Eyring absorption coefficient
$\bar{\alpha}$	average value of the absorption probability or mean room surface absorption coefficient
Δt	time step [s]
ε	energy carried by a particle [J] (particle-tracing code)
γ	function of the mean free path (revised theory)
γ_{pu_r}	coherence between sound pressure and particle velocity
λ	mean free path of a room [m]
Λ	sound wavelength [m]
ω	angular frequency [rad/s]
ρ	air density [kg/m^3]
σ	total absorption per unit of time [1/s] (diffusion theory)
$\sigma(T)$	standard deviation of the reverberation time [s]
∇	gradient operator
∇^2	Laplace operator

Introduction

This thesis collects the research activities performed during the Ph.D. in Engineering Science, carried out from 2009 to 2011 at the Engineering Department of University of Ferrara. Part of the activities were carried out at the PPRIME Institute of University of Poitiers (France), where a seven months research period was spent.

The thesis is focused on the room-acoustics diffusion theory and its validation by means of both numerical and experimental results.

The room-acoustics diffusion theory is a recently developed model for the prediction of the sound field inside enclosures. It was initially introduced by Picaut *et al.* in 1997 [1] and it is based on the use of a diffusion equation to describe the acoustic quantities inside urban streets or rooms with diffusely reflecting boundaries. The underlying assumption is that the multiple diffuse reflections that take place on these surfaces yield to a sound field whose propagation can be described as a diffusion process, employing the same equations that govern the propagation of particles inside a scattering medium.

The model was further extended in the last ten years for taking into account the main aspects of the sound propagation inside rooms (atmospheric or boundaries absorption, sound transmission...) and a numerical solution was introduced, allowing the prediction of the sound field inside rooms of complex shape, or big dimensions, with limited computational times and resources. The obtained results, expressed in terms of sound pressure level and reverberation time, show a good agreement with both experimental and simulated data (especially for coupled rooms [2, 3]).

Anyway, during these years, no systematic studies were carried out for validating the model, starting from the analysis of the basic equation of the diffusion theory. The model relies in fact on two main equations: a conservation equation and a diffusion gradient equation that relates the energy density gradient and the sound intensity by means of a proportionality constant named diffusion coefficient (Fick's law). The equation states that the motion of particles from an high density area to a low density one, that is the energy flow, is generated by the presence of an energy density gradient. This relationship does not follow from the acoustic wave equation but derives from the so-called "diffusion approximation" in the hypothesis of a small rate of change of the considered acoustic quantities with the mean free path of the room.

The analysis of the diffusion gradient equation is therefore believed to be an important issue in order to understand when the diffusion model can be successfully

applied and which is the "real" value of the diffusion coefficient. Moreover this kind of analysis can be also employed for finding out if the model, which is intrinsically limited to rooms with diffusely reflecting boundaries, could be extended to the more realistic case of enclosures characterized by mixed diffuse and specular reflections.

Therefore, in this study, the basic equation of the room-acoustics model is systematically investigated through a numerical and experimental estimate of the diffusion coefficient inside enclosures with different geometries and acoustic properties of the boundaries. The numerical investigation was performed with the aim of outlining the basic features of the problem and thus providing a starting point for the experimental part of the research.

The thesis is divided in four main chapters, organized according to the following structure.

In *Chapter 1* the room-acoustics diffusion theory is reviewed. Firstly the formulation of the analytical model is detailed, starting from the analogy between a gas of elementary particles in a scattering medium and the reverberant part of the sound field inside a room. The theoretical expression of the diffusion constant is introduced, as derived from the diffusion theory applied to the particles propagation. Then the numerical solution of the diffusion equation is presented and the limits of validity of the diffusion model are discussed. Finally, in the last part of the Chapter, two studies dealing with the extension of the model to the description of the sound field inside rooms with mixed reflections are briefly discussed.

Then, in *Chapter 2* the numerical estimate of the diffusion coefficient is presented. The numerical analysis was carried out by means of a particle-tracing code, whose typical features are detailed at the beginning of the Chapter. The choice of this code was led by the possibility of modelling the sound field relying on the same basic concepts of the diffusion model; moreover the direct calculation of energy density and sound intensity at each receiver position, irrespective to each other, performed by the code allowed to numerically investigate the diffusion gradient equation. The relationship between the two acoustic quantities is initially assessed for a proportionate room with both uniform and non-uniform surface absorption. Then a long room is considered, where a systematic analysis of the diffusion coefficient sensitivity to the geometrical and acoustic characteristics of the room was carried out.

The experimental part of the research is presented in *Chapter 3* where the measurements performed inside a scale model of a long room are described. The first part of the Chapter deals with the intensimetric p-u probe employed for the collection of the data: in particular, the calibration of the probe is carefully detailed, describing the measurements performed inside a small anechoic chamber and the numerical elaboration of the digital filters to be employed for the correction of the raw signal. The measurements were performed inside two different configurations of the scale model, varying the scattering and absorption properties of the boundaries; the acquired data (pressure and three velocity components) allowed to retrieve the energy density and the sound intensity along the three axes. Hence, in the final part of the Chapter the basic characteristics of the investigated sound fields are carefully investigated, by means of energetic and intensity based quantities.

Finally, in *Chapter 4*, the experimental estimate of the diffusion coefficient inside the two investigated long rooms is presented and the validity of the diffusion equation is discussed, as a function of the reflection properties of the room boundaries. In the same Chapter a comparison between simulated and measured quantities is also performed, with the aim of validating the sound intensity prediction performed by the particle-tracing code.

Chapter 1

The room-acoustics diffusion theory

1.1 Introduction

Sound field modelling is a topic of primary interest in architectural acoustics; during the years several analytical and numerical models have been proposed in literature with the aim of exactly predicting the sound field, in both its temporal and spatial distribution.

However, given the complexity of the physical phenomena involved, it is not possible to reach a single, all-comprehensive model and during the time a variety of approaches has been suggested, each one with specific fields of analysis and restrictions in the application. For example the solution of the wave equation (employing either analytical or numerical methods) leads to an accurate description of the sound field in terms of modal distribution but, given the computational load, it is suitable only for the low frequency range. On the contrary, statistical methods allow to deal with medium and high frequencies, providing correct results even with a limited knowledge of the room under study, but they can not describe the sound field characteristics at the low frequencies. Anyway, all these different models yield to the prediction of the majority of the acoustical effects and, on the whole, cover a wide range of configurations, useful from a practical point of view.

In this Chapter a recently developed model for the prediction of the sound field inside enclosures, named room-acoustic diffusion theory, is presented. The model is based on the analogy between the sound field inside a room with diffusely boundaries and the propagation of elementary particles in a scattering medium. The analogy, initially proposed by Ollendorff in 1969 [4, 5] was further developed by Picaut *et al.* in 1997 [1, 6] with reference to urban acoustics. A numerical implementation of the analytical formulation was then derived in 2006 [7], in order to employ the model for describing and predicting the sound field inside enclosures of various shapes and preparations, for example coupled rooms [2, 3, 8, 9] or fitted rooms [10]. During the years the model has been further extended for taking into account high absorption coefficients of the room boundaries [11, 12], atmospheric attenuation [13] and sound transmission through the walls [7]. Few attempts were

also carried out to extend the model and describe the case of enclosures characterized by mixed (diffuse and specular) reflections [14, 15].

In the following Sections the theoretical derivation of the diffusion equation is presented, starting from the more general representation of the diffusion problem (transport equation) and focusing on the analogy between the diffusion of particles in a scattering medium and the sound field inside rooms. The numerical implementation of the model and its principal extensions proposed in the last years are then briefly introduced and finally, in the last part of the Chapter, the problem of correctly predicting the main parameter of the equation (i.e., the diffusion constant) is discussed.

1.2 Room-acoustics diffusion theory: theoretical model

1.2.1 Sound particles concept

The mathematical formulation of the diffusion model is based on the concept of sound particles and the equivalence between the sound energy density and the particles distribution function inside an enclosure.

The sound particle concept stems directly from geometrical room acoustics: the sound rays can in fact be regarded as trajectories of the sound particles (*phonons*) [16] or, alternatively, the sound particles can be described as "short pulses with a broad spectral distribution propagating along sound rays path" [17]. Following this approach, geometrical room acoustics can be considered as a special case of particle dynamics and the sound field assimilated with a gas of sound particles, where the local sound energy density is represented by the density of particles at each receiver position. Hence, in models based on the sound particles concept the target shifts from the prediction of the sound field to the analytical or numerical calculation of the local density of sound particles.

The main assumptions of this kind of models can be summarized in the following points:

1. In the sound field the particles propagate at the sound velocity c along straight lines, without mutual interaction and carrying an infinitesimal amount of energy. When a particle strikes a wall, or an obstacle if the room is fitted, it can be absorbed or reflected, according to the local absorption coefficient α; if the particle is reflected, a new straight trajectory is identified, whose direction depends on the reflection law of the surface.

2. As it derives from geometrical acoustics, the sound particle approach disregards the undulating nature of the sound waves and is suitable only for the description of the sound field in the high frequency range, where the phase effects can be neglected. The sound field is therefore regarded as a superposition of an high number of plane waves, mutually incoherent, with phases in a random relationship [18].

3. The sound field can be properly represented with a particles model only after a large number of reflections has occurred, when it can be described as a complex energy mixing [19]. It follows that only the reverberant part of the sound field, result of a "complex mixing of specular reflections, diffraction and scattering phenomena" [20], can be properly modelled by a particle approach.

4. This kind of models do not take into account expressly the notion of frequency which anyway can be introduced via the acoustics properties of the room surfaces and the source (absorption and scattering coefficients, source power, atmospheric absorption...).

1.2.2 Analogy between room acoustics and particle diffusion

As introduced in the previous Section, the reverberant part of the sound field inside a room can be modelled through a multitude of phonons, propagating along straight lines and striking the room boundaries. According to the room-acoustics diffusion model, this propagation can be considered analogous to the movement (diffusion) of elementary particles in a space containing scattering objects (figure 1.1), as described by Morse and Feshbach [21]. In particular the analogy regards the case of scattering objects more massive than the elementary particles where, even if collisions between elementary particles occur, their effect can be neglected; from a physical point of view, the model describes for example the propagation of electrons through massive nuclei or the movement of photons through fog particles.

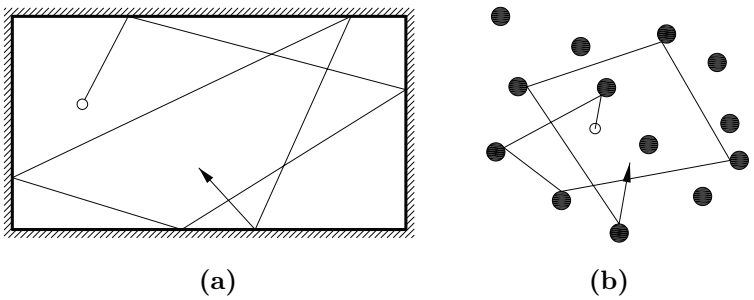

Figure 1.1: Analogy between the diffusion of a sound particle inside a room (a) and the diffusion of an elementary particle in a scattering medium (b). (from [1])

Therefore, following the proposed analogy, the room boundaries are assimilated to a set of scattering elements and the average absorption coefficient of the room is considered analogous to the absorption probability $\bar{\alpha}$ of the scattering elements. Moreover the phonons velocity c (i.e., the speed of sound) is supposed to be equal to the propagation velocity of the elementary particles.

The scattering objects, which can be described as elastic spheres of radius R, are randomly distributed inside the space with a density n_t; their total scattering cross section is $Q_t{=}\pi R^2{=}s_e/4$, being $s_e{=}4\pi R^2$ the surface of each sphere. When a particle hits a scattering object, it is absorbed with an average probability $\bar{\alpha}$

and reflected with a probability $(1 - \bar{\alpha})$; the total cross section of the scattering elements can therefore be written as the sum of an absorption cross section Q_a and a scattering cross section Q_s, as:

$$Q_t = Q_a + Q_s = \bar{\alpha}\, Q_t + (1 - \bar{\alpha})\, Q_t. \tag{1.1}$$

In order to apply the analogy between the diffusion of gas particles and the sound field inside a room of volume V and surface S, it is moreover necessary that the surface per room volume is equal to the scattering objects surface per unit volume, that is:

$$\frac{S}{V} = n_t\, s_e. \tag{1.2}$$

Finally, let's define $P(x)$ as the probability that a particle covers a distance x without collisions. A particle will cover a distance $x + dx$ without collisions only if it does not experiment collisions along the length x and inside the volume of thickness dx and unit surface perpendicular to the propagation direction. This, in terms of probability, can be expressed as:

$$P(x + dx) = P(x) \cdot (1 - Q_t n_t dx), \tag{1.3}$$

where $Q_t n_t dx$ is the number of diffusing elements inside the defined volume. Starting from equation (1.3), it is possible to derive the average distance λ between two successive collisions (mean free path), expressed as:

$$\lambda = \int_0^\infty x P(x) dx = \frac{1}{Q_t n_t}. \tag{1.4}$$

According to the defined analogy, inside an enclosure equation (1.4) leads to:

$$\lambda = \frac{4V}{S}, \tag{1.5}$$

which is the value classically chosen for expressing the mean free path inside rooms with diffusely boundaries [17, 22].

1.2.3 Transport equation

In this Section the transport equation is analytically derived. This equation can be considered as the most general representation of the diffusion problem; starting from its integral formulation and applying the so-called "diffusion approximation" it will be then possible to derive the analytical expression of the diffusion equation.

Let's define the phase space $V_r \times V_v$, where the state of a single particle can be specified at each instant of time by its six coordinates x, y, z, v_x, v_y, v_z, expressing position and velocity.

In order to analytically derive the density of sound particles at each position of the space it is necessary to move from the description of the motion of the single particles to a description of the average motion of the whole cloud of particles. The link between small-scale phenomena and large-scale motion of the fluid as a

whole, can be provided by the distribution function, according to the methods of the kinetic theory.

The distribution function $f(\boldsymbol{r}, \boldsymbol{v}, t)$ returns the probability for a particle to be localized at position $\boldsymbol{r}$ in the position space V_r with a velocity $\boldsymbol{v}$ (with norm c, speed of sound) in the velocity space V_v at the instant t.

Hence, all the large-scale properties can be obtained conveniently integrating the distribution function.

Integrating the function over both position and velocity spaces gives the total number of particles:

$$N = \iiint f(\boldsymbol{r}, \boldsymbol{v}, t)\, dV_v dV_r. \tag{1.6}$$

Integrating the function over the only velocity space returns the average number of particles per unit volume of position space, that is, following the analogy with the propagation of sound particles, the sound energy density:

$$w(\boldsymbol{r}, t) = e \iiint f(\boldsymbol{r}, \boldsymbol{v}, t)\, dV_v. \tag{1.7}$$

Similarly, the total average velocity per unit volume expresses the sound energy flow, or acoustic intensity:

$$\boldsymbol{I}(\boldsymbol{r}, t) = e \iiint \boldsymbol{v} f(\boldsymbol{r}, \boldsymbol{v}, t)\, dV_v. \tag{1.8}$$

In the following, a unit mass e will be considered, corresponding to the case of a unit energy carried by each sound particle.

Let's now consider the propagation of the particles inside a space. If collisions on the scattering elements do not take place, all the particles in a given element of velocity space V_v will travel with the same velocity $\boldsymbol{v}$ and there will be $f(\boldsymbol{r}, \boldsymbol{v}, t) dV_v dV_r$ of them in the element dV_r at the position $\boldsymbol{r}(x, y, z)$ and at the time t. The same particles, at the time $t + dt$, will be found at the position $\boldsymbol{r} + \boldsymbol{v}dt$. Therefore, if collisions and absorption phenomena are neglected, the distribution function at the position $\boldsymbol{r}$ at time t must be equal to the distribution function at the position $\boldsymbol{r} + \boldsymbol{v}dt$ and at the time $t + dt$:

$$f(\boldsymbol{r}, \boldsymbol{v}, t) = f(\boldsymbol{r} + \boldsymbol{v}dt, \boldsymbol{v}, t + dt), \tag{1.9}$$

meaning that during the propagation there is no loss of sound particles:

$$\frac{\mathrm{d}}{\mathrm{d}t} f(\boldsymbol{r}, \boldsymbol{v}, t) = \left[\frac{\partial}{\partial t} + \frac{\partial}{\partial \boldsymbol{r}} \frac{\mathrm{d}\boldsymbol{r}}{\mathrm{d}t} + \frac{\partial}{\partial \boldsymbol{v}} \frac{\mathrm{d}\boldsymbol{v}}{\mathrm{d}t} \right] f(\boldsymbol{r}, \boldsymbol{v}, t) = 0. \tag{1.10}$$

Given that the velocity $\boldsymbol{v}$ is a constant over the time (i.e. $\mathrm{d}\boldsymbol{v}/\mathrm{d}t = 0$) and $\mathrm{d}\boldsymbol{r}/\mathrm{d}t = \boldsymbol{v}$, it is possible to simplify equation (1.10) and obtain the equation of continuity for the distribution function, that describes the spatial and temporal evolution of the local particles density:

$$\frac{\partial}{\partial t} f(\boldsymbol{r}, \boldsymbol{v}, t) = -\boldsymbol{v} \cdot \nabla f(\boldsymbol{r}, \boldsymbol{v}, t), \tag{1.11}$$

where the gradient operator ∇ operates only on the space dependence of $f(\boldsymbol{r}, \boldsymbol{v}, t)$.

Equation (1.11) can also be seen as the transport equation of a free molecular flow, also called Liouville equation; the evolution of sound particles density is described in analogy with the evolution of the molecular density in a rarefied (or Knudsen) gas [23].

When the particles propagate inside a space filled with scattering elements, the possibility of collisions modifies the distribution function, which is no longer the same from point to point; in fact, due to collisions, some particles vanish from the velocity space element dV_v, while other particles, originally in other velocity space elements, are scattered inside it. In this Section the absorption of the particles due to collisions with the scattering elements is neglected: it will be considered in § 1.2.6 where the boundary conditions are discussed.

The particles vanishing from the velocity space element dV_v due to collisions are responsible for a rate of loss of the distribution function, expressed as:

$$\frac{\partial}{\partial t} f(\boldsymbol{r}, \boldsymbol{v}, t) = -(Q_t n_t c) f(\boldsymbol{r}, \boldsymbol{v}, t) = -\frac{c}{\lambda} f(\boldsymbol{r}, \boldsymbol{v}, t), \tag{1.12}$$

where $Q_t n_t c$ expresses the fraction of particles that experiment collisions and change their direction.

On the other hand, there is also a fraction of particles, originally in other velocity space elements, which are scattered into dV_v by collisions. Assuming that the particles are scattered with equal probability in all directions and that there is no change in the velocity of the particles undergoing collisions, the increase rate of $f(\boldsymbol{r}, \boldsymbol{v}, t)$ can be written as:

$$\frac{\partial}{\partial t} f(\boldsymbol{r}, \boldsymbol{v}, t) = \left(\frac{Q_t n_t c}{4\pi} \right) \int f(\boldsymbol{r}, \boldsymbol{v'}, t)\, dV_{v'}, \tag{1.13}$$

where $dV_{v'}$ represents the velocity space elements where the particles scattered inside dV_v are originally located. Hence, the continuity equation can be generalized for taking into account the scattering phenomena, leading to:

$$\frac{\partial}{\partial t} f(\boldsymbol{r}, \boldsymbol{v}, t) = -\boldsymbol{v} \cdot \nabla f(\boldsymbol{r}, \boldsymbol{v}, t) - \frac{c}{\lambda} f(\boldsymbol{r}, \boldsymbol{v}, t) + \frac{c}{4\pi\lambda} \int f(\boldsymbol{r}, \boldsymbol{v'}, t)\, dV_{v'}. \tag{1.14}$$

1.2.4 Diffusion approximation

Applying the transport model to a specific problem, requires the resolution of the transport equation together with some appropriate boundary conditions. Unfortunately, at the moment exact analytical solutions for this system of equations are not available, a part from the case of simple geometries [24, 25].

Anyway, it is possible to find asymptotic solutions of the system, moving from the integral formulation to a differential equation, easier to solve but not always valid. In fact, a differential equation is a good approximation of the transport equation only when the changes in $w(\boldsymbol{r}, t)$ and $\boldsymbol{I}(\boldsymbol{r}, t)$ per mean free path are small, that is, when the distribution function is nearly independent of the angle of direction of the velocity and the energy flow $\boldsymbol{I}(\boldsymbol{r}, t)$ is small [21].

Therefore, let's consider the angle-dependent part of $f(\boldsymbol{r}, \boldsymbol{v}, t)$ to be quite small; in this case the density function $f(\boldsymbol{r}, \boldsymbol{v}, t)$ can be expanded in power of $\boldsymbol{v}$, giving the first order approximation:

$$f(\boldsymbol{r}, \boldsymbol{v}, t) \approx \frac{1}{4\pi} w(\boldsymbol{r}, t) + \frac{3}{4\pi c^2}\, \boldsymbol{v} \cdot \boldsymbol{I}(\boldsymbol{r}, t). \tag{1.15}$$

Considering this last relation, equation (1.14) becomes:

$$\frac{\partial}{\partial t} w(\boldsymbol{r}, t) + \frac{3}{c^2} \boldsymbol{v} \frac{\partial}{\partial t} \boldsymbol{I}(\boldsymbol{r}, t) = -\boldsymbol{v} \cdot \nabla w(\boldsymbol{r}, t) - \frac{3}{c^2}\, \boldsymbol{v} \cdot \nabla (\boldsymbol{v} \cdot \boldsymbol{I}(\boldsymbol{r}, t)) - \frac{3}{c\lambda}\, \boldsymbol{v} \cdot \boldsymbol{I}(\boldsymbol{r}, t), \tag{1.16}$$

which can be separated in two equations on the basis of symmetry, by considering separately the terms that change sign when the direction of $\boldsymbol{v}$ is reversed and the terms that do not. The terms that change sign lead to:

$$\boldsymbol{I}(\boldsymbol{r}, t) = -D_{th}\, \nabla w(\boldsymbol{r}, t), \tag{1.17}$$

where the term $\partial \boldsymbol{I} / \partial t$ of equation (1.16) has been neglected, given the slow rate of change with the time of the involved quantities. This equation, relating the acoustic energy flow to the acoustic energy density is a diffusion gradient equation and states that an energy gradient produces a motion of sound particles from an high density area to a low density one [1]. The same type of equation was employed in different fields of acoustics, for example in the context of porous materials [26] or structural vibrations [27].

In equation (1.17) it is introduced the diffusion constant of the room D_{th}, expressed, for rooms of arbitrary shape with diffusely reflecting walls, as:

$$D_{th} = \frac{\lambda c}{3} = \frac{4V}{S} \frac{c}{3}, \tag{1.18}$$

where the expression of the mean free path λ is taken up from equation (1.5).

On the other end, the terms that do not change sign lead to:

$$\frac{\partial}{\partial t} w(\boldsymbol{r}, t) = -\frac{3}{c^2}\, \boldsymbol{v} \cdot \nabla \left[\boldsymbol{v} \cdot \boldsymbol{I}(\boldsymbol{r}, t) \right]. \tag{1.19}$$

Replacing $\boldsymbol{I}(\boldsymbol{r}, t)$ with the expression defined in equation (1.17) and averaging over all the possible directions of $\boldsymbol{v}$, the diffusion equation can be obtained as:

$$\frac{\partial}{\partial t} w(\boldsymbol{r}, t) - D_{th} \nabla^2 w(\boldsymbol{r}, t) = 0, \tag{1.20}$$

where ∇^2 is the Laplace operator.

It is worth noticing that the diffusion equation can be seen as a direct consequence of the general principle of energy conservation:

$$\frac{\partial w}{\partial t}(\boldsymbol{r}, t) + \nabla \cdot \boldsymbol{I}(\boldsymbol{r}, t) = 0, \tag{1.21}$$

provided that the intensity is proportional to the energy density gradient as stated in equation (1.17).

1.2.5 Introducing a source function

In the present form, the diffusion equation does not contain a term accounting for the introduction of new particles into the scattering space, that is a source function. This term can be added in the transport equation (1.14), bringing to the following modified expression of the diffusion equation:

$$\frac{\partial}{\partial t}w(\boldsymbol{r},t) - D_{th}\nabla^2 w(\boldsymbol{r},t) = P(\boldsymbol{r},t), \tag{1.22}$$

where $P(\boldsymbol{r},t)$ accounts for a source located in $\boldsymbol{r}$ and emitting particles with a defined distribution in the time t.

For example, the case of a point source emitting q particles per second may be modelled by the term $q\delta(\boldsymbol{r}-\boldsymbol{r_s})$, $\boldsymbol{r_s}$ being the source position [21]. Following the analogy between elementary particles propagation and sound field inside a room [7], the diffusion equation inside a room with a point source of power $W(t)$ located at $\boldsymbol{r_s}$ can be therefore expressed as:

$$\frac{\partial}{\partial t}w(\boldsymbol{r},t) - D_{th}\nabla^2 w(\boldsymbol{r},t) = W(t)\,\delta(\boldsymbol{r}-\boldsymbol{r_s}). \tag{1.23}$$

If an impulsive point source is considered, the diffusion equation will become instead:

$$\frac{\partial}{\partial t}w(\boldsymbol{r},t) - D_{th}\nabla^2 w(\boldsymbol{r},t) = E_0\,\delta(\boldsymbol{r}-\boldsymbol{r_s})\delta(t-t_0), \tag{1.24}$$

where E_0 is the energy emitted from the source at the time $t = t_0$.

The particular case of a sound source occupying a volume v and radiating a sound power $W(t)$ (which will be employed in the numerical implementation of the diffusion equation in § 1.2.9) can be modeled instead with the following source term:

$$P(\boldsymbol{r},t) = \frac{W(t)}{v} f_s(\boldsymbol{r}), \tag{1.25}$$

where the function $f_s(\boldsymbol{r})$ is equal to 1 inside the volume v and 0 otherwise; the integration of equation (1.25) over v returns the sound power of the source.

1.2.6 Boundary conditions

In the derivation of the transport equation it was supposed that the absorption of the scattering elements (or equivalently the absorption of the room boundaries) was negligible. This phenomenon, which leads to a rate of loss in the distribution function, can be both integrated in the expression of the diffusion equation (homogeneous Neumann boundary conditions) or directly considered in the boundary conditions (mixed boundary conditions). The solutions obtained with both methods are equivalent, but, while the first one deals only with the average absorption coefficient of the room $\bar{\alpha}$, the second one allows to handle local variations of absorption.

1.2.6.1 Homogeneous Neumann boundary conditions

The absorption of the room boundaries is integrated in the model by adding a term to the transport equation (1.14), accounting for a rate of loss of the distribution function $f(\boldsymbol{r}, \boldsymbol{v}, t)$:

$$\frac{\partial}{\partial t} f(\boldsymbol{r}, \boldsymbol{v}, t) = -\boldsymbol{v} \cdot \nabla f(\boldsymbol{r}, \boldsymbol{v}, t) - n_t (Q_s + Q_a)\, c\, f(\boldsymbol{r}, \boldsymbol{v}, t) + \\ + \frac{Q_s n_t c}{4\pi} \int f(\boldsymbol{r}, \boldsymbol{v'}, t)\, dV_{v'} + p(\boldsymbol{r}, \boldsymbol{v}, t), \tag{1.26}$$

where $p(\boldsymbol{r}, \boldsymbol{v}, t)$ is the function modelling the sound source and $n_t Q_a c$ expresses the fraction of particles absorbed by the scattering elements.

In this case, the diffusion equation becomes:

$$\frac{\partial}{\partial t} w(\boldsymbol{r}, t) - D_{th} \nabla^2 w(\boldsymbol{r}, t) + \sigma\, w(\boldsymbol{r}, t) = P(\boldsymbol{r}, t), \tag{1.27}$$

where $\sigma = c\bar{\alpha}/\lambda$ is the probability rate of a sound particle to be absorbed during one second.

In this approach the absorption phenomena are exclusively handled inside the volume of the room by the diffusion equation; on the boundaries (where the absorption actually takes place) it is only necessary to state the impossibility of the particles to be transmitted through the walls: when a particle strikes a surface it can only be absorbed or reflected, but it can not escape from the volume. The associated boundary conditions state therefore a null energy flow through the walls ($\partial w/\partial n = 0$).

The system of equations that has to be solved therefore becomes equal to:

$$\frac{\partial}{\partial t} w(\boldsymbol{r}, t) - D_{th} \nabla^2 w(\boldsymbol{r}, t) + \sigma w(\boldsymbol{r}, t) = P(\boldsymbol{r}, t) \qquad \text{in} \quad V, \tag{1.28}$$

$$\boldsymbol{I}(\boldsymbol{r}, t) \cdot \boldsymbol{n} = -D_{th} \nabla w(\boldsymbol{r}, t) \cdot \boldsymbol{n} = 0 \qquad \text{on} \quad \partial V, \tag{1.29}$$

where V expresses the room volume, ∂V denotes the room boundaries and $\boldsymbol{n}$ is the local vector normal to the surface.

1.2.6.2 Mixed boundary conditions

In order to take into account the local variations of the surface absorption and their effect on the sound field, a different set of boundary conditions was presented in ref. [7]. In this case the absorption is entirely handled through the boundary conditions, expressed in the form:

$$\boldsymbol{I}(\boldsymbol{r}, t) \cdot \boldsymbol{n} = -D_{th} \nabla w(\boldsymbol{r}, t) \cdot \boldsymbol{n} = h\, w(\boldsymbol{r}, t), \tag{1.30}$$

where h is the so-called local exchange coefficient.

The expression of h can be derived observing that the energy flow through the room boundaries S has to be equal to the absorption over the room volume V, as expressed by the term $\sigma w(\boldsymbol{r}, t)$ in equation (1.27):

$$\int_V \sigma\, w(\boldsymbol{r}, t) dV = \int_{\partial V} h(S)\, w(\boldsymbol{r}, t) dS. \tag{1.31}$$

If the sound field is supposed to be totally diffuse[1], that is, if the energy density is uniform throughout the volume, the exchange coefficient can be expressed as a function of the absorption coefficient as:

$$\frac{\bar{\alpha} c S}{4} = \int_{\partial V} h(S)\, dS. \tag{1.32}$$

If the room boundaries are composed of n surfaces S_i with constant sound absorption α_i, then the exchange coefficient h_i of each surface portion can be expressed as:

$$h_i = \frac{\alpha_i c}{4},\ i = 1, ..., n. \tag{1.33}$$

Therefore, if the mixed boundary conditions are employed, the following system of equation will be solved:

$$\frac{\partial}{\partial t} w(\boldsymbol{r}, t) - D_{th} \nabla^2 w(\boldsymbol{r}, t) = P(\boldsymbol{r}, t) \qquad \text{in} \quad V, \tag{1.34}$$

$$D_{th} \frac{\partial}{\partial n} w(\boldsymbol{r}, t) + \frac{c\alpha}{4} w(\boldsymbol{r}, t) = 0 \qquad \text{on} \quad \partial V. \tag{1.35}$$

The exchange coefficient h, but also the coefficient σ, are based on the Sabine absorption coefficient, restricting the validity of diffusion model to rooms with low surface absorption. To overcome this limitation a new expression for the exchange coefficient h was suggested in ref. [11, 12], based on the Eyring absorption coefficient $\alpha_E = -\ln(1 - \alpha)$:

$$h_{E,i} = -\frac{c \ln(1 - \alpha_i)}{4}. \tag{1.36}$$

This expression can be applied when the absorption coefficient is high, improving the results in terms of reverberation time, for rooms with both non-homogeneous and high absorption.

This model shows anyway a singularity when the absorption coefficient becomes equal to 1.0 (i.e., when portions of the room walls are open); in order to overcome the problem, a modified boundary condition was proposed in ref. [28], where the exchange coefficient is expressed as:

$$h_{M,i} = \frac{\alpha_i c}{2 \cdot (2 - \alpha_i)}. \tag{1.37}$$

The three boundary conditions return the same results in the low absorption region, whereas they show considerable discrepancies in the high absorption region.

1.2.7 Considering the atmospheric absorption

The atmospheric absorption has a relevant contribute in the distribution of the sound field, especially in big rooms and at high frequencies. As shown in ref. [11],

[1]These boundary conditions are therefore obtained relaying on a quite specific (and ideal) assumption, which could represent a critical point in the solution of the model.

it can be integrated into the room-acoustic diffusion model by adding a specific rate of loss to the distribution function, which will be rewritten as:

$$\frac{\partial}{\partial t}f(\boldsymbol{r},\boldsymbol{v},t) = -\boldsymbol{v}\cdot\nabla f(\boldsymbol{r},\boldsymbol{v},t) - \left[\frac{c}{\lambda}+mc\right]f(\boldsymbol{r},\boldsymbol{v},t) + \\ + \frac{Q_s n_t c}{4\pi}\int f(\boldsymbol{r},\boldsymbol{v'},t)\,dV_{v'} + p(\boldsymbol{r},\boldsymbol{v},t), \tag{1.38}$$

where m is the coefficient of atmospheric attenuation [m^{-1}].

Consequently the diffusion equation (in the hypothesis of mixed boundary conditions) changes its expression in:

$$\frac{\partial}{\partial t}w(\boldsymbol{r},t) - D'_{th}\nabla^2 w(\boldsymbol{r},t) + mcw(\boldsymbol{r},t) = P(\boldsymbol{r},t). \tag{1.39}$$

Therefore the presence of atmospheric absorption alters the expression of both diffusion equation and diffusion coefficient, that becomes:

$$D'_{th} = D_{th}\cdot\frac{1}{1+m\lambda} \tag{1.40}$$

However as the effect of the atmospheric absorption is usually quite small per mean free path (i.e. $m\lambda \ll 1$) it can be assumed that $D'_{th} \approx D_{th}$.

1.2.8 The diffusion model as an extension of the statistical theory

According to classical theory [17], the energy balance for a room of volume V and surface S containing a source of sound power $W(t)$ and with an average surface absorption $\bar{\alpha}$, can be expressed as:

$$V\frac{d}{dt}w(t) + V\frac{c\bar{\alpha}S}{4V}w(t) = W(t). \tag{1.41}$$

This expression can be compared with the energy balance of the same room given by the diffusion theory and expressed integrating equation (1.28) over the room volume:

$$\int_V \frac{\partial}{\partial t}w(\boldsymbol{r},t)dV + \int_V \frac{c\bar{\alpha}S}{4V}w(\boldsymbol{r},t)dV - D_{th}\int_V \nabla^2 w(\boldsymbol{r},t)dV = \int_V W(t)\delta(\boldsymbol{r}-\boldsymbol{r_s})dV. \tag{1.42}$$

By using Gauss's theorem and the condition of null energy flow through the boundaries, the term containing the Laplacian operator is shown to be null:

$$D\int_V \nabla^2 w(\boldsymbol{r},t)dV = D_{th}\int_{\partial V}\frac{\partial w}{\partial n}(\boldsymbol{r},t)dS = 0, \tag{1.43}$$

and, if the order of derivative and integral in the first term are exchanged, the expression will become:

$$\frac{\partial}{\partial t}\int_V w(\boldsymbol{r},t)dV + \frac{c\bar{\alpha}S}{4V}\int_V w(\boldsymbol{r},t)dV = \int_V W(t)\delta(\boldsymbol{r}-\boldsymbol{r_s})dV. \tag{1.44}$$

This last expression is clearly an extension of equation (1.41) for a spatially varying sound field: the room acoustics diffusion theory can be therefore considered as an extension of the classical statistical theory, as pointed out in ref. [1, 7].

However it is necessary to clarify the differences between the "diffuse" sound field (as defined by the classical theory) and the sound field considered in the diffusion model.

The "diffuse" sound field rests classically on two main hypothesis [17, 29]:

- spatial diffusion: the stationary energy density is uniform inside the room;
- directional diffusion: the incidence of sound energy at any point of the sound field does not depend on the direction of incidence.

This two conditions can be realized inside rooms with irregular shape and low absorption. The geometry helps in scattering the sound rays in all possible directions and providing an high modal distribution; the absorption is instead needed to be low, as otherwise it will affect the diffusion of the field by continuously extinguish potential ray paths. In order to create the diffuse field, enclosures with diffusely reflecting boundaries are particularly efficient, as the irregularities on the surfaces scatter and redistribute the sound field in a wide range of directions.

On the contrary the room-acoustic diffusion theory deals with sound field characterized by non-uniform energy density, which varies inside the room according to the geometry and the absorption of the walls. The differences in the temporal and spatial distribution of the energy density are just responsible for the energy flow inside the room.

1.2.9 Validity of the diffusion equation

As already pointed out, the diffusion process is based on the assumption that a large number of reflections happens inside the room and the sound field can be regarded as a complex energy mixing; this hypothesis assures that only small variations of the acoustic quantities take place per mean-free path. It also implies that this kind of model can properly describe only the reverberant part of the sound field or, looking at the problem in the time domain, that it is valid only after a certain amount of time after the source activation, necessary for the first reflections to take place. In the first instants after the source activation the diffusion theory returns in fact non physical results [1, 7].

Several values for the time limit after which the model leads to correct results were proposed. Morse and Feshbach [21] and Valeau *et al.* [7] suggested that a limit of one mean free time (i.e. λ/c) could be considered for the diffusion equation to have physical meaning; before this time, the high probability of the particles of not having hit a scatterer/surface yet leads to non valid results. Equation (1.3) states in fact that the particles have some chance to hit a surface even at infinitely small distance from the source, which is clearly not physical. Then, in ref. [3], a time interval of two mean free time was proposed, in order to find an agreement between the reverberation time obtained with the diffusion model and measured inside coupled rooms. Finally, a systematic study focused on this

topic was recently published, where diffusion theory and ray-tracing results are compared [30]. The authors suggest that the diffusion equation could be considered certainly valid after the mixing time (the time at which the transition from early reflections to late reverberation occurs), conventionally equal to three mean-free path; in addition the equation can also correctly predict a certain fraction of early reflections (approximately one mean free path) prior the time at which mixing occurs.

1.3 Numerical implementation of the diffusion model

The room-acoustic diffusion equation can be analytically solved only in few cases, when the shape of the enclosure and the associate boundary conditions are especially simple. For example, a solution was calculated inside long rooms with uniform absorption for both stationary and time-varying states, yielding to the analytical expressions of sound attenuation and reverberation time in finite, semi-infinite and infinite long rooms [6].

In all the other cases (complex room shape, complicate distribution of the sound absorption...), it is instead necessary to numerically solve the diffusion equation, following the procedure developed in ref. [7].

In particular a FEM-based method was proposed to solve the equation that, in its time-varying form, can be rewritten as:

$$\frac{\partial}{\partial t} w(\boldsymbol{r}, t) - D_{th} \nabla^2 w(\boldsymbol{r}, t) = 0 \qquad \text{in} \quad V, \tag{1.45}$$

$$\frac{\partial}{\partial t} w(\boldsymbol{r}, t) - D_{th} \nabla^2 w(\boldsymbol{r}, t) = \frac{W}{v} \qquad \text{in} \quad V_s, \tag{1.46}$$

The diffusion equation is solved in two separate sub-domains (V and V_s) with different source terms, ensuring that the constant sound power of the source W can be retrieved by integrating equation (1.46) over V_s. Here V_s identifies the sob-domain of volume v centered in the source location and V is the whole room volume minus V_s, representing the sub-domain where the sound energy density is calculated. The associated boundary conditions will be of the mixed-type.

When the finite-element method is employed for solving the Helmholtz equation, its application is limited at the low frequency range, as the size of the mesh elements has to be smaller than the considered wavelength ($< \Lambda/6$). If the same method is employed for solving the diffusion equation, the parameter that influence the mesh size will be no longer the wavelength but the mean-free path of the room: the same mesh size can therefore be employed for all the frequency bands and the size of the elements is required to be smaller than one mean free path. It follows that the finite-elements method can be employed for solving the diffusion equation even in big rooms with limited meshing and low computational times.

From the numerical solution of the diffusion equation expressed in terms of energy density $w(\boldsymbol{r}, t)$ it is possible to obtain the square pressure, classically employed in room acoustics for describing the sound field. To express this quantity,

it is necessary to recall the concept of the random wave theory, introduced in ref. [31, 32] and further discussed by Pierce [33] and Nelson [18], where the sound field in a room is described by a superimposition of an infinite number of plane waves. Provided that all quantities are spatially averaged through a volume of space that is large compared to the acoustic wavelength at the considered frequency, but much smaller than the room mean free path [18], the energy density can be related to the square pressure according to the expression:

$$p^2(\boldsymbol{r}, t) = \rho c^2 w(\boldsymbol{r}, t), \tag{1.47}$$

where ρ is the air density and c the speed of sound. Let us stress here that equation (1.47) does not rely on the "diffuse field" assumption, but considers locally-averaged quantities. In the same way, the energy density $w(\boldsymbol{r}, t)$ governed by the diffusion equation can be seen as a local spatial average of the energy density, smoothing the local modal effects that could occur in practice throughout the room.

Finally, it is important to recall that in order to obtain the total sound field inside the room, the direct field contribution has to be added to equation (1.20) that provides only the reverberant component of the sound field. The direct part of the energy density can be expressed as:

$$w_d(\boldsymbol{r}, t) = \frac{W(t)}{4\pi c r^2}. \tag{1.48}$$

1.4 Diffusion coefficient estimate

In equation (1.18) the diffusion coefficient was theoretically defined as a constant, depending only on the mean free path of the room. Its expression was directly derived from the diffusion theory applied to the propagation of particles and only few attempts have been done to investigate the real value of the parameter.

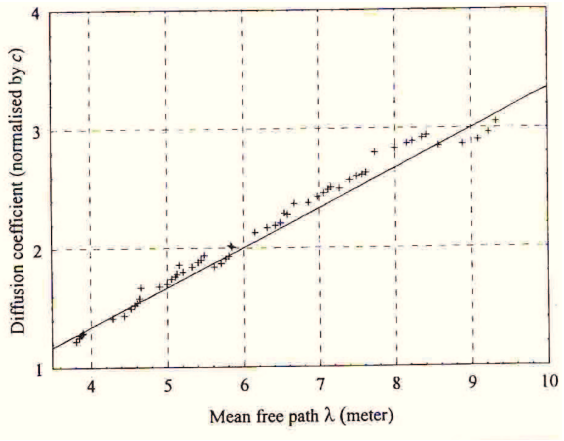

Figure 1.2: Variation of the normalized diffusion coefficient D_{th}/c with the mean free path λ of the room; (+) numerical estimation with the radiosity method, (–) diffusion model. (from [1])

For example, in ref. [1] a numerical estimate of the constant is provided, by comparing the diffusion equation and a numerical model. The comparison was

performed with the radiosity method, proposed by Kuttruff [17] and based, similarly to the diffusion theory, on the hypothesis of purely diffusely reflections inside the room. Numerical simulations were carried out for long rooms with different dimensions and aspect ratios, showing a close agreement between the numerical estimate and the theoretical value, as represented in figure 1.2.

A different approach is instead proposed in ref. [6], were the reliability of the expression chosen to describe the mean free path of a room is discussed. In fact, for the long room considered in the study, the best agreement between experimental measurements and diffusion model results was obtained for a different expression of the mean free path, that is:

$$\lambda = \sqrt{\frac{S}{4\pi}}. \tag{1.49}$$

This expression, introduced in ref. [34], derives from the application of the image source method to rectangular rooms.

This study proves that it is necessary to further investigate the diffusion coefficient value as it could differ from the theoretical value, varying, for example, as a function of the room shape.

1.4.1 Diffusion coefficient inside rooms with mixed diffuse and specular reflections

Another issue to be tackled is the possibility of extending the diffusion model to the most general case of rooms with mixed reflections. The model, and therefore the expression of the diffusion coefficient, is intrinsically limited to the rather ideal condition of rooms characterized by purely diffuse reflections. This conditions is frequently assumed for prediction models but it is hardly encountered in real situations as the surfaces diffuse only a fraction of the incident sound whereas the remaining part is reflected into specular directions, according to the scattering coefficient s.

In order to model this phenomenon LePollès *et al.* [23] analytically derived an expression for the diffusion coefficient $\mathcal{K}$, starting directly from the transport equation solved in its asymptotic form, for the particular case of a street canyon. Being b the width of the street, the diffusion coefficient $\mathcal{K}$ is expressed as:

$$\mathcal{K} = \frac{(1+d)}{(1-d)}\frac{bc}{4}, \tag{1.50}$$

where d is the accomodation coefficient, varying from 0 for diffuse reflections to 1 for purely specular reflections. In figure 1.3 the variation of the diffusion coefficient with d and b is represented showing that, as the fraction of specular reflections increases the diffusion coefficient increase, that is a faster diffusion of the sound energy takes place. In the same way the energy is distributed very quickly when the distance between the façades of the street canyon is large, while remains for a long time at the same place when the planes are close to each other.

A systematic study on the estimation of the diffusion coefficient inside enclosures with mixed diffused and specular reflections was initially proposed in ref. [10] and then developed, for the case of a stationary sound field by Foy *et al.* [14, 15].

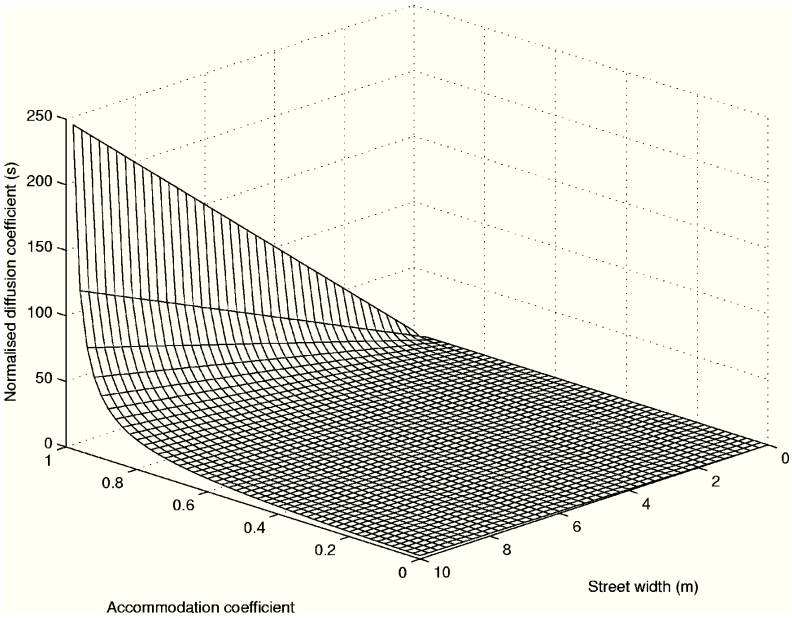

Figure 1.3: Variation of the normalized diffusion coefficient $\mathcal{K}/c$ as a function of the accomodation coefficient d (accounting for the fraction of specular reflections inside the room) and the width of the street b. (from [23])

In these studies the presence of mixed reflections is taken into account by empirically adjusting the theoretical diffusion coefficient with a correction factor K:

$$D_{emp} = K\, D_{th}. \tag{1.51}$$

The values of the parameter K were empirically obtained, for a variety of room shapes, by comparing the diffusion model with cone-tracing simulations: the most probable value for K is determined as the one that provides the best fit between the SPL curves estimated with the two methods.

The main results of the study can be summarized in the following remarks:

1. Inside enclosures with purely diffuse reflections it is possible to identify a narrow interval of values for K optimal for all the investigated geometries and centred around $K \approx 1.2$ (that is, the theoretical expression slightly underestimates the diffusion coefficient). Inside proportionate rooms the solution of the diffusion equation is almost independent on the diffusion coefficient.

2. The acoustical behaviour of long and flat rooms is significantly affected by variations of the scattering coefficient, whereas inside rooms with proportionate dimensions the sound field is relatively unaffected by the amount of specular reflections inside the rooms; the range of possible values for the diffusion coefficient is very broad.

3. Inside enclosures with mixed reflections the estimated values of K are always higher then those obtained for the same room with diffusely reflecting boundaries. The variation of the correction factor with the scattering coefficient s

can be expressed through the following empirical law:

$$K = -2.238 \ln(s) + 1.549, \tag{1.52}$$

where the scattering coefficient varies between 10^{-3} and 1. This expression is found to be valid only for enclosure with low absorption ($\alpha < 0.4$) where even for mixed reflections the diffusion process seems to be still valid.

This empirical model was validated by comparison with experimental measurements, for both SPL and reverberation time.

1.5 Open problems

The theoretical frame outlined in the previous Sections highlights that the diffusion equation is a powerful numerical method that allows to predict the sound field inside rooms of various shape with low calculation times and limited computational resources. Even though in the last years several studies were published on this topic, still some aspects of the diffusion theory remain unsolved, as they were never systematically investigated by an experimental point of view:

- the "real" value of the diffusion coefficient as a function of the room geometry;
- the possibility of describing with a diffusion process the sound field inside enclosures with mixed reflections

Obviously these problems could be tackled from an analytical point of view, for example newly deriving the diffusion equation in the hypothesis of a variable diffusion coefficient. This kind of approach is for example employed for the description of the sound propagation in non-homogeneous materials or for the heat transfer.

Anyway, it is believed that prior to proceed with this kind of analysis, it is necessary to clearly understand the limits of the diffusion equation in its present form by means of numerical and experimental tools. The recognized open issues will be therefore investigated in the following Chapters, analysing one of the basic equations of the room-acoustics diffusion model, that is, the equation relating sound energy density and sound intensity through D_{th} (Fick's law of diffusion). If the validity of equation (1.17) is assessed in different geometrical and acoustical configurations, then an estimate of the diffusion coefficient could be provided allowing to model the sound field inside the considered room with a diffusion process.

In *Chapter 2* the gradient equation will be investigated numerically, employing a particle-tracing code, whereas in *Chapter 3* it will be analysed from an experimental point of view, by means of measurements inside the scale model of a long room.

Chapter 2

Numerical anaylsis of the diffusion gradient equation inside proportionate and long rooms

2.1 Introduction

In this Chapter, the local value of the diffusion coefficient is numerically investigated inside both proportionate (cubical) and non-proportionate (long) rooms.

To do so, the diffusion equation in its stationary form was numerically solved, together with appropriate boundary conditions, by using a FEM-based software. The results, in terms of Sound Pressure Level (SPL) and Sound Intensity Level (SIL) were compared with those predicted by a numerical code based on particle-tracing simulations, with the aim of investigating the diffusion gradient equation and verifying the relationship between sound energy density and sound intensity. A local, numerical estimation of the diffusion coefficient was then derived as a function of the room shape and of the boundaries reflection law.

The choice of employing a particle-tracing code, instead of other well established methods (such as, for example, ray-tracing methods) is based on two principal remarks:

1. the particle-tracing code models the sound field starting from the same basic concept of the diffusion equation, that is, as a cloud of elementary particles, propagating inside the room and carrying infinitesimal amounts of energy.

2. the particle-tracing code allows a direct calculation of the net sound intensity, irrespective of the sound energy density (making thus possible to assess the diffusion gradient equation and predict the diffusion coefficient value).

In the following Section the particle-tracing code is described in detail, especially focusing on its calculation principle and the main advantages and downsides of the model. Then, some numerical applications of the diffusion equation and the particle-tracing code are presented, with reference to the sound field inside a cubical room with diffuse reflections and both uniform and non-uniform absorption; moreover, an analytical correction of the diffusion solution is introduced. Finally

the sound field inside a long room is numerically analysed and the local value of the diffusion coefficient is obtained for different geometrical configurations (varying length and aspect ratio of the room) and various acoustic properties of the surfaces.

2.2 A particle-tracing software

The particle-tracing algorithm employed in this study is named SPPS (Sound Particles Propagation Simulation) and is based on the concept of tracking, both in time and space, the elementary particles that form the sound field. The code follows the approach originally suggested by Stephenson [35, 36] and was developed by Picaut *et al.* for investigating the acoustic parameters within street canyons and enclosures [37, 38].

As the code is based on the sound particle concept, it is suitable only for simulating the sound field in the high frequency range, where the modal density is high. The concept of frequency is not directly taken into account but different simulations have to be carried out for each frequency band, varying the absorption and scattering properties of the surfaces, the atmospheric absorption coefficient and the power of the sound source.

In the model the particles are emitted from a source with sound power W, through a closed (or partially closed) enclosure and each particle carries an initial energy $e_{init} = W/N$ (N being the number of particles emitted from the source). The particles propagate along straight lines, without any mutual interaction and with a velocity $\boldsymbol{v}$, whose norm is equal to the speed of sound c. When a particle hits a wall (or a diffusing obstacle), it is absorbed or reflected into a new direction, according to the local reflection law. All the simulations presented in the following Sections were obtained by employing the *energetic* approach proposed by the code [39]: the absorption phenomena do not lead to the disappearance of the particle from the propagation domain, but at each collision the particle energy is weighted according to the local absorption coefficient. The same calculation principle is applied for the absorption of particles during their propagation, due to the atmospheric absorption.

On the other hand, the reflection phenomena are modelled by successive drawings of random numbers following a procedure which can be assimilated to a Monte Carlo method and allows to determine the new propagation direction. In practice the choice of the reflection angle is made by drawing a number ξ between 0 and 1, to be compared with the local value of the scattering coefficient s. If $\xi > s$ the particle is specularly reflected and the reflection angle is equal to the incident angle, according to the Snell's law. On the other hand, if $\xi < s$, the particle reflection will be diffuse: the new propagation direction depends only on the form of the reflection law of the surface and its numerical representation should respect the density probability of the physical phenomenon. For the purpose of this study, a cosine Lambert's law was considered, where the probability of reflection is maximum along the normal direction whereas is null on the grazing angles. In this particular case the propagation direction can be obtained by using the inverse cumulative distribution function technique [40]. The probability $f(\hat{\phi})$ that a particle

is reflected in the solid angle ϕ', included between 0 and $\hat{\phi}$, is obtained as:

$$f(\hat{\phi}) = 2\int_0^{\hat{\phi}} \cos\phi' \sin\phi' d\phi' = \sin^2\hat{\phi}. \tag{2.1}$$

As the probability is between 0 and 1, the choice of the angle $\hat{\phi}$ can be simply done by drawing a random number $u \in [0, 1]$, that is:

$$\hat{\phi} = \sin^{-1}\sqrt{u} = \cos^{-1}(1-u)^{0.5}. \tag{2.2}$$

Obviously, the reflection and absorption phenomena are better represented when the number of random drawings is high, that is when the number N of particles is high in comparison with the room dimensions.

Since SPPS is a numerical tool, in order to describe the sound propagation inside the room, spatial and temporal discretizations are required.

Temporal discretization is carried out calculating the position of each particle within the room every multiple of a constant time step Δt. Of course, in order to obtain an accurate description of the propagation in the time domain, it would be better to select a time step as smaller as possible but in practice its value is a compromise between the precision requirements and the computation time.

On the other hand, spatial discretization is performed by dividing the three dimensional propagation domain into a finite number of tetrahedral elements, using algorithms of Delaunay type [41]. Moreover, the punctual receivers are represented through finite spherical volumes (V_{rec}), in order to compute the number of particles located at the receiver position at time t. The choice of the volume dimension is once again a compromise: it should be small enough to generate a precise spatial description, but not too small, as in this case the probability that a sound particle is located inside the volume becomes too small.

In order to derive the acoustic quantities inside the simulated enclosures, all the contributions of all the particles are collected at the receiver position, as the sound energy density in a receiver volume is proportional to the distribution of sound particles in its volume.

The sound energy density (in J/m^3) is estimated for each time step n at every receiver position as the sum of the amount of energy carried by each particle that crosses the receiver volume V_{rec} (figure 2.1):

$$w_{rec}(n) = \frac{E_{rec}(n)}{V_{rec}} = \frac{W}{N}\frac{1}{V_{rec}}\sum_{i=1}^{N_0}\epsilon_i\frac{l_i}{c}. \tag{2.3}$$

In equation (2.3), N is the total number of emitted particles, N_0 is the number of particles that cross the receiver volume, $l_i/c = \Delta t_i$ is the amount of time that the i^{th} particle spends inside the receiver volume, the coefficient ϵ_i depending on the reflections that this particle has undergone (i.e., $\varepsilon_i = \frac{W}{N}\Delta t_i \epsilon_i$ is the energy carried by the i^{th} particle).

The particle-tracing code provides also results for the net sound intensity vector at each receiver position, calculated as the sum of the intensity vectors of the particles that pass through V_{rec}. Considering that each particle travels through

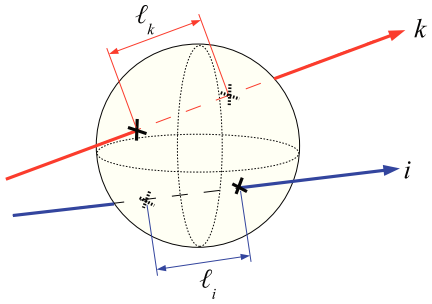

Figure 2.1: Calculation principle of the energy density at a receiver position with the particle-tracing code: each particle crosses the receiver volume and cover a distance l_i inside it. (from [37])

V_{rec} with a velocity vector $\boldsymbol{v}_i$ (with $\|\boldsymbol{v}_i\| = c$) and carries the energy ε_i, the net sound sound intensity vector is then calculated according to:

$$\boldsymbol{I}_{rec}(n) = \sum_{i=1}^{N_0} \varepsilon_i \, \boldsymbol{v}_i = \frac{W}{N} \frac{1}{V_{rec}} \sum_{i}^{N_0} \epsilon_i l_i \frac{\boldsymbol{v}_i}{c}. \tag{2.4}$$

The acoustic quantities $w_{rec}(n)$ and $\boldsymbol{I}_{rec}(n)$ can be summed for all the time steps, yielding the stationary energy density and the stationary net intensity vector.

The numerical code was extensively validated for the prediction of both sound pressure level and reverberation time, comparing the obtained results with other numerical models, experimental data or analytical formulations. On the contrary, no comparisons are available for the prediction of the sound intensity: the comparison between numerical results and experimental data which will be presented in *Chapter 4* is the first attempt of validation of the code.

2.3 Numerical investigation of proportionate rooms

The concept of diffuse sound field employed in room-acoustics predictions is based on the hypothesis of uniform spatial and directional diffusion of the sound energy density inside a room: plane waves with uniform amplitude and random phase arrive at each point of the room with equal probability from all directions, leading to a uniform energy density and a null net energy flow throughout the enclosure. Typical examples of enclosures where the sound field is regarded as diffuse (above the Schroeder frequency) are proportionate rooms with uniform boundaries absorption, where the main acoustic quantities are usually predicted employing Sabine's statistical theory.

Anyway, this theory can provide only a rough estimation of these quantities since the ideal "diffuse sound field" does not exist in reality [42–44]: the reverberant part of the energy density is not uniformly distributed but undergoes a spatial decay from the source to the boundaries of the room [45], and a non-null reverberant energy flow is then present inside the room.

Recent studies [46, 47] have investigated and described the energy flow within rooms at low frequencies, where the sound field is dominated by strong modal effects. In this Section, on the other hand, the high-frequency case (where the phenomena can be described in a statistical way) is investigated. First, an analytical correction for the diffusion equation is presented, which is valid in the region close to the source, where the diffusion approximation is invalid. Then, the link between the spatial variations of the stationary reverberant acoustic energy density and the acoustic intensity vector (defined as the local acoustic energy flow) is analysed inside proportionate enclosures.

As both diffusion model and particle-tracing code do not directly deal with the concept of frequency or frequency bands, all the results will be presented with reference to a unique frequency identified by the acoustic properties of the surfaces and the characteristics of the sound source.

2.3.1 Analytical correction close to the source

As explained in § 1.2.9, close to the sound source (i.e., for source-receiver distances smaller than the mean free path of the room), the solution of the diffusion equation is invalid, as the diffusion process is not established yet [7].

In order to better understand the phenomenon, the solution of the diffusion equation in its stationary state can be analysed [21]. When the source emits a constant sound power and the steady-state is reached, the diffusion equation can be expressed as an Helmholtz equation:

$$D_{th}\nabla^2 w(\boldsymbol{r}) - \sigma w(\boldsymbol{r}) = W\,\delta(\boldsymbol{r}-\boldsymbol{r_s}). \tag{2.5}$$

The Green function of equation (2.5) for an unbounded medium is:

$$G(\boldsymbol{r},\boldsymbol{r}_s) = \frac{W}{4\pi D_{th} r}\exp\left(-\sqrt{\frac{\sigma}{D_{th}}}r\right), \tag{2.6}$$

where W is the sound power, $\boldsymbol{r}_s$ is the source location, $r = \|\boldsymbol{r}-\boldsymbol{r}_s\|$ is the source-receiver distance, and $\sigma = \bar{\alpha}c/\lambda$ ($\bar{\alpha}$ being the mean absorption coefficient of the room). An interpretation of this function was proposed in ref. [7], and it was pointed out that for $r \to 0$, the Green function $G(\boldsymbol{r},\boldsymbol{r}_s)$ reduces to:

$$G(\boldsymbol{r},\boldsymbol{r}_s) = \frac{W}{4\pi D_{th} r}. \tag{2.7}$$

This $1/r$ singularity involves a non-physical behaviour of the diffusion solution close to the source, where an incorrect direct field is predicted due to the lack of validity of the analogy with a diffusion process.

On the other hand, the intensity $\boldsymbol{I}(\boldsymbol{r},t)$ is correctly described by the diffusion process, even close to the source. Indeed, applying the diffusion gradient equation (1.17) to the Green function of equation (2.7) retrieves the correct value of the direct field intensity:

$$\boldsymbol{I}(r) = -D_{th}\frac{\partial}{\partial r}\left(\frac{W}{4\pi D_{th} r}\right) = \frac{W}{4\pi r^2}. \tag{2.8}$$

The conclusion is that the spurious part of the energy density solution of equation (2.7), is the part of the energy whose flow creates the direct field intensity, the remaining part accounting for the reverberant energy density.

The idea is then to calculate a "corrected" energy density, $w_r(\boldsymbol{r})$, from the solution of the diffusion equation $w_{diff}(\boldsymbol{r})$, by removing the non-physical contribution of the diffusion process in the region close to the source:

$$w_r(\boldsymbol{r}) = w_{diff}(\boldsymbol{r}) - \frac{W}{4\pi D_{th} r}. \tag{2.9}$$

The quantity $w_r(\boldsymbol{r})$ is then expected to be an improved estimation of the energy density of the reverberant field, as the shortcoming of the $1/r$ singularity is removed from the original solution $w_{diff}(\boldsymbol{r})$. Following this, the total net intensity vector (including the contributions of direct field and reverberation) is calculated by computing $\boldsymbol{I}(\boldsymbol{r}) = -D_{th}\nabla w_{diff}(\boldsymbol{r})$, while the contribution of the reverberant field, $\boldsymbol{I}_{rev}(\mathbf{r})$, will be calculated as:

$$\boldsymbol{I}_{rev}(\boldsymbol{r}) = -D_{th}\nabla w_r(\boldsymbol{r}) = \boldsymbol{I}(\boldsymbol{r}) - \frac{W}{4\pi r^2}. \tag{2.10}$$

The vector $\boldsymbol{I}_{rev}(\boldsymbol{r})$ is termed "reverberant intensity vector", while $\boldsymbol{I}(\boldsymbol{r})$ is the "total intensity vector" (including the direct and reverberant fields contribution).

In the following this analytical correction is verified for the case of a cubical room with diffuse reflections and uniform absorption coefficient.

2.3.2 Cubical room with uniform aborption coefficient

In this Section the sound field inside a $10 \times 10 \times 10$ m^3 cubical room, with a uniform absorption coefficient $\alpha = 0.1$ is investigated; an omni-directional source is located in its centre, and emits a constant sound power level $L_W = 100$ dB. An upper view of the cubical enclosure, together with source and receivers positions on the plane at z=5 m, is shown in figure 2.2.

Inside the room, particle tracing simulations were carried out with $N = 5 \times 10^6$ particles and a time step $\Delta t = 0.002$ s; a scattering coefficient $s = 1$ was assigned

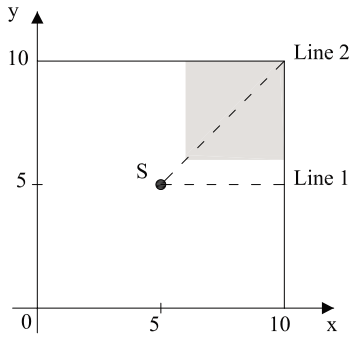

Figure 2.2: Upper view of the investigated $10 \times 10 \times 10$ m^3 room, with the two lines along which sound pressure and sound intensity levels are evaluated. The gray zone refers to the area where the spatial distribution of the intensity vectors is investigated.

to all the surfaces, which can thus be regarded as purely diffusely reflecting. The diffusion equation was numerically solved by using a software based on the finite elements method, where a cubical domain was defined and meshed with about 420×10^3 quadratic Lagrange-type elements.

The SPL at each point in the room is calculated from the energy density, by using the estimation of the square pressure introduced in equation (1.47). For the purposes of this analysis only the reverberant part of the energy density was taken into account, calculated as the difference between the total sound energy density $w(\boldsymbol{r})$ and the energy density of the direct field $w_d(\boldsymbol{r})$ for particle-tracing simulations, and as the corrected energy density $w_r(\boldsymbol{r})$ for diffusion model simulations.

In order to understand if the empirical correction of the energy density leads to correct results, the predicted SPL was compared with that obtained applying the theory developed by Barron *et al.* [45, 48], widely known as "revised theory". This theory, originally developed for the prediction of the sound field in concert-halls and auditoria, stems from geometrical room-acoustics and the image source method. It provides reliable results when dealing with proportionate enclosures and uniform boundaries absorption, and it finds a good agreement with data measured inside the enclosures. In this model the energy density at the receiver is obtained by adding the contribution of the image sources weighted by the absorption coefficient of the walls and the mean free path of the room, as:

$$w(\boldsymbol{r}) = \frac{W}{4\pi c r^2}\exp\left(-\gamma r\right), \tag{2.11}$$

where $\gamma = -\ln\left(1-\bar{\alpha}\right)/\lambda$, λ being the mean free path of the room. The integration of all these contributions over the totality of the image sources, will then provide the reverberant energy density at the receiver position, decreasing with the distance according to an exponential law. In terms of sound pressure level the relationship can be expressed as:

$$\mathrm{SPL}(\boldsymbol{r}) = L_W + 10\,\log\left(\frac{1}{V}\frac{\exp\left(-\gamma r\right)}{\gamma}\right). \tag{2.12}$$

The calculated SPL curves, obtained with the three different methods, are depicted in figure 2.3, showing that the models lead to similar results, with relative differences lower than 0.3 dB; in the same graph, for comparison, the SPL decay obtained from $w_{diff}(\boldsymbol{r})$, solution of the diffusion equation, is plotted, demonstrating the need for removing the $1/r$ singularity as in equation (2.9). Finally, it is worth noticing that, although the general trend of the SPL distribution has to be considered almost constant, all the models predict slight variations of the SPL value in the position closest to the boundaries, that will inherently produce energy flows (i.e., intensity vectors) throughout the room.

The SIL at position $\boldsymbol{r}$ is calculated as:

$$\mathrm{SIL}(\boldsymbol{r}) = 10\,\log\left(\frac{I(\boldsymbol{r})}{I_{ref}}\right), \tag{2.13}$$

where $I(\boldsymbol{r})$ is the norm of the calculated intensity vector and $I_{ref} = 10^{-12}$ W/m^2.

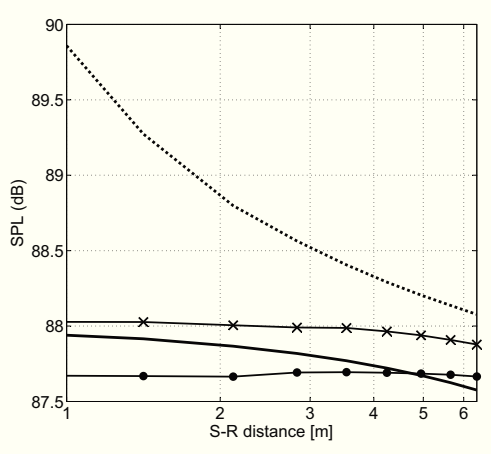

Figure 2.3: Sound pressure level (SPL) of the reverberant field as a function of the distance between source and receiver (S-R distance) inside a cubical room with $\alpha = 0.1$, along Line 2: revised theory (solid line), particle tracing simulations ($\times$); $(\cdots)$ and $(\bullet)$ indicate respectively the SPL calculated with the diffusion model from $w_{diff}(\boldsymbol{r})$ and $w_r(\boldsymbol{r})$.

In figure 2.4 the predicted total SIL is plotted along Line 1 and Line 2 (as defined in figure 2.2): both numerical tools provide the same results, in spite of their differences in the calculation method of the sound intensity. This agreement demonstrates that the gradient equation of equation (1.17) is valid, even though the energy density variations are very weak throughout the room. Indeed the obtained intensity matches the one obtained from the particle-tracing calculation.

The numerical results of figure 2.4 are compared with the SIL decay of the direct field (with norm $I_{\text{dir}} = W/4\pi r^2$), decreasing 6 dB for doubling of distance [29]. Close to the source the total field is completely dominated by the direct sound, while, near the boundaries a discrepancy between the total and direct SIL is found, that reaches almost 1.5 dB for the considered geometry. In these regions therefore the norm of the reverberant intensity vectors becomes of the same order of magnitude as the norm of the direct intensity vectors.

This effect is related to the presence of edges and vertices: a numerical simulation of a sphere with radius $R = 5$ m, uniform absorption coefficient $\alpha = 0.1$ and diffuse boundaries was carried out employing the diffusion model, the source being located at the sphere centre. The total SIL estimated along a line from the source to a wall, is depicted in figure 2.4, demonstrating that in such a room, due to the spherical symmetry, the reverberant energy density flow is null all over the enclosure: the total sound intensity at any internal point is then equal to its direct component, and the reverberant field is found to be ideally diffuse in this case [49, 50].

In order to explain the different SIL decay trends on Line 1 and Line 2, the spatial distribution of the reverberant intensity vectors inside the cubical room was represented over an horizontal plane in figure 2.5. Only the region outside the reverberant radius $r_r = 1.15$ m (calculated according to the classical theory [17]) is depicted, shown as the grey zone in figure 2.2. The intensity vectors are shown to follow a well-defined pattern from the source toward the edges of the

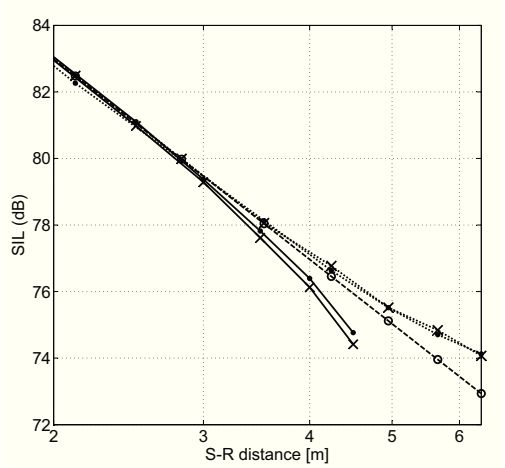

Figure 2.4: Total sound intensity level (SIL) in the $10 \times 10 \times 10$ m^3 cubical room ($\alpha = 0.1$), as a function of the source-receiver distance, along Line 1 (solid lines) and Line 2 (dotted lines): particle tracing simulations for the room with diffusely reflecting boundaries ($\times$), diffusion model ($\bullet$), theoretical value of the direct sound field (- -); ($\circ$) refers to the total SIL calculated with the diffusion model inside a sphere with radius $R = 5$ m and $\alpha = 0.1$.

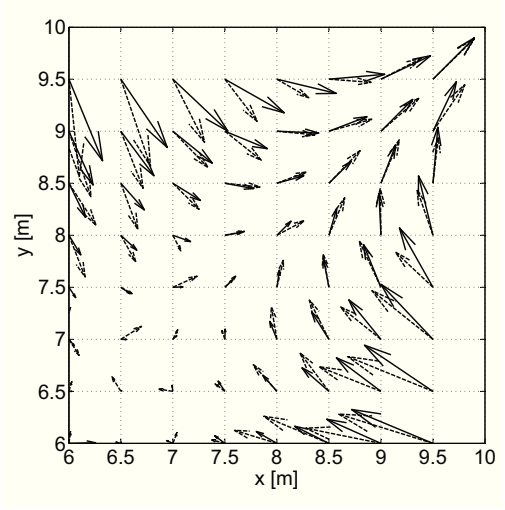

Figure 2.5: Reverberant intensity vectors distribution over the horizontal plane at z=5 m inside a $10 \times 10 \times 10$ m^3 cubical room with $\alpha = 0.1$: particle-tracing simulations (solid arrows) and diffusion theory (dashed arrows).

room, and the norm of the reverberant intensity is more intense close to the room boundaries. Both models provide the same pattern, in spite of local differences in the vectors direction, which, again, demonstrates the validity of the diffusion gradient equation.

Additionally, it is observed that close to the room corner, the reverberant intensity vectors point toward the same direction as the direct field intensity vectors: in this region the total SIL is therefore higher than the direct one, as observed in figure 2.4 for Line 2. Conversely, along Line 1, the total SIL is lower than the SIL of the direct field, as a consequence of the reverberant intensity vectors orientation, opposite to the one of the direct field intensity vectors.

Similar effects were pointed out also by Waterhouse in ref. [51], showing that the reverberant field departs from the ideal condition of diffusiveness due to interference phenomena that occur close to the walls of the room between the sound wave and its reflections. The different combinations of the phase of the waves are responsible for an increase of the sound pressure level close to the boundaries of the room. Anyway, the results of this analysis can not be entirely reproduced with the diffusion model (or with the particle-tracing code) as the latter is an energetic model, and thus can not model the interference phenomena.

Finally, having numerically assessed the validity of the diffusion gradient equation, a local estimate of the diffusion coefficient was obtained, starting from the particle-tracing software results and inverting the expression in equation (1.25), as:

$$D_{est}(\boldsymbol{r}) = \frac{|\boldsymbol{I}_{rev}(\boldsymbol{r})|}{|\nabla w_{rev}(\boldsymbol{r})|}, \tag{2.14}$$

where $\boldsymbol{I}_{rev}(\boldsymbol{r})$ and $w_{rev}(\boldsymbol{r})$ are the simulated reverberant intensity vector and energy density. Only the reverberant part of the sound field was considered in the estimate, being the only one properly modelled through the diffusion equation.

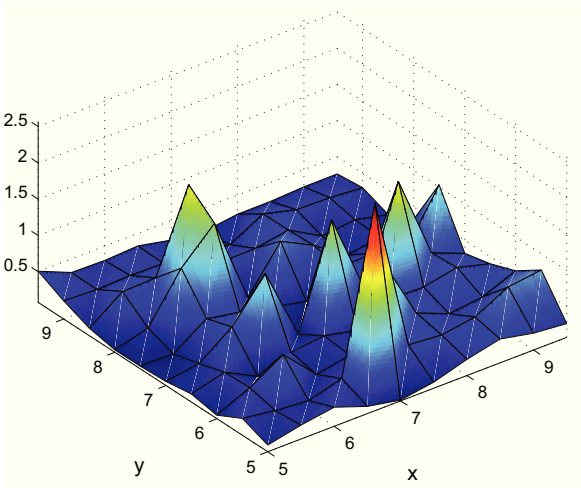

Figure 2.6: Ratio between the estimated diffusion coefficient D_{est} and the theoretical value D_{th} inside the cubical room $10 \times 10 \times 10$ m^3 with $\alpha = 0.1$, over a quarter of the horizontal plane at z=5 m.

In figure 2.6 the ratio between the estimated value of the diffusion coefficient and the theoretical one, as obtained by equation (1.18), is represented over the horizontal plane: the values of the estimated coefficient are basically lower than that of the theoretical one, as a consequence of a slightly bigger variation of the energy density simulated with the particle-tracing model. Anyway, D_{est} varies from point to point over the plane, with values between $0.1 \cdot D_{th}$ and $2.5 \cdot D_{th}$, without any kind of regularity or organized trend: therefore it is not possible to define a unique value for the coefficient inside the room. The result is in agreement with the conclusions drawn by Foy *et al.* in ref. [15] in the analysis of the SPL decay inside rooms with proportionate dimensions, where, especially if the source is located in the centre and the shape of the room is cubical, the solution of the diffusion equation is found to be almost independent of the diffusion coefficient.

2.3.3 Cubical room with non-uniform absorption coefficient

A cubical room with non-uniform absorption properties was then investigated: in this case all the walls are featured with an absorption coefficient $\alpha = 0.1$, except for the ceiling where $\alpha = 0.5$.

Inside this room, as an effect of the non-homogeneous absorption coefficient, the reverberant intensity vectors are attracted from the surface with the higher absorption, leading to an energy flow from the floor to the ceiling of the room. Both particle-tracing model and diffusion model provide the same vector distribution, as shown in figure 2.7.

In figure 2.8 the total SIL predicted by the two models is reported along the x=5 m line, together with the SIL of the direct field. Again, a very good agreement is found between the diffusion gradient modelling of the intensity, and the direct calculation obtained with the particle-tracing code. As for the cubical room with uniform absorption coefficient, in the region close to the walls the norm of the reverberant intensity vector is of the same order of magnitude as the norm of the direct one, leading to a discrepancy between the direct and the total field. Close to the floor, where the reverberant intensity vectors are oriented in the opposite direction to the direct intensity vectors, the total SIL is lower than the direct SIL. Close to the ceiling, where both reverberant and direct sound intensity vectors point toward the same direction, the total SIL is higher than the direct one.

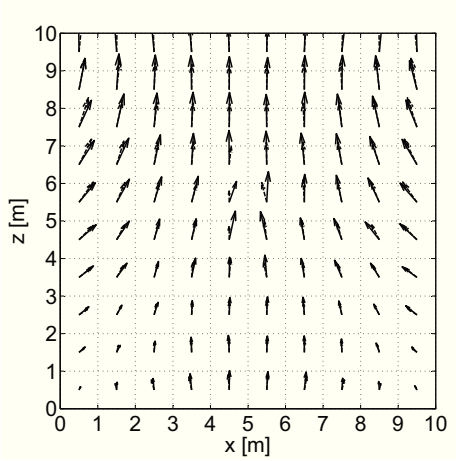

Figure 2.7: Reverberant intensity vector distribution over the vertical plane at y=5 m inside a $10 \times 10 \times 10$ m^3 cubical room with $\alpha = 0.5$ for the ceiling and $\alpha = 0.1$ for the remaining surfaces: particle-tracing simulations (solid arrows) and diffusion theory (dashed arrows).

Some deviations of SIL from the one of the direct field were already reported and discussed by Van Zyl *et al.* [29], for enclosures with poor directional diffusion; in particular the differences can be interpreted as positive or adverse additions of the reverberant intensity field to the direct intensity field. More generally, inside a room with non homogeneous absorption distribution, the reverberant energy flows from reflecting to absorbing surfaces are responsible for the non-diffuseness of the reverberant sound field [1].

[1]The same conclusion was pointed out also in ref. [52] where it is remarked the unsuitability

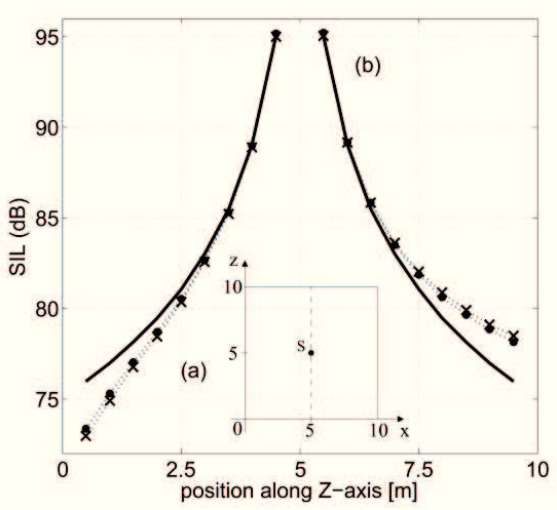

Figure 2.8: (a) Side view of the $10 \times 10 \times 10$ m^3 cubical room: the ceiling is featured with $\alpha = 0.5$ while the other surfaces with $\alpha = 0.1$; the sound intensity level is evaluated along the x=5 m vertical line, over the y=5 m plane. (b) Total sound intensity level (SIL): particle-tracing simulations ($\times$), diffusion theory ($\bullet$), direct sound field (solid line).

2.4 Numerical estimation of the diffusion coefficient inside long rooms

In this Section the numerical methodology introduced in § 2.3.2 for the estimation of the diffusion coefficient is applied to the case-study of a long room.

The choice of investigating this particular kind of enclosures was determined by several different considerations:

1. Inside long rooms, as a consequence of the disproportion between the geometrical dimensions, the sound field is far from diffuse and the classical statistical formula can not be employed for predicting the acoustic quantities which vary continuously along the length of the room [52]. Hence, in order to study the sound field inside this kind of enclosures, it is necessary to employ other models, such as the radiosity method (for rooms with diffusely reflecting boundaries), or the image source method (for room with geometrically reflecting boundaries). The room-acoustics diffusion theory represents a valid alternative to these methods (at least, in the case of diffuse reflections) as it can be regarded as an extension of the statistical theory to non-diffuse sound fields.

2. The sound field inside long rooms can be considered as one-dimensional: this observation allows to investigate the local value the diffusion coefficient only along one of the room dimensions, diminishing the number of independent factors affecting its variation.

of the classical theory for describing the sound field inside enclosures with normal shape but extremely uneven absorption distribution.

3. As reported in ref. [15], inside elongated rooms the solution of the diffusion process is very sensitive to the value of the diffusion coefficient: so, unlike the case of cubical rooms, with this geometrical configuration a variation of the diffusion coefficient should be observed inside the room.

The relationship between energy density and sound intensity was numerically investigated firstly inside a long room room with diffusely reflecting boundaries; then the geometrical (length, aspect ratio) and acoustic (boundaries reflection law and surface absorption coefficient) properties of the room were systematically varied. As for the cubical room, the aim of the analysis was to identify, if exists, the diffusion coefficient that allows the stationary sound field to be governed by a diffusion process.

2.4.1 Remarks on the one-dimensional Green function

Inside long enclosures the sound field varies mainly along the length of the room and can be considered constant over the cross-section; this behaviour allows to define the sound field as one-dimensional and investigate the acoustic parameters only along the main dimension of the room. If the boundary conditions are "simple" (such as, for example, uniform boundaries absorption), the diffusion equation can be analytically solved, as proposed in ref. [6]. For example, in the limit case of an infinitely long room with the sound source located in $x = 0$, the one-dimensional Green function is expressed as:

$$G(\boldsymbol{x}) = \frac{W}{2\sqrt{D_{th}\sigma}} \exp\left(-x\sqrt{\frac{\sigma}{D_{th}}}\right), \tag{2.15}$$

where W is the sound power and σ accounts for the absorption at the room boundaries. The function predicts an exponential decay of the energy density with the distance from the source, thus a linear decrease of the sound pressure level within the room.

It is worth noticing that for one-dimensional enclosures the whole solution $w_{diff}(\boldsymbol{r})$ provided by the diffusion equation is satisfactory, as the $1/r$ singularity that occurs close to the source in proportionate rooms, is not present here; therefore, in long rooms is not necessary to employ the correction introduced in § 2.3.1 for dealing with sound-receiver distances smaller than one mean free path. The reason is twofold: firstly, the correction is needed only where the sound field is three-dimensional, condition that inside proportionate room is met in the whole propagating space, while in long rooms happens only in the position closest to the source (near field). Secondly, the correction is needed inside a region of the size of one-two mean free paths but while in proportionate room the mean free path is significant in comparison with the room dimensions, in the case of long enclosures it is always much smaller of the biggest dimension of the room, where the sound field is usually investigated.

Therefore, in all the simulations that will be presented in the following, the empirical correction was never applied and it was chosen to study only the total sound field, which is everywhere coincident with its reverberant part, except for

positions closest to the sound source, where the direct field is predominant. The total energy density at each position $\boldsymbol{r}$ of the room is calculated as:

$$w(\boldsymbol{r}) = \frac{W}{4\pi c r^2} + w_{diff}(\boldsymbol{r}), \tag{2.16}$$

where $w_{diff}(\boldsymbol{r})$ describes the reverberant part of the sound field obtained as the solution of the diffusion equation.

2.4.2 Numerical estimation of the diffusion coefficient

To start with, a long room with dimensions $40 \times 4 \times 4$ m^3 is considered, with a uniform absorption coefficient $\alpha = 0.1$ and completely diffusely reflecting boundaries. The sound source is located 2 m apart from one of the end walls and emits a constant sound power level $L_W = 100$ dB. An upper view of the investigated geometry is depicted in figure 2.9, with the source position and the line, from the source to the opposite end wall, along which the acoustic quantities were investigated.

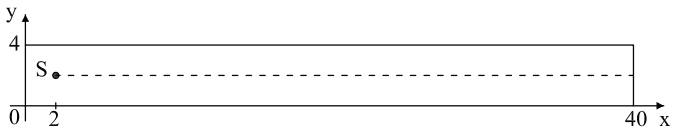

Figure 2.9: Upper view of the $40 \times 4 \times 4$ m^3 room with the line at $z = 2$ m along which sound pressure and/or sound intensity were evaluated.

Particle-tracing simulations were carried out with $N = 5 \cdot 10^6$ particles, a time step $\Delta t = 0.002$ s and a total time $T_s = 2$ s; for the numerical solution of the diffusion equation with a FEM-based software the domain was meshed with 6114 quadratic Lagrange-type elements. For the calculation of the energy density gradient it was chosen to apply central finite differences, with a 4^{th} order accuracy; the same method was employed for both simulation tools.

The predicted acoustic quantities are depicted in figure 2.10, as function of the distance from the source.

As expected, the sound field inside the room is not diffuse and the SPL decreases continuously along the length. The two simulation tools provide quite similar results for the SPL decay, up to 25 m from the source, where the difference between the models is almost equal to 1 dB and the slope of the decay curve predicted by the particle-tracing model starts diminishing, affected by the reflections from the surrounding walls. This effect, mainly related to the presence of the end wall, was already pointed out by Kang [53] and Picaut *et al.* [6]. Kang explains the change of slope in long rooms with geometrically reflecting boundaries and highly reflective end walls with a difference in the contribution of the image sources: the first order image source plane plays a more important role than the others, that become important instead only in the area close to the end wall, producing a decrease (or even a slight increase) of slope in the SPL decay. On the other hand, Picaut *et al.* study the influence of the absorption coefficient on this change of slope in the case of long rooms with diffusely reflecting walls, concluding that it raises when

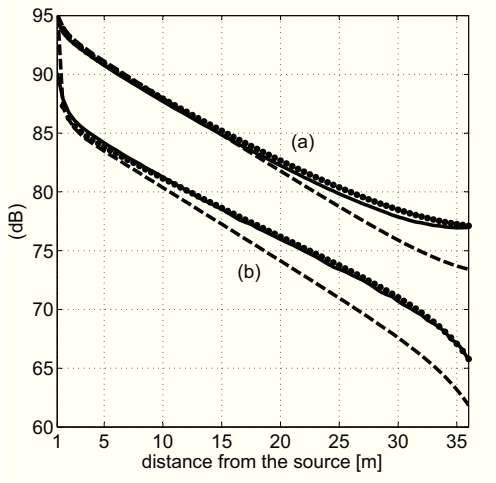

Figure 2.10: SPL (a) and SIL (b) inside a long room $40 \times 4 \times 4$ m^3 with $\alpha = 0.1$ and diffusely reflecting boundaries (s=1): particle tracing simulations (solid line), diffusion model solved with the constant D_{th} $(--)$, diffusion model solved with the estimated diffusion coefficient $(\bullet)$.

the absorption at the end and on the side walls increases. Anyway, this effect is not properly modelled by the diffusion theory and leads to differences between the numerical simulations that, close to the end wall of the room, reach 4 dB.

The predicted SIL shows differences between the two models starting from 12 meters from the sound source and increasing with the distance; the diffusion equation always predicts for the sound intensity smaller values than the particle-tracing code.

It is worth stressing here an important restriction of both diffusion model and particle-tracing code. Neither of them allows to take into account the concept of frequency band and bandwidth and this lack leads to an incorrect representation of the acoustic phenomena as, for example, the dependence of the level difference between pressure and intensity on the considered bandwidth (increasing with the enlargement of the frequency band) [54]. This is clearly an intrinsic limitation of the models, that can not be overcome without a complete revision of their basic hypothesis; therefore, great attention has to be paid in comparing the predicted acoustic quantities.

In order to find a better agreement between the two simulation tools, the diffusion coefficient was numerically investigated inside the room, starting from the particle-tracing results and employing the relationship expressed in equation (2.14). The ratio between D_{est} and D_{th} is represented in figure 2.11: starting from the theoretical value, the estimated diffusion coefficient increases linearly with the distance, up to 30 m from the source where the slope of the curve increases sharply. The linear increase of D_{est} explains the erroneous results predicted by the diffusion theory, which is based on the constant value D_{th}.

The experimental curve was therefore fitted with the linear approximation shown in the same figure, to be employed for solving the diffusion equation. The results, in terms of SPL and SIL, are represented in figure 2.10, showing, as expected, a close agreement with the particle-tracing predictions, with differences

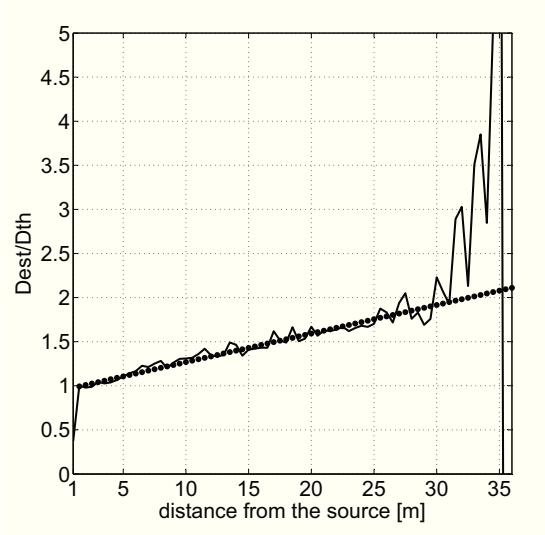

Figure 2.11: Ratio between the estimated and the theoretical value of the diffusion coefficient as a function of the distance between source and receiver inside a long room $40 \times 4 \times 4$ m^3 with $\alpha = 0.1$ and diffusely reflecting boundaries ($s = 1$): particle-tracing simulations (solid line), linear approximation ($\bullet$).

smaller than 1 dB everywhere, even in the region close to the end wall, where the SPL increase is finally properly modelled.

In the linear approximation only the part of the curve with a constant slope was considered, as it seems to be the only one affecting the behaviour of the sound field. The final change of slope is due to the end wall reflections, which lead to an increase of energy density in the area; this physical effect is probably enhanced in the diffusion coefficient estimation by the numerical computational errors related to an energy density gradient with values close to zero.

Finally, the local value of the diffusion coefficient was estimated over the cross-section of the room in x=13 m; the results are shown in figure 2.12.

It can be seen that the diffusion coefficient is not a constant over the section but varies slightly, increasing its value from the boundaries to the centre of the room of about 15%. The variation is related to the changes over the cross section of both energy density and sound intensity, originated by the presence of the room boundaries. In fact the assumption of semi-diffuse sound field (that is of constant sound energy density over the cross section) is a useful simplification of the problem but variations of the acoustic parameters over the cross section are always present, that become smaller with increasing distance between the cross-section and the source [53].

2.4.3 Diffusion coefficient inside long rooms with different length

In this Section the influence of the room length on the diffusion coefficient value is investigated. In particular, three rooms with the same cross-section 4×4 m^2 and length $L_1 = 20$ m, $L_2 = 40$ m and $L_3 = 60$ m are considered, with a uniform

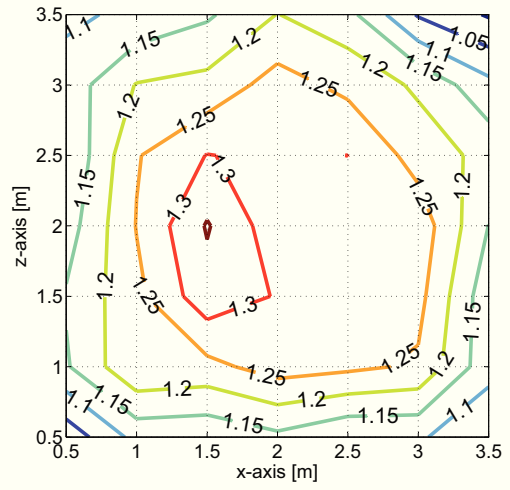

Figure 2.12: Contour plot of the ratio between the estimated and the theoretical value of the diffusion coefficient inside a long room $40 \times 4 \times 4$ m^3 with $\alpha = 0.1$ and diffusely reflecting boundaries. Results for the cross-section in x=13 m.

absorption coefficient $\alpha = 0.1$ and completely diffusely reflecting boundaries ($s = 1$).

In figure 2.13 the predicted SPL and SIL decays inside the three rooms are represented. Both quantities are somehow independent of the length of the room: the decays follow always the same trend, as far as 10 m from the end wall, where the reflection effects become important and the decay in each room experiments a deviation from the main path. It is worth noticing that increasing the length of the room, increases also the spatial variation of the energy density at the end of the room: inside the enclosure with $L = 60$ m close to the end wall an increase of sound pressure level can in fact be noticed.

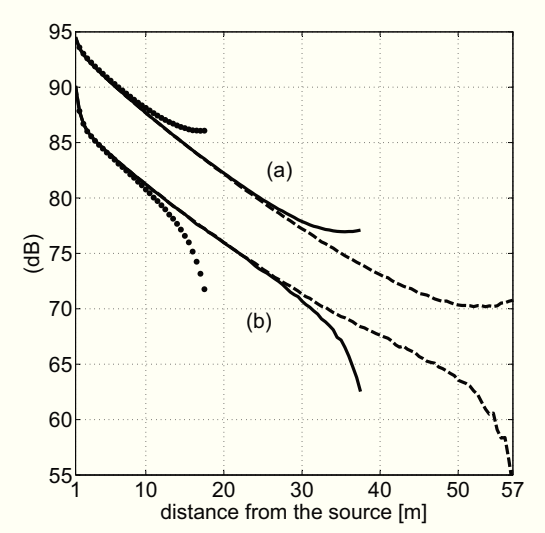

Figure 2.13: SPL (a) and SIL (b) inside a long room with cross-section 4×4 m^2, uniform absorption coefficient $\alpha = 0.1$ and diffusely reflecting boundaries. Particle-tracing results for different lengths of the room: $L_1 = 20$ m (•), $L_2 = 40$ m (solid line), $L_3 = 60$ m (- -).

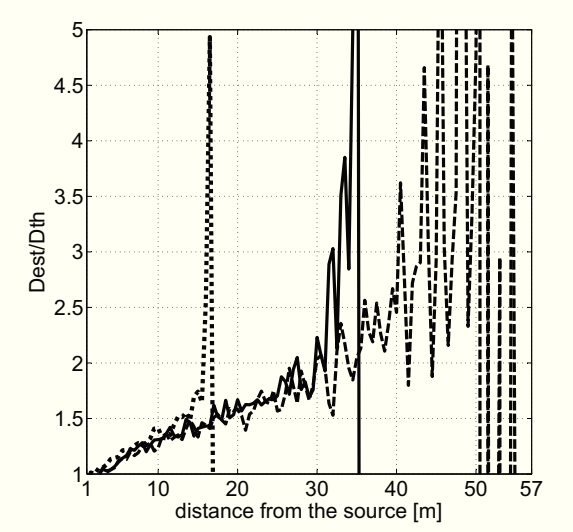

Figure 2.14: Ratio between the numerically estimated and the theoretical diffusion coefficients within a long room with cross-section 4×4 m^2, absorption coefficient $\alpha = 0.1$ and diffusely reflecting boundaries. Results for different length of the room: $L_1 = 20$ m (•), $L_2 = 40$ m (solid line), $L_3 = 60$ m (- -).

In the special case of long rooms with square cross-section it can be easily demonstrated that the mean free path is equal to the height (or the width) of the room and, consequently, the diffusion coefficient does not depends on the length of the room. It means that, for the positions farther from the source and the end wall, where the Green function of equation (2.15) can be considered valid, the energy density follows always the same decay trend, regardless of the length of the room.

This is confirmed also by the diffusion coefficient estimate, which can always be approximated using the same regression law, as depicted in figure 2.14.

2.4.4 Diffusion coefficient inside long rooms with different cross-section

Then the influence of the cross-section dimension on the diffusion coefficient variation inside a long room was investigated. For the analysis, three different elongated enclosures were considered, with the same length (L=40 m) and cross sections respectively 2×2 m^2, 4×4 m^2, 6×6 m^2.

In figure 2.15 the spatial decay of the acoustic quantities decays are represented; it can be seen that the behaviour is quite different, depending on the distance from the sound source. Close to it the acoustic parameters are higher inside the rooms with the smaller cross-sections but, on the opposite, close to the end wall, SPL and SIL are found to have the biggest values in the room with the biggest cross section. So, when comparing rooms with the same L_W, the overall attenuation is lower inside the room with the biggest cross-section; this numerical evidence can be explained according to ref. [53] where it is suggested that as the cross-sectional area increases, the sound field become closer to diffuse, and thus, the decay slope

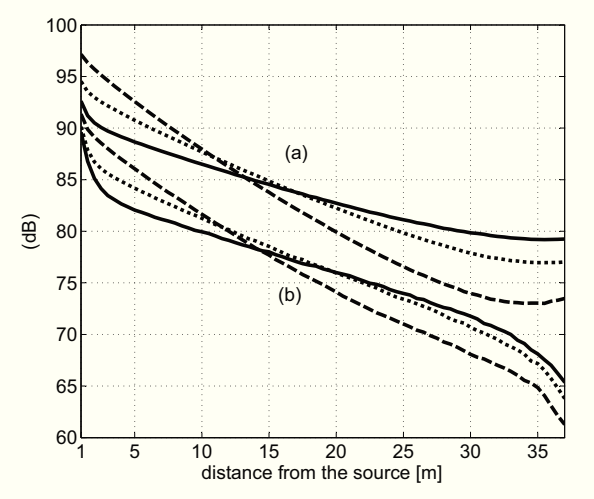

Figure 2.15: SPL (a) and SIL (b) inside long rooms with length L=40 m, $\alpha = 0.1$ and diffusely reflecting boundaries. Particle-tracing results for different cross-sections: 2×2 m^2 (- -), 4×4 m^2 (•), 6×6 m^2 (solid line).

of the acoustic parameter diminishes[2]. Moreover, the change of slope at the end of the SPL decay curve (which is related to the particular geometrical shape of the rooms) is stronger inside the room with the small cross-section.

The diffusion coefficient value was numerically estimated in the three cases (figure 2.16), showing again a linear increase with the distance but with different slopes, depending on the room dimensions. In particular, the slope is found to be inversely proportional to the cross-sectional area, that is to be higher inside rooms with an high ratio between cross-section and length.

2.4.5 Diffusion coefficient as a function of the absorption coefficient

In this Section the dependence of the sound field inside a long room on the overall amount of absorption is investigated. Three long room with dimensions $40 \times 4 \times 4$ m^3 are considered, characterized by diffuse reflections ($s = 1$) and different values of the boundaries absorption coefficient: $\alpha_1 = 0.1$, $\alpha_2 = 0.2$ and $\alpha_3 = 0.3$.

In figure 2.17(a) the spatial decays of SPL and SIL are represented, as obtained by particle-tracing simulations. The increase of surface absorption leads, as expected, to steeper spatial decays of both acoustic quantities, even though the slope increase is more pronounced when the SPL is considered. The absorption coefficient affects also the slope variation of the SPL close to the end wall of the room, enhancing the reflection effects due to the surrounding boundaries; evidences of this effect were also pointed out in ref. [6].

[2]According to ref. [52] "since the unsuitability of the classic theory depends on both dimension and absorption conditions, it seems that there is not a fixed lenght/cross section ratio to characterise the long enclosure. In other words, to define a long enclosure, the dimension condition as well as the amount and distribution of the absorbers should be considered.".

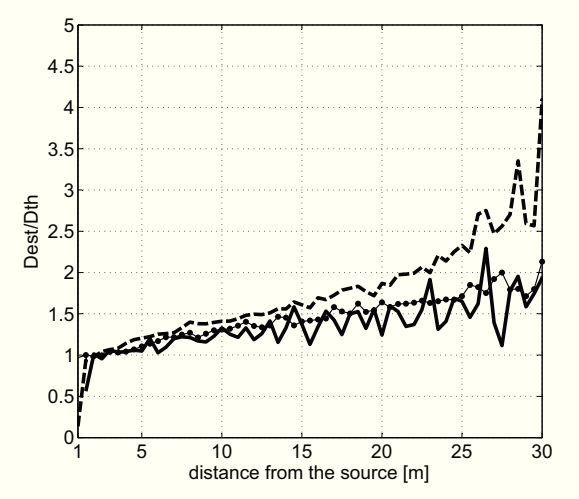

Figure 2.16: Ratio between estimated and theoretical diffusion coefficients within long rooms with lenght L=40 m, absorption coefficient $\alpha = 0.1$ and diffusely reflecting boundaries. Results for different cross-sections: 2×2 m^2 (- -), 4×4 m^2 (•), 6×6 m^2 (solid line).

A numerical estimate of the local value of the diffusion coefficient was obtained for the three enclosures (figure 2.17(b)), showing again a linear increase of the coefficient, with an initial value always coincident with the theoretical value. The surface absorption affects only the slope of the distance - D_{est} curve that increases with the raise of the absorption coefficient.

Even though the diffusion coefficient estimate with the particle-tracing code could be extended to absorption coefficients higher than $\alpha = 0.3$, only the results obtained for the interval $\alpha = [0.01, 0.4)$ can be considered meaningful. In fact, when D_{est} is employed to solve the diffusion equation (as illustrated in § 2.4.2), absorption coefficient values bigger than 0.4 lead to non-physical estimate of the SIL spatial decay[3]; on the contrary correct results were always returned for the SPL prediction. This behaviour is supposed to be related to a lack of validity of equation (1.17) when dealing with disproportionate enclosures and high absorption coefficients. No evidences of this effect were found in literature, as the results inside these kind of enclosures always refers to the energy density spatial distribution [12] or to the reverberation time [11].

2.4.6 Diffusion coefficient as a function of the scattering coefficient

Finally, the variation of the acoustic parameters inside a long room was numerically investigated as a function of the reflection law of the boundaries. The same long room described in § 2.4.2 was considered, with three different values of the boundaries scattering coefficients (s=0.1, s=0.5, s=1).

The SPL and SIL spatial decays calculated in the three cases are represented in figure 2.18. It can be seen that as the amount of specular reflections inside

[3]In the numerical resolution of the diffusion model all the formulations of the exchange coefficient presented in § 1.2.6 were tested.

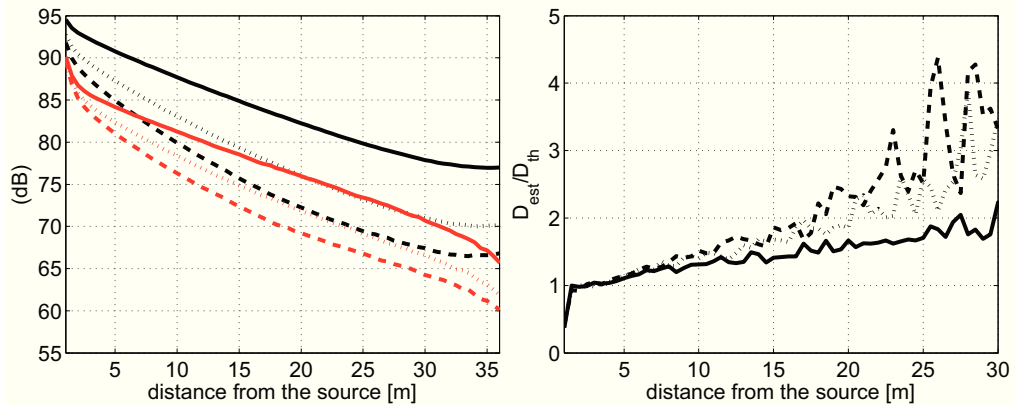

(a) **(b)**

Figure 2.17: (a) SPL (black lines) and SIL (red lines) inside a $40 \times 4 \times 4$ m^3 long room with diffusely reflecting boundaries. Particle tracing results for different values of the absorption coefficient: α=0.1 (–), α=0.2 (•), α=0.3 (- -). (b) Ratio between the estimated D_{est} and the theoretical D_{th} diffusion coefficient within a $40 \times 4 \times 4$ m^3 long room with diffusely reflecting boundaries. Results for different values of the absorption coefficient: α=0.1 (–), α=0.2 (•), α=0.3 (- -).

the room increases, the sound field starts to behave more similarly to a diffuse one, diminishing the spatial attenuation of the SPL. Therefore, inside long rooms, increasing the roughness of the boundaries, leads to greater spatial variations of the acoustic quantities and not to a more diffuse sound field.

As suggested in ref. [53] the reason can be related to the highest chance of the sound rays to hit the surfaces inside rooms with diffusely boundaries with respect to the case of a long room with specularly reflecting boundaries; as the scattering coefficient increases, the sound rays have therefore an highest probability of being absorbed from a surface and consequently the total energy inside the room decreases.

Moreover, it can be observed that the variation of the scattering coefficient differently affects the SPL decay, depending on the distance from the source. In fact close to the sound source the biggest SPL values are found inside the room characterized by purely diffuse reflections (due to backscattering), whereas close to the end of the room an opposite trend verifies and the long room with $s = 1$ shows the smallest SPL values [55]. The crossing point between the three curves is found around x=8 m.

Let's now consider the SIL spatial decay: as for the energy density, the SIL attenuation is smaller inside the long room with diffuse reflections. According to the gradient equation (1.17), solved with a constant diffusion coefficient, what one should expect is instead the opposite trend, as the lowest energy gradients should originate the lowest values of intensity. The observed SIL decay therefore suggests that if the stationary sound field is expected to be modelled with a diffusion process, then the diffusion coefficient should locally variate, increasing with the fraction of specular reflections inside the room.

The local estimate of the diffusion coefficient is depicted in figure 2.19, showing

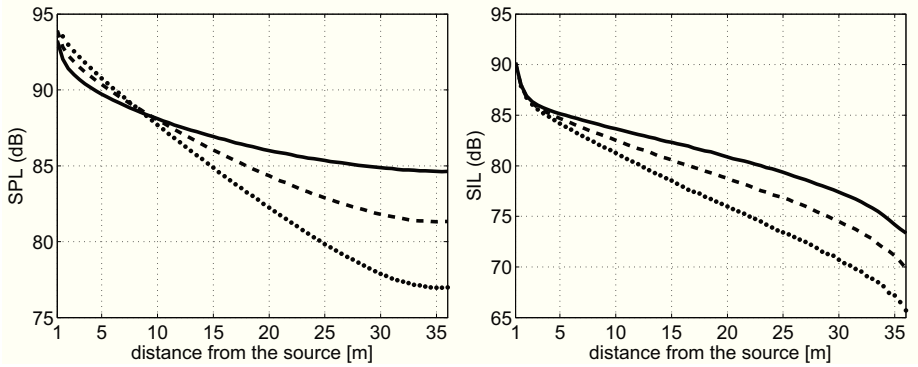

Figure 2.18: SPL (a) and SIL (b) inside a $40 \times 4 \times 4$ m^3 long room with uniform absorption $\alpha = 0.1$. Particle tracing results for different values of the scattering coefficient: s=0.1 (solid line), s=0.5 (- -), s=1 (•).

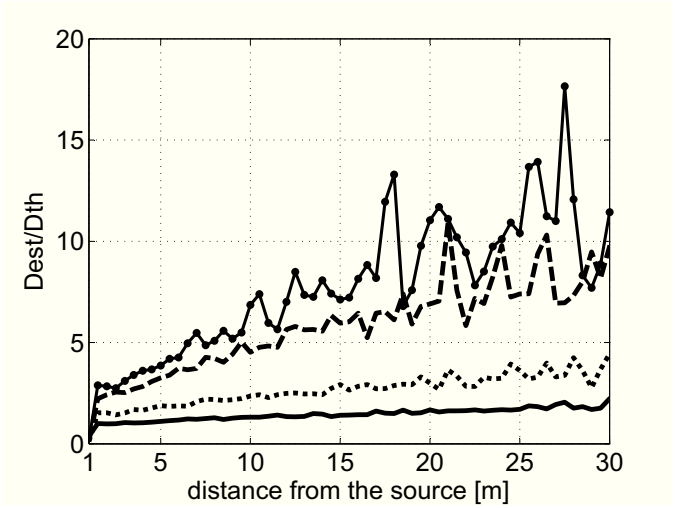

Figure 2.19: Ratio between estimated and theoretical diffusion coefficient within a $40 \times 4 \times 4$ m^3 long room with $\alpha = 0.1$. Particle tracing results for different values of the scattering coefficient: s=1 (solid line), s=0.5 (•), s=0.1 (- -), s=0.01 (-•-).

that both slope and the initial value of the curve distance-D_{est} increases with the amount of specular reflections inside the room. Only when $s = 1$, the initial value of the curve coincides with the theoretical value D_{th}.

In the same figure, also the diffusion coefficient estimate for $s = 0.01$ is represented, which can be considered as the lowest limit of application of the described methodology. Scattering values lower than 0.01 returns in fact a non correct matching between particle-tracing results and the diffusion equation solved with the corresponding diffusion coefficient estimates. Therefore it is possible to conclude that the case of purely specular reflections can not be modelled as a diffusion process, being based on a different propagation mechanism.

2.5 Conclusions

In this Chapter the sound field inside both proportionate and elongated rooms was investigated by means of the diffusion equation and a particle-tracing numerical code, which allows a direct and independent calculation of energy density and sound intensity. The ratio between the two quantities was employed to perform a numerical investigation of the local value of the diffusion coefficient inside the two kind of enclosures.

In particular, the main results obtained with the numerical part of the research can be summarized in the following remarks:

1. The presence of a spurious part in the solution of the diffusion equation was assessed, whose energy flow produces the direct field intensity. An empirical correction was derived, in order to obtain a correct description of the reverberant part of the sound field inside the rooms; the correction was proved to be necessary especially close to the sound source (where the sound field is three-dimensional) or, more generally, in the region within one (or two) mean-free paths from the source.

2. Inside proportionate rooms with homogeneous absorption, where the sound field is classically supposed to be diffuse, the diffusion equation with the analytical correction provides correct results and highlights the presence of weak variations of the reverberant energy density, producing an energy flow throughout the room. This energy flow (which correspond to the reverberant intensity inside the room) is well-organized, emanating from the source and the walls central areas, and converging toward the room's edges and vertices. The intensity vector pattern derived from the energy density gradients was compared with that obtained by direct calculation, showing a good agreement and proving the reliability of the diffusion gradient equation for the reverberant intensity.

3. The diffusion coefficient was numerically investigated inside the proportionate room: it was not possible to define a unique value (or an organized trend) of the coefficient, confirming that, when dealing with proportionate rooms, the solution of the diffusion equation is almost independent of the diffusion coefficient.

4. The numerical analysis of the long rooms showed that inside this kind of enclosures the diffusion coefficient is not a constant but increases linearly along the length of the room, starting, when the boundaries are diffusely reflecting, from the theoretical value D_{th}. The dependence of the diffusion coefficient on the length, the aspect ratio and the absorption properties of the room was assessed. The analysis confirmed the necessity of experimentally investigate the relationship between energy density and intensity inside long rooms, in order to understand if the sound field inside them can be modelled as a diffusion process.

5. Finally, long rooms characterized by mixed reflections were considered; the increase of the amount of specular reflections inside the room was proved to influence both slope and initial values of the curve describing the variation of the numerically estimate diffusion coefficient with the distance. The numerical analysis allowed to estimate the diffusion coefficient only inside long rooms where a residual amount of diffuse reflections is still present ($s > 0.01$); the case of purely specular reflections can not be correctly represented with a diffusion process, being based on a different propagation mechanism.

Chapter 3

An experimental energetic description of the scale model of a long room

3.1 Introduction

This Chapter is focused on the experimental investigation of the sound field inside a scaled long room.

In the previous Chapter the main results of the numerical part of the research were presented: in particular, the diffusion gradient equation was analysed inside long rooms finding that the diffusion coefficient varies with the length of the room and the acoustic properties of the boundaries. The numerical simulations gave therefore a clear outline of the basic features of the issue and provided a starting point for the experimental part of the research.

To assess the real relationship between energy density and intensity in long rooms, measurements were performed inside a 1:16 scale model employing a p-u probe to collect the data. A three-dimensional pressure-velocity probe, that Microflown kindly lent us, was employed, for accomplishing the required measurements. Two different configurations, with different acoustic properties of the boundaries, were set up and the sound field inside them was described by means of energetic and intensity based quantities.

A careful description of the sound field inside the scaled long rooms was a main target of this study, as it represents the mean to understand the results, in term of diffusion coefficient estimate, that will be presented in the next Chapter.

The first step in the acquisition of reliable data inside the model was the calibration of the employed p-u probe, accomplished by means of measurements inside an anechoic chamber, where the probe was exposed to a sound field of spherical waves. The description of the measurements and the numerical elaboration of the digital filters are the main topics of the following Section.

The second part of the Chapter is, on the other hand, focused of the measurements performed inside the scale models, firstly to assess the acoustic properties of the different surface materials and then to investigate the acoustic quantities

inside the scaled long rooms. Two set ups were considered, differing in the type of finishing of the interior surfaces: flat in the first model (corresponding to the case of purely specular reflections) and scattering inside the second (corresponding to the case of mixed reflections inside the room). The description of the sound fields basic features is reported in the final part of the Chapter.

3.1.1 State of the art: intensity in reverberant sound fields

During the years several theoretical formulations have been proposed for describing the sound intensity inside reverberant sound fields.

A perfectly "diffuse" field is classically described through an infinite number of plane waves, propagating from uniformly distributed directions and having random phase relations (hypothesis of directional diffusion). Therefore, the net flow of reverberant energy through a receiver is supposed to be null inside the room [17, 29] whereas, close to the room boundaries the norm of the intensity can be expressed as $I(\boldsymbol{r}) = c\, w(\boldsymbol{r})$ [17].

In ref. [54] the reverberant sound field inside an ideal pure-tone diffuse field is analysed: in this context, in the hypothesis of unit normalized spatial variances of the mean square pressure and the mean square velocity, all the phase angles between pressure and every component of the particle velocity are equally likely. Hence, the spatial-average value of the active intensity component $\boldsymbol{I}_a$ is zero in every direction, that is the spatial distribution of $\boldsymbol{I}_a$ is symmetric around zero, implying that the local value of the active intensity could be non-null. In such a pure-tone sound field it is demonstrated that the intensity level is about 5.5 dB below the sound pressure level. On the contrary, if the room is excited by a "band of random noise", the level differences will depend on the bandwidth and the reverberation time of the enclosure.

In ref. [56] a distinction between "diffuse" sound field produced by a single source and "true" diffuse sound field (as created by uncorrelated sources) is proposed. In the first sound field the coherence between sound pressure and particle velocity $\gamma^2_{pu_r}$ is almost unit and the field is "no more active than reactive". On the other hand, in the second case, the sound field can be considered as homogeneous and isotropic, $\gamma^2_{pu_r} = 0$ and the field is not reactive.

The classic description of the diffuse field can be extended to take into account the interference phenomena that occur near the walls of the room [31, 51], showing that the interference between each wave and its reflected (and correlated) counterpart originates interference pattern near the boundaries. This approach was applied to the region of high modal overlap and but an application to the low-frequency region is proposed in [46, 47, 57] where the statistical properties of active and reactive sound intensity are investigated.

3.2 Characterization of the employed *p-u* probe

The instantaneous sound intensity along a direction is defined as the product of the sound pressure and the component of the particle velocity in that direction [42]. Starting from the definition, it is clear that measuring the sound intensity is never a straightforward task, as, in principle, it involves the concurrent measure of two acoustic quantities by means of transducers of different type.

An historical review of the techniques employed for measuring the sound intensity in air can be found in ref. [42], where the basic features of the two available categories of probes (*p-p* and *p-u*) are also described. As is common knowledge, while the *p-p* probes provide an indirect measure of the particle velocity (according to the Euler's equation), the *p-u* probes are able to directly measure the particle velocity. The main drawback of this kind of probes is the phase mismatch between the two transducers, which is always present (as derives from differences in the transduction method of the devices) and leads to important bias errors in the intensity estimate, especially at low frequency when the measurements are carried out in the near field of a source [18, 58].

For this research a Microflown® USP probe was employed, performing the measure of the particle velocity according to the principles of the two hot wires anemometry. The choice of employing this probe was mainly led by the possibility of acquiring three independent measurements of velocity along the Cartesian axes at the same time; moreover the dimensions of the probe are small enough to avoid perturbations of the sound field.

3.2.1 Description of the probe

The Microflown® device performs a direct measure of the velocity of air particles by means of two closely spaced wires [59–62]; a detail of the particle velocity transducer is shown in figure 3.1 The wires, heated by an electric power to a temperature of 300°C, work as resistors sensitive to temperature fluctuations. In fact, when an acoustic airflow propagates orthogonally across the two wires, the temperature distribution around the resistors alters asymmetrically and generates a voltage signal proportional to the particle velocity. The upstream wire is always cooled down more than the downstream one and this feature makes the system able to discriminate between positive and negative velocity, according to the reversal of the temperature difference.

The sensitivity of the device is not flat over the frequency; the response curve is a combination of one high-pass and two low-pass filters, with the following characteristics:

- at low frequency the sensitivity increases 6 dB per octave; this effect is found to be related to the thermal boundary layer of the wires;
- between 100 Hz and 1 kHz the frequency response is relatively flat;
- at high frequencies the sensitivity decreases. A first roll-off (6 dB per octave) happens between 1 and 10 kHz, caused by diffusion effects. A second roll-off

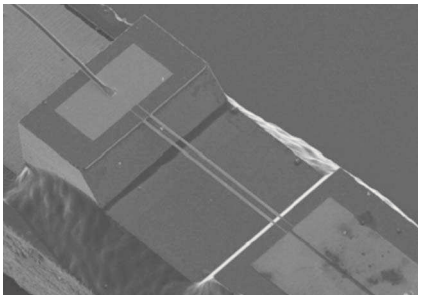

Figure 3.1: SEM photo of a Microflown probe; detail of the two heated wires. (from [61])

happens then above 10 kHz, where the sensitivity decreases an additional 6 dB per octave; the decrease depends on the heat capacity (thermal mass), the geometry and the operating temperature.

The sensitivity curve for each device is directly provided by the manufacturer, in terms of an analytical parametric function [63]. This analytical model predicts the corner frequencies of the system and provides magnitude and phase of the filters to be applied for correcting the measured values; the correction can be directly applied during the measurements by using the signal conditioner provided together with the probe. Anyway, this method prevents the possibility of checking the calibration procedure, which has to be a-priori considered as correct.

Therefore, in this study, an alternative procedure was employed for the equalization and calibration of the signal: raw (uncorrected) data were initially acquired and afterwards processed by using digital filters, expressly designed and derived from calibration measurements.

For the measurements inside the scaled long room a 1/2 in. USP probe was employed: this is a three dimensional device where three orthogonally positioned particle velocity sensors are combined with a small electret microphone, as shown in figure 3.2. The use of this kind of probe allowed to completely characterize pressure and intensity (in modulus and direction) inside the scale model, over a suitable frequency range.

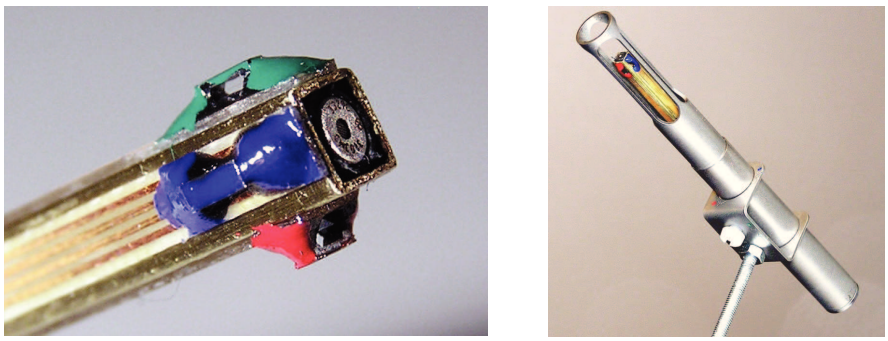

Figure 3.2: A Microflown® USP probe with the three particle velocity sensors positioned on the sides and the pressure microphone mounted on the top of the device.

3.2.2 Directivity measurements

Before staring the calibration measurements, a preliminary investigation of the employed probe was carried on, assessing its frequency and directional responses.

All the measurements were accomplished inside a small silent chamber, which can be considered as anechoic above 250 Hz; moreover, in order to avoid spurious reflections all the possible reflecting objects were covered with absorbent material. The sound source, an highly directive unit at the high frequencies, was placed at an height of 138 cm from the floor; the probe was placed at the same height, 70 cm far from the source.

The measurement chain was then completed by a portable personal computer equipped with a MOTU® Traveler sound card set up with a sampling rate of 96 kHz, the loudspeaker's power amplifier and the signal conditioner of the tested probe. In this phase the measurements were performed enabling the hardware correction of the signal. The acquired impulse responses (IRs), obtained with the sine sweep technique, were employed to retrieve the level of the signal for each one-third octave band in the frequency interval between 800 Hz and 20 kHz.

In a first set of measurements the probe was maintained in the vertical position and rotated clockwise around its axis by means of a turntable placed underneath; a measure was accomplished every 10°. In figure 3.3 a sketch of the measurement set-up at the 0° position is shown, where the relative position of the three velocity sensors is identified through their distinctive colour. In this configuration only the directional response of the two vertical sensors (red and blue) can be investigated, as the wave front is orthogonal to their heated wires; the third sensor, the green one, should instead register a null, or at least constant, signal, well separated from the others.

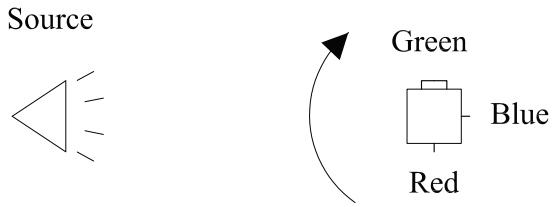

Figure 3.3: Sketch of the set-up for the directivity measurements (upper view); source and probe configuration for the angular position of 0°. The relative position and orientation of the three velocity sensors are identified by their distinctive colour: the red and the blue sensors are oriented along the axis of the probe, while the green one is in the orthogonal direction.

The results, in terms of polar pattern, are reported in figure 3.4: the red and the blue sensors show the expected figure-of-eight directionality and a good agreement between each other. The signal acquired with the green sensor is instead almost constant over all the directions and well separated from the others, with differences of about 15 dB. The pressure microphone can be considered omnidirectional for all the investigated frequency range.

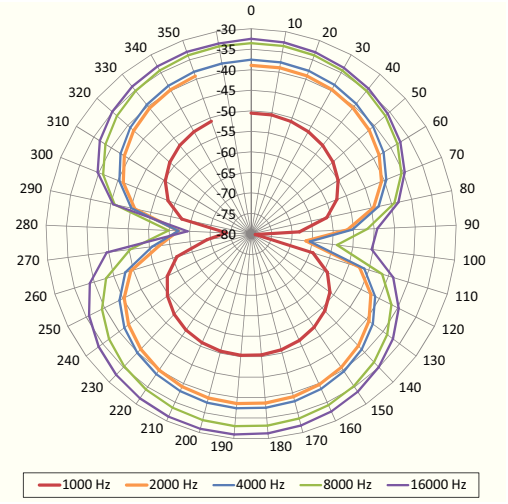

(a) Red device

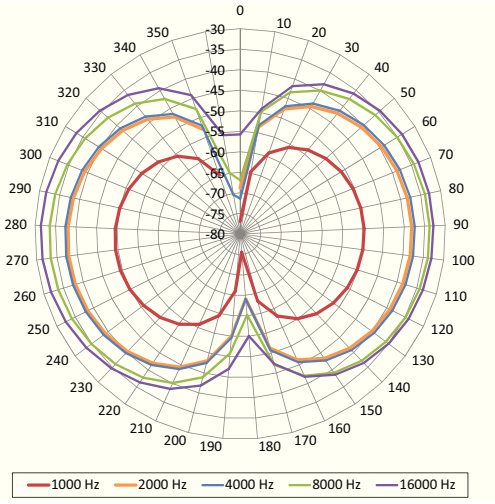

(b) Blue device

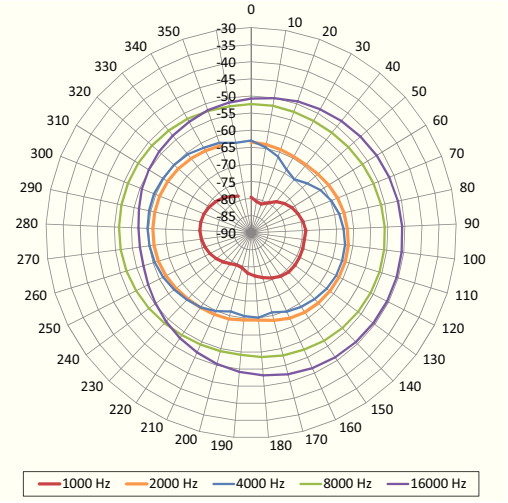

(c) Green device

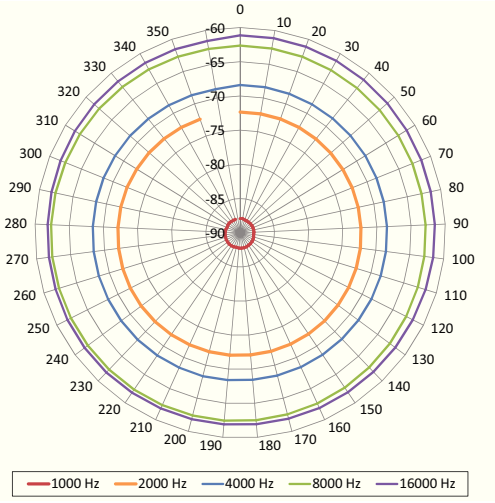

(d) Pressure microphone

Figure 3.4: Polar plots of the four transducers forming the p-u probe, for five different one-third octave bands; the measurements were carried out inside a silent chamber with the probe maintained in the vertical position and rotated around the vertical axis. Results acquired every 10°.

A second set of measurements was then performed to investigate the directional response of the green sensor: in this case the probe was maintained in the horizontal position and rotated around the vertical axis. The polar plot (figure 3.5) shows again the expected cosine behaviour but with a slight asymmetry for the 90°-270° positions, due to the influence of the probe chassis on the sound field and the small changes in the sensor position during the rotation. Again the red and blue sensors acquired a constant signal, well separated from that of the device under test.

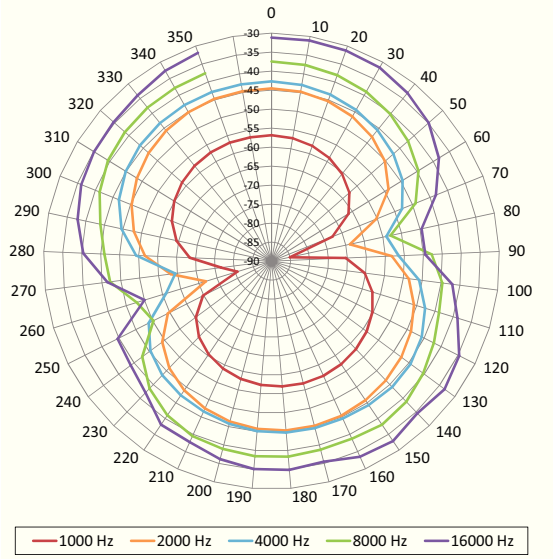

Figure 3.5: Polar plot of the particle velocity green device for five different one-third octave bands; the measurements were carried out inside a silent chamber with the probe maintained in the horizontal position and rotated around the vertical axis. Results acquired every 10°.

Finally, in figure 3.6 the frequency responses of the four devices for a frontal incidence of the sound field are reported: the data are referred to the measurement set up with the vertical probe for the pressure, the red and the blue device (respectively in the angular position 0°, 0° and 90°) and to the set up with the horizontal probe for the green device (angular position 0°). In the graph the pressure signal is attenuated of 30 dB with respect to the others. It can be seen that the frequency response of the three devices can be considered relatively flat (with deviations of ± 3dB) up to 17 kHz.

On the whole, the tested p-u probe demonstrated its suitability for carrying out precision measurements inside a scale model.

3.2.3 Calibration measurements

At present, there is no established method for calibrating the p-u probes; in fact, while it is quite easy to calibrate the pressure microphone, a comparison calibration of the velocity sensor is still not possible, as a standard reference particle velocity transducer does not exist. So, the solution is to carry out a relative calibration, that is, to calibrate the velocity sensor with respect to the pressure one, exposing the whole probe to a sound field with a known relationship between pressure and

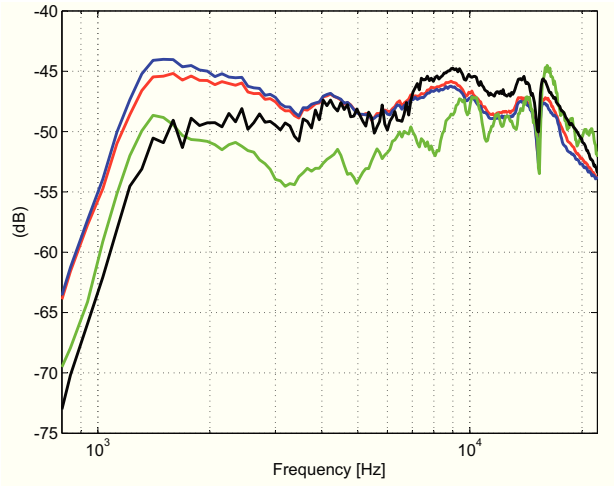

Figure 3.6: FFT analysis of the frequency response of the three velocity sensors (identified by their colour) and the pressure microphone (black line) for frontal incidence. The pressure signal is attenuated of 30 dB with respect to the others.

velocity. Then, the reference velocity signal will be obtained as the ratio between the measured and the theoretical value of the impedance of the sound field.

With reference to the employed p-u probe, during the last years several calibration methods have been proposed, as, for example, the calibration inside an anechoic room [58], the calibration inside a standing wave tube [61] and the calibration with a spherical baffle [64, 65]; see, for a review of the different techniques ref. [64]. In addition, a new calibration procedure was recently proposed, employing a plane progressive wave generated along a wave guide as reference sound field [66]. The main targets of these methods are to cover at once all the considered frequency range (without any change in the measurement set up) and to allow an in-field calibration that does not require specially equipped rooms to be performed.

For this study it was chosen to calibrate the probe following the method proposed by Jacobsen *et al.* in ref. [58]. The calibration measurements were performed inside a small anechoic chamber, where the probe was exposed to a field of spherical waves. When the distance between source and receiver is conveniently large, the impedance of the field equals that of the plane progressive waves, that is $\rho_0 c$. If the calibration is carried out close to the sound source (as in the present case, due to the limited dimensions of the available chamber) the theoretical value of the impedance is no longer valid: the hypothesis of far field is not verified and the loudspeaker can not be considered a perfect monopole. This remark is especially true at low frequency where a correction for the "near field effect" has to be set. No additional phase-correction procedures (as those suggested in ref. [58]) were employed in the calibration, given that the scale model measurements were performed at frequencies higher than 500 Hz.

The measurements set-up is shown in figure 3.7. The sound source was an highly directive unit, positioned at an height of 141 cm. The probe was placed, together with a reference microphone, 55 cm apart from the source, at the same height. The reference microphone was a 1/8 in. B&K® type 4165 free-field microphone,

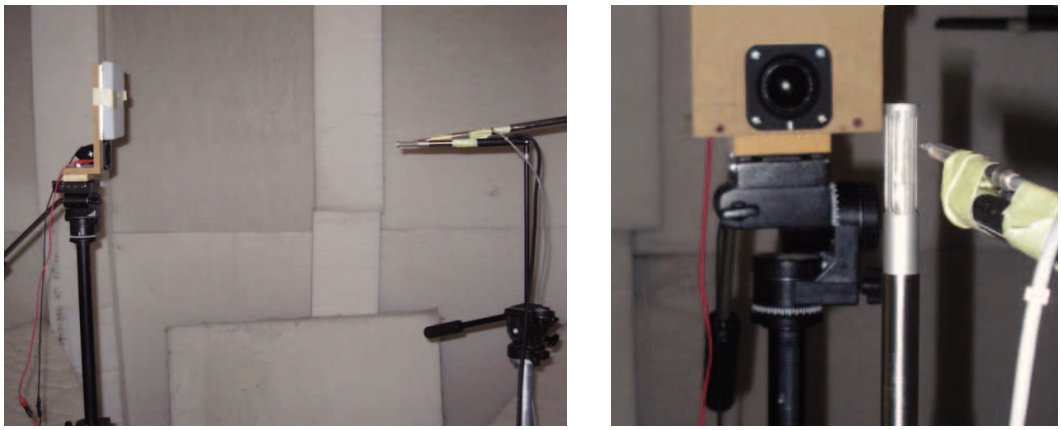

Figure 3.7: Measurement set ups for the calibration of the p-u probe inside the anechoic chamber, with the highly directive source and the reference microphone.

chosen in order to minimize the effects of its presence on the sound field close to the probe.

The measurement chain was therefore composed by the sound source with the power amplifier, the reference microphone, the p-u probe with the related preamplifiers and a MOTU® Traveler sound card, operating at 192 kHz sampling rate. During the measurements, the correction of the velocity signals provided by the manufacturer was not applied.

The test signal was a sine sweep, varying from 700 Hz up to 23 kHz. The lower limit of the frequency range was chosen in accordance to the supposed Schroeder frequency of the scale model where the measurements had to be performed. The upper limit was, on the other hand, imposed by the sensibility of the velocity transducer, which greatly decreases above 20 kHz.

During the calibration, three sets of measurements were acquired, one for each of the velocity transducers: each calibration was hence performed rotating the device under test in the direction of maximum sensibility (condition of orthogonality between the source and the velocity sensor).

3.2.4 Elaboration of the calibration filters

The measured impulse responses were elaborated following a two-step procedure:

1. comparison of the built-in pressure microphone of the probe with the reference microphone over the whole frequency range; this step is required for aligning the frequency response of the probe over the flat response of the reference microphone.

2. adjustment of the velocity sensor frequency response over the calibrated pressure one, according to the known impedance of the sound field.

All the data were elaborated with dedicated Matlab® routines. A temporal windowing was first applied, to avoid the presence of spurious reflections and

retrieve only the direct part of the signal. The signals were then numerically elaborated for obtaining the three series of calibration transfer functions, expressed in FFT with a spectral resolution of 1.5 Hz over the calibration frequency range [67, 68].

Firstly, the transfer function between the two measured pressure signals, named $H_{p\hat{p}}$, was obtained, expressed as:

$$H_{p\hat{p}}(\omega) = \frac{p_{ref}(\omega)}{\hat{p}(\omega)}, \tag{3.1}$$

where $p_{ref}(\omega)$ is the pressure signal measured with the reference microphone and $\hat{p}(\omega)$ is the pressure signal acquired with the built-in microphone.

As three set of measurements were performed, three pressure signals of the built-in microphone were obtained, which in principle should coincide. However a slight difference in the high frequency range can be instead observed, due to the different orientation of the probe (vertical for the calibration of the red and blue sensors and horizontal for the calibration of the green one): in particular a decrease in the frequency response of the microphone at the high frequency is observed when the probe is in the vertical position. Therefore, as the $H_{p\hat{p}}$ transfer function has to be unique, it was chosen to employ the function obtained by elaborating the signals acquired during the calibration of the green device, when the built-in and the reference microphones were similarly oriented.

Amplitude and phase of the transfer function in FFT are shown in figure 3.8: as the built-in microphone has a flat response up to almost 5 kHz, the correction will affect only the high frequency range. Applying the $H_{p\hat{p}}$ transfer function to a measured (uncorrected) pressure signal $p(\omega)$, allows to calculate its "corrected" value $p_{corr}(\omega)$, as:

$$p_{corr}(\omega) = p(\omega) \cdot H_{p\hat{p}}(\omega). \tag{3.2}$$

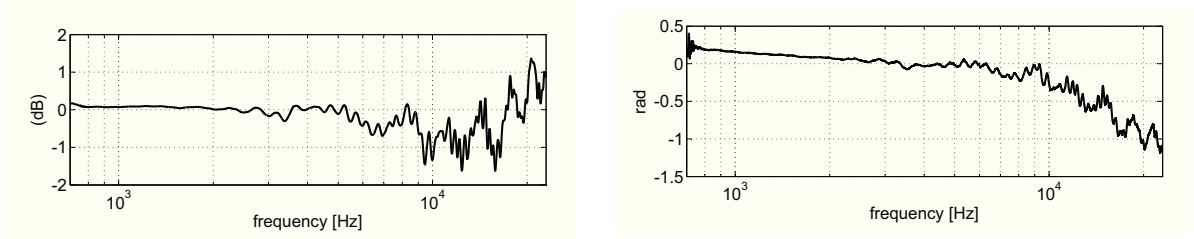

(a) Amplitude **(b)** Phase

Figure 3.8: Amplitude and phase of the transfer function $H_{p\hat{p}}$ between the pressure signals measured with the built-in and the reference microphones (spectral resolution 1.5 Hz).

Then the transfer functions for the relative calibration of the velocity devices were elaborated. The underlying idea was to obtain a "virtual" reference velocity starting from the reference pressure signal and the theoretical impedance of the sound field, to be compared with the velocity signal acquired during the calibration measurements.

The probe was exposed to a sound field of spherical waves, where the admittance of the medium can be expressed as:

$$H_{th}(\omega) = \frac{u(\omega)}{p(\omega)} = \frac{1}{\rho c}\left(1 + \frac{1}{ikr}\right). \tag{3.3}$$

In the expression ρ is the air density, k the wave number and r the distance between the source and the probe. The term within brackets, which accounts for the correction of the near field effect, affects the results only in the low frequency range.

On the other hand, the "true" specific admittance measured in the calibration position with the probe, will differ from the theoretical one, due to the mismatch in the frequency response of the two transducers. The measured impedance (that is, the inverse of the admittance) can be expressed as:

$$H_{\hat{p}\hat{u}}(\omega) = \frac{\hat{p}(\omega)}{\hat{u}(\omega)}, \tag{3.4}$$

where $\hat{p}(\omega)$ and $\hat{u}(\omega)$ are the measured uncorrected signals in the calibration conditions.

Therefore, the corrected velocity signal can be expressed through a combination of the transfer functions defined above, as:

$$u_{corr}(\omega) = u(\omega) \cdot H_{p\hat{p}}(\omega) \cdot H_{th}(\omega) \cdot H_{\hat{p}\hat{u}}(\omega) = u(\omega) \cdot H_{u\hat{u}}(\omega). \tag{3.5}$$

In figure 3.9 the amplitude and the phase of the $H_{u\hat{u}}$ filters obtained for the three velocity sensors are represented. Obviously, being above 1 kHz, the sensitivity of the velocity devices diminishes continuously with the frequency and the amplitude of the $H_{u\hat{u}}$ filters shows an increasing trend.

In order to assess the reliability of the obtained transfer functions, some relevant acoustic quantities were calculated for the calibration conditions, where the sound field, as well as its principal characteristics, are known.

First of all, the ratio between the corrected pressure and velocity signals was investigated for each of the three channels, with the aim of evaluating the presence of numerical errors and defining the range of validity of the elaborated filters.

A similar trend of variation was obtained for all the devices, shown in figure 3.10 with reference to the green transducer. The measured ratio, in spite of the presence of slight variations in the FFT representation, is in satisfactory agreement with the corresponding theoretical value ($1/H_{th}$) starting from 1.5 kHz; below this value the elaborated filters do not provide the right correction of the acquired signals and can not be applied. Hence, the value of 1.5 kHz will represent the lower limit of the investigated frequency range inside the scale models.

Then the sound intensity in the calibration position was evaluated. The distribution of the mean intensity in frequency was obtained via FFT analysis of the corrected pressure and velocity signals, combined through their cross-spectrum, as:

$$I_r + iJ_r = S_{pu}\ |H_{p\hat{p}}|^2\ H_{\hat{p}\hat{u}}\, H_{th}. \tag{3.6}$$

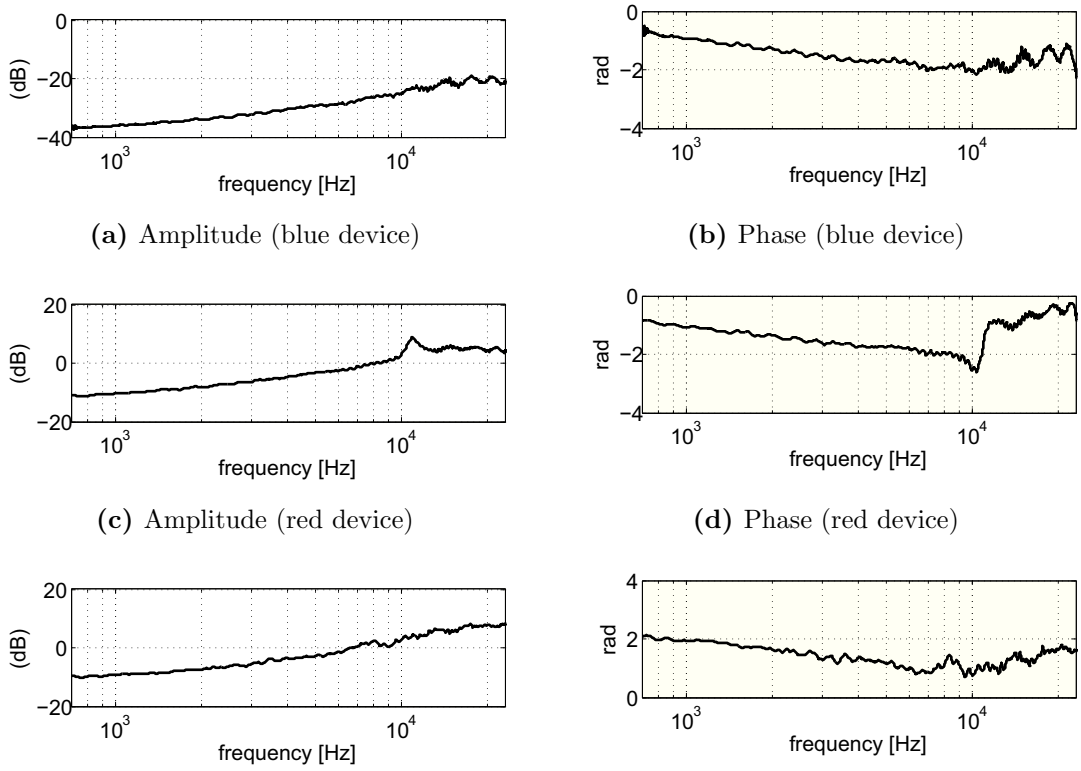

(a) Amplitude (blue device)

(b) Phase (blue device)

(c) Amplitude (red device)

(d) Phase (red device)

(e) Amplitude (green device)

(f) Phase (green device)

Figure 3.9: Amplitude and phase of the three transfer functions $H_{u\hat{u}}(\omega)$ between the measured velocity signal and a "virtual" velocity obtained from the reference pressure signal and the theoretical impedance; spectral resolution 1.5 Hz.

In equation (3.6) I_r and J_r are respectively the active and reactive components of the intensity along a direction r, whereas S_{pu} is the cross-spectrum between the measured sound pressure and particle velocity. Given the hypothesis on the sound field in the calibration conditions, the sound intensity was expected to be purely active, with similar frequency distributions for the three sets of acquired data.

The active and reactive components of the intensity, measured with the three devices, are represented in figure 3.11; the analysis of the results leads to the following remarks:

- The sound field can be considered purely active; the difference between active and reactive intensity is in fact nearly 15 dB for all the investigated frequency range. If the linear value of the two intensity components is represented, it can be seen that the reactive component varies rapidly with the frequency but has a null mean.

- The results provided by the three velocity sensors are in fair agreement, with small differences at high frequency (around 20 kHz) between the green device and the other two. The difference derives from the choice of always employing the same transfer function $H_{p\hat{p}}$ for correcting the particle velocity.

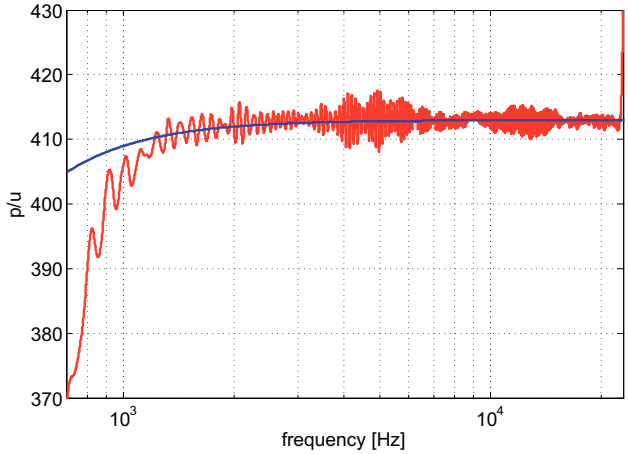

Figure 3.10: Comparison between the theoretical (blue line) and the measured (red line) ratio between pressure and velocity signals; the measured values were corrected with the elaborated transfer functions, according to equations 3.2 and 3.5. The two functions are found to be equal starting from 1.5 kHz.

- The measured active component of the intensity has a satisfactory flat response in the frequency range between 1.5 and 18 kHz, where the calibration procedure can be considered valid.

Moreover, the sign of the intensity calculated in the calibration conditions, allows the assessment of the internal reference system of the probe that will be necessary, during the measurements inside the scale model, to evaluate the positive or negative direction of the intensity vectors.

Finally, it is worth noticing that in the elaboration of the transfer functions was not introduced the sensitivity of the reference pressure microphone; therefore, even though the relative calibration between the pressure and the velocity devices is correct and provides a flat and in-phase response of the two transducers, the absolute level of the acquired signal can not be retrieved. Anyway, for the purposes of this study this aspect can be neglected as the focal point are the relationship between the acoustic quantities and their variations inside the enclosures

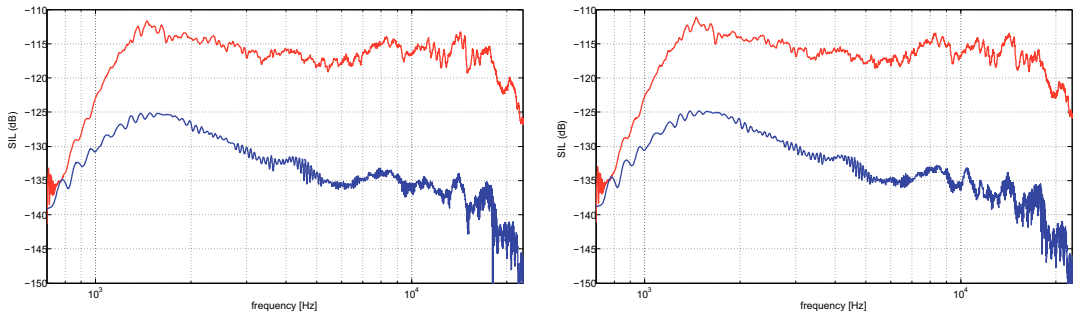

(a) Blue sensor

(b) Red sensor

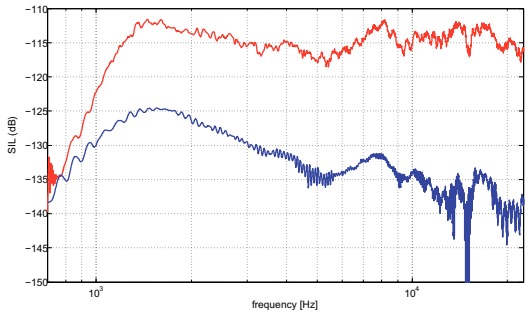

(c) Green sensor

Figure 3.11: Sound intensity level (SIL) derived from the calibration measurements (spectral resolution 1.5 Hz): active component (red line) and reactive component (blue line).

3.3 Measurements inside the scale model of a long room

The experimental investigation of the diffusion coefficient value was accomplished by means of measurements inside a scale model.

The choice of employing a scale model was led by the possibility of performing measurements inside an enclosure where the acoustic properties of the surfaces could be estimated with good accuracy and the sound field carefully described.

The main issue of taking measurements inside a scale model is the effect of the air absorption as it does not vary linearly with the frequency and affects the measurements at high frequency. The effect can be diminished by replacing the air inside the model with dry air or other gas, as nitrogen, with smaller decay parameters. However in this case, the relatively large dimensions of the model made these solutions impractical and quite expensive.

An alternative possibility is to numerically correct the measurements according to the standard ISO 9613-1 [69]; the procedure was successfully applied to the measurements for the characterization of the materials, in order to obtain the correct absorption and scattering coefficients. The procedure was accomplished with the commercial software Dirac® that automatically provide a rescale on the time axis of the measured impulse responses, retrieving their full scale equivalent.

Hence, a 1:16 scale model of a long room was set up, conceived as a modu-

	Model scale (MS)	Full scale (FS)
Length	0.500 m	8 m
Width	0.500 m	8 m
Height	0.250 m	4 m
Surface	1.000 m^2	288 m^2
Volume	0.063 m^3	256 m^3

Table 3.1: Geometrical dimensions of the scaled reverberant chamber. The dimensions are given with both model scale values (MS) and their full-size equivalents (FS).

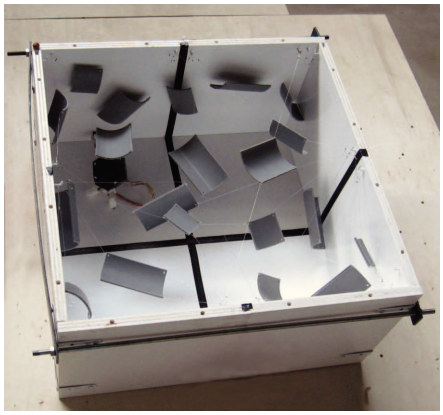

Figure 3.12: The scaled reverberant chamber.

lar structure made of fir-tree wooden panels, with the possibility of patching the interior surfaces with different kind of finishing. Two configurations were set up, corresponding to the cases of purely specular and mixed (specular and diffuse) reflections inside the room. Prior to the measurements inside the scaled long room a characterization of the different superficial finishing was made, obtaining their absorption and scattering coefficients. These values will be then employed in the numerical particle-tracing model of the scaled room.

All the results presented in this Section are expressed as a function of the full-size equivalent frequency for the scale of 1:16 (FS).

3.3.1 Characterization of the materials

The acoustic characterization of the materials was accomplished by measurements inside a 1:16 scaled reverberation chamber, with the dimensions reported in table 3.1.

The chamber was set up following the advices of the standard ISO 354 [70] on geometrical dimensions, sound absorption area and diffusers, for obtaining the desired diffuse conditions inside the room. In particular, all the interior surfaces were varnished with an acrylic paint to limit their sound absorption and curved plastic elements of suitable dimensions were randomly distributed throughout the space. An image of the final set up is shown in figure 3.12.

The same chamber could also be prepared for accomplishing scattering measure-

ments, by modifying the configuration of the floor with the addition of a circular section flush with the rest of diameter 5.6 m in full scale (FS). This section was connected to a turntable underneath providing the required rotation of the sample under test [71]. The measurement principle of the scattering coefficient measure is in fact based on the isolation of the specular (correlated) part of the reflections from the uncorrelated one: this can be obtained by synchronized averaging the impulse responses acquired for different orientation of the sample. The set up for the scattering measurements is shown in figure 3.13.

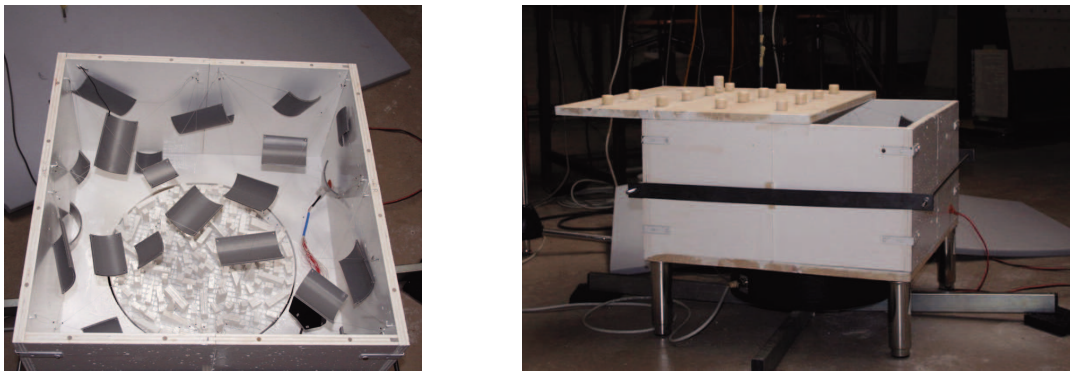

Figure 3.13: The scaled reverberant chamber set up for scattering measurements, with the rotating central section in the centre of the floor connected to the turntable underneath.

The measurement chain consisted of a miniaturized piezoelectric dodecahedron (with a diameter of 7 cm) with the related power amplifier, a 1/4 in. free-field B&K® microphone with its preamplifier and a MOTU® Traveler sound card operating at 192 kHz sampling rate.

The measurements were accomplished by inserting the microphone inside the model from holes in the ceiling (figure 3.14); the holes not involved in the current measure were plugged with silicon stoppers, treated with the same varnish employed for all the surfaces of the chamber. For the absorption measurements 4 source positions and 16 microphone positions were chosen, evenly distributed into the available space. The impulses responses obtained with the sine sweep technique were processed with the Dirac® software for calculating their full scale equivalents and correcting the effect of the air absorption. For each position was then calculated the reverberation time RT30.

Before starting the characterization of the materials, the grade of diffusion of the reverberation chamber was tested, varying the position and the number of reflectors. The test was performed applying the Davy's criterion, which assesses the grade of diffusion of the sound field from the spatial variance of the measured reverberation time [72, 73]. In particular, the theoretical value of the relative standard deviation is calculated as:

$$\frac{\sigma(T)}{T} = \frac{0.96}{\sqrt{BT}}, \tag{3.7}$$

where T is the spatial average of the reverberation time, $\sigma(T)$ its standard deviation and B the statistical bandwidth. When the measured relative standard deviation is lower than the theoretical one, the sound field can be considered as

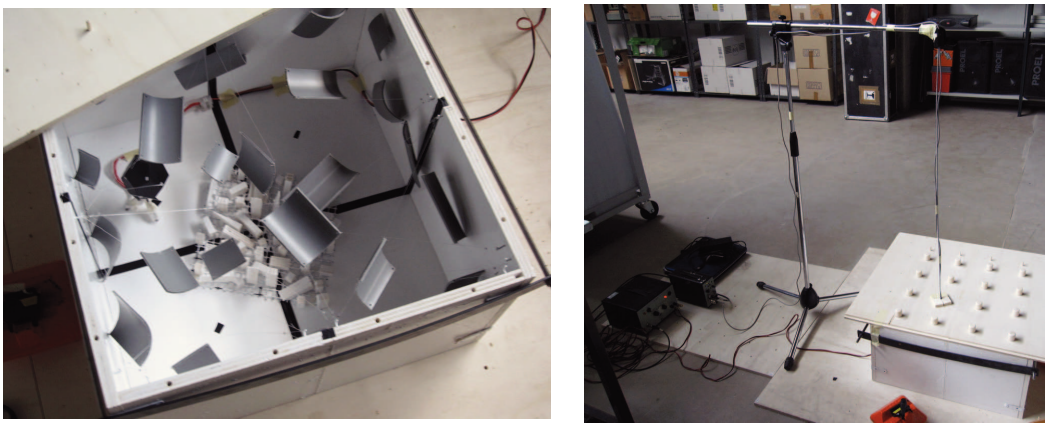

Figure 3.14: Measurement set up with the tested material inside the scaled reverberant chamber for the absorption measurements.

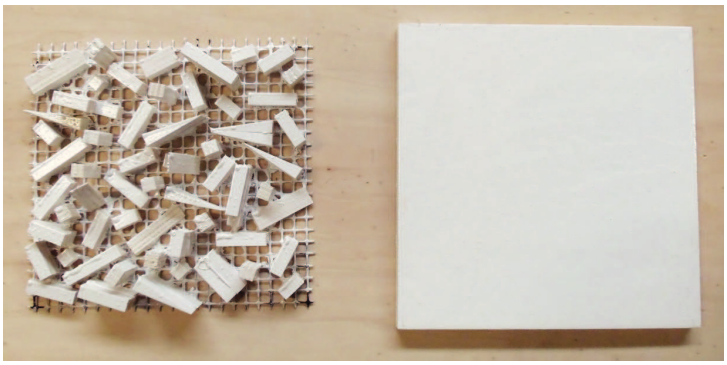

Figure 3.15: Materials tested inside the reverberation chamber: a patch of varnished scattering elements (on the left) and a flat varnished tile (on the right).

diffuse. Otherwise non-diffuse conditions prevail. The comparison, for the chosen configuration of the reverberation chamber, is reported in table 3.2. It can be seen that the sound field can be considered as diffuse for the one-third octave bands between 125 Hz and 1 kHz (FS), which therefore represent the range of validity of the obtained absorption and scattering coefficient.

Then, the materials employed in the scale model were tested inside the reverberation chamber: the varnished finishing and the scattering elements (figure 3.15). The scattering patch was obtained by gluing small wooden pieces in random order over a plastic grid; the elements, all with different geometries and dimensions (ranging from 0.16 m to 1.28 m FS) had been previously varnished for limiting their sound absorption. The absorption coefficient of the varnish finishing was obtained performing a first measurement with a Perspex tile (which provided an highest reference reverberation time) and a second measure with a varnished tile.

In figure 3.16 the measured values of the absorption and scattering coefficients in one-third octave bands are presented. It is worth noticing that the scattering elements, in spite of the varnish finishing, still present a residual absorption due to the material porosity which will affect the measurements inside the model; the absorption of the flat surface is instead quite negligible. The scattering coefficient

Frequency band (MS) Hz	**Frequency band (FS)** Hz	**Theoretical std. deviation** %	**Measured std. deviation** %
1000	63	12.19	20.63
1350	80	11.68	12.79
1600	100	10.83	13.10
2000	125	10.43	9.43
2500	160	10.09	7.50
3150	200	8.86	8.83
4000	250	7.58	6.79
5000	315	6.68	5.82
6300	400	6.02	4.87
8000	500	5.70	4.61
10000	630	5.51	4.41
12500	800	4.92	4.80
16000	1000	4.45	4.17

Table 3.2: Application of the Davy's criterion to the RT30 measurements inside the reverberation chamber: the sound field can be considered as diffuse when the measured standard deviation is lower than the theoretical one. The results are expressed as a function of the frequency in both model scale (MS) and full scale (FS).

of the flat, varnished surface is almost null: the sound will therefore be reflected in a specular manner from this elements. On the other hand, the scattering patches, due to the random surface roughness, are characterized by a coefficient s increasing with the frequency.

In table 3.3 the standard deviations of the measured coefficients are reported for each of the rescaled frequency bands, showing great uncertainties especially in the evaluation of the scattering coefficients at low frequency.

Frequency	**Scattering el.**		**Flat surfaces**	
	$\boldsymbol{\alpha}$	**s**	$\boldsymbol{\alpha}$	**s**
125	0.005	0.152	0.150	0.110
160	0.006	0.172	0.100	0.107
200	0.006	0.118	0.080	0.071
250	0.004	0.142	0.070	0.070
315	0.004	0.106	0.030	0.054
400	0.004	0.138	0.030	0.076
500	0.003	0.175	0.040	0.086
630	0.004	0.196	0.030	0.046
800	0.007	0.166	0.020	0.051
1000	0.002	0.152	0.020	0.073

Table 3.3: Standard deviations of the measured absorption and scattering coefficients of the scattering elements and the flat surfaces employed inside the model. Results expressed as a function of the full-size equivalent frequency (FS).

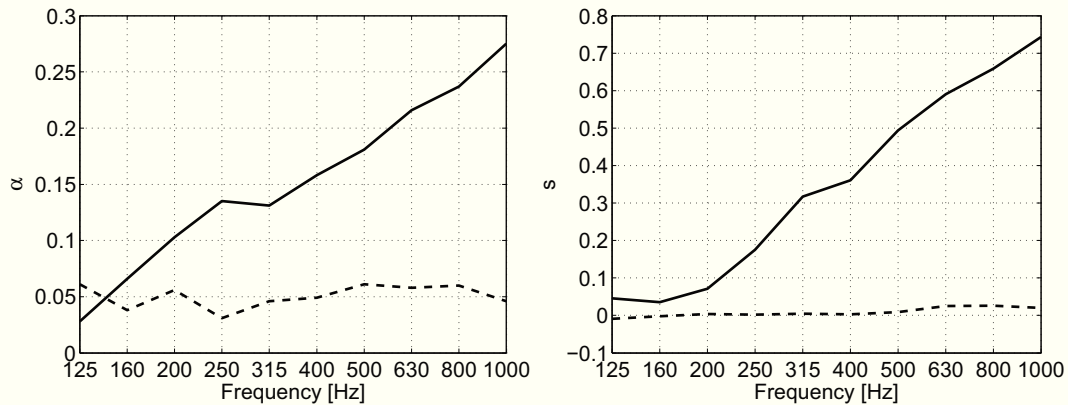

(a) Absorption coefficients **(b)** Scattering coefficients

Figure 3.16: Measured absorption coefficient α and scattering coefficient s for the varnish finishing $(--)$ and the scattering elements (solid line) in one-third octave bands; the results are expressed as a function of the full-size equivalent frequency (FS).

	Model scale (MS)	**Full scale (FS)**
Length	2.500 m	40 m
Width	0.500 m	8 m
Height	0.250 m	4 m
Surface	4.000 m^2	1024 m^2
Volume	0.3125 m^3	1280 m^3

Table 3.4: Geometrical dimensions of the scaled long room. The dimensions are given with both madel scale values (MS) and their full-size equivalents (FS).

3.3.2 Scale model set-up

Then, the scale model of a long room was set up, with the dimensions reported in table 3.4.

The model was composed by modular square elements of 4 m (FS) side, tightly connected together to build the floor and the walls of the room; the minimal fissures between the elements were sealed with tape for avoiding any leakage of sound. The ceiling was instead formed by one whole piece, provided with holes at regular positions for introducing the microphone and performing the measurements inside the model. During the measurements all the holes (a part from that corresponding to the current receiver position) were plugged with stoppers, varnished on the interior side for preventing sound absorption. The size of the holes was specifically designed to allow the passage (and a minimal movement) of a 1/2 in. transducer.

For the purposes of this study, two different configurations were set up, by differently patching the interior surfaces:

1. a long room with flat boundaries (figure 3.17);

2. a long room with surfaces equipped with a great number of scattering frames (almost 80% of the total surface was covered); this set up is shown in figure 3.18. Each modular square element was patched with a scattering frame

Figure 3.17: Measurement set up of the scaled long room with flat boundaires.

of the same dimension, suspended with small hooks from the lateral walls, appended to the ceiling or simply laid on the floor.

The measurements were performed with a portable personal computer with a CLIO® sound card operating at 192 kHz sampling rate, connected to a miniaturized piezoelectric dodecahedron with the related amplifier and to a Microflown® USP probe with the signal conditioner[1]. In both configurations the sound source was placed close to an end wall of the model and the measurements were accomplished in 23 receiver positions at two different heights: z=1.60 and z=2.72 in FS (corresponding to z=0.1 m and z=0.17 m in MS). An upper view of the source and receivers positions is shown in figure 3.19. At each receiver position 4 impulse responses were collected at the same time with the sine sweep technique, one for each of the independent channels of the *p-u* probe.

As the aim of the measurements was to investigate experimentally the diffusion gradient equation, it was necessary to collect data which could be useful for the estimate of the energy density gradient. Hence, around each receiver positions other six measures were collected, two for each of the principal directions (one at each side of the "main" central position). Each additional point was 8 cm far from the central one (FS).

For performing this kind of measurements, that require great precision in the probe displacement, the acquisition system was automatized through the use of a three dimensional scanner (figure 3.20). The scanner, which has a movement precision of 1 mm, allowed independent movements along the three directions and was controlled with a dedicated LabView® application.

The two systems (probe displacement and signal acquisition) were conveniently synchronized for performing all the measurements in an automatic way.

[1]As the equalization of the recored signal was performed in post-processing by using the elaborated digital filters, during the acquisition the correction of the signal was disabled.

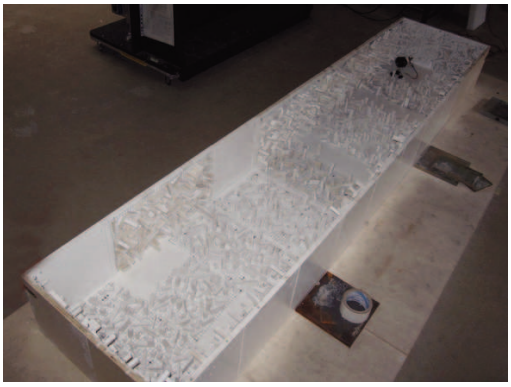

(a) Long room

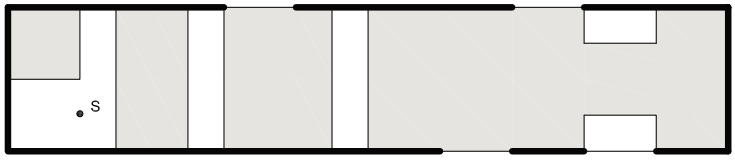

(b) Upper view (floor)

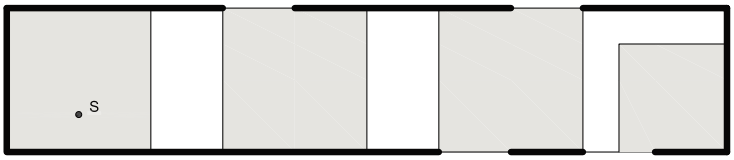

(c) Upper view (ceiling)

Figure 3.18: (a) Measurement set up of the scaled long room with scattering boundaires. (b) and (c) Sketch of the surfaces of the room covered with the scattering patches, identified by the gray areas for floor (b) and ceiling (c), and thick lines for the walls.

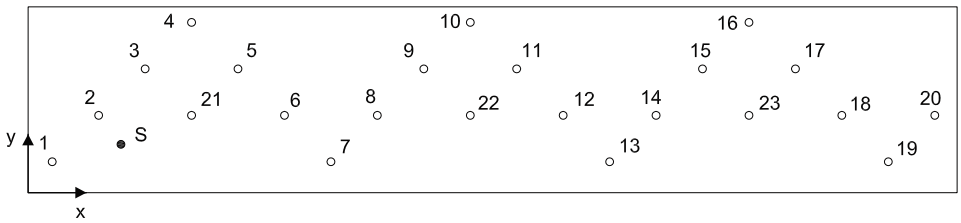

Figure 3.19: Source (S) and receivers (1-23) positions inside the scaled long room (upper view).

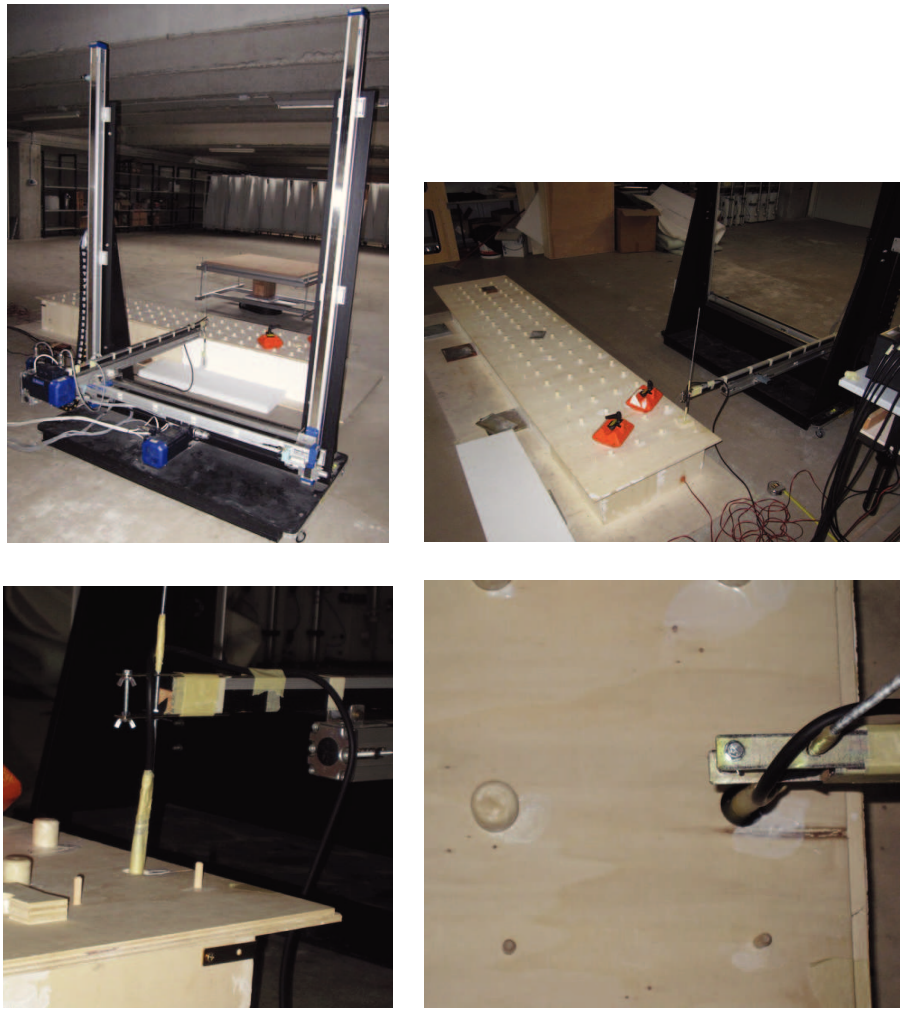

Figure 3.20: Automatic acquisition of the measurements inside the scale model with a three dimensional scanner.

3.3.3 Characterization of the sound field inside the scale model

The impulse responses measured inside the scale model were elaborated with Matlab® routines for obtaining the principal acoustic quantities at each receiver position. All the elaborations were carried out in the frequency range from 1.5 to 18 kHz (MS), where the calibration filters provide a reliable signal correction.

The results will be therefore presented, with reference to the full-size equivalent frequency, in one-third octave bands from 125 to 1000 Hz. In this Section only the results concerning the bands of 500 and 800 Hz will be presented; the results obtained for all the considered bands are reported in *Appendix A*.

Two principal quantities were obtained from the elaborations: energy density and intensity. The calculation procedure for obtaining the sound intensity has already been detailed in § 3.2.4; the energy density, on the other hand, was evaluated as the sum of its potential and kinetic components [51], calculated as the auto-spectra of pressure and velocity:

$$e_{pot} = \frac{S_{pp}}{2\rho_0 c^2}, \tag{3.8a}$$

and:

$$e_{kin,r} = \frac{\rho_0}{2} S_{u_r u_r}, \tag{3.8b}$$

where $e_{kin,r}$ and u_r (velocity signal) are referred to the direction r.

3.3.3.1 Long room with flat surfaces

First, the Schroeder frequency was calculated for the scaled long room with flat surfaces, employing the spatially averaged value of the measured RT30, equal to 4.30 ± 1.03 s (the value refers to all the considered bands). The Schroeder frequency is equal to 116 Hz, meaning that the first analysed band, 125 Hz, is (partially) characterized by a modal behaviour: it will not be considered in the analysis of the sound field which is limited to the frequencies of high modal overlap.

The first analysed parameter is the energy density level L_e: its spatial decay inside the room, together with that of its potential and kinetic components, is represented in figure 3.21. As inside long rooms the sound field is supposed to vary mainly with the length of the room, only the receiver positions along a line at z=1.6 m from the source to the end wall of the room were considered for the analysis (positions n° 2 - 21 - 6 - 8 - 22 - 12 - 14 - 23 - 18 - 20, with reference to figure 3.19).

From figure 3.21 it can be seen that inside the room the energy density attenuation is almost null: in fact, except for the near field positions, the variation of the parameter along the length is quite limited. The same trend can be observed for both its components, that, moreover are always coincident. This almost null spatial variation is related to the presence of the highly reflective end wall, whose presence greatly affects the last part of the temporal decay, reducing the variation of the acoustic quantities; evidences of this effect can also be found in ref. [53].

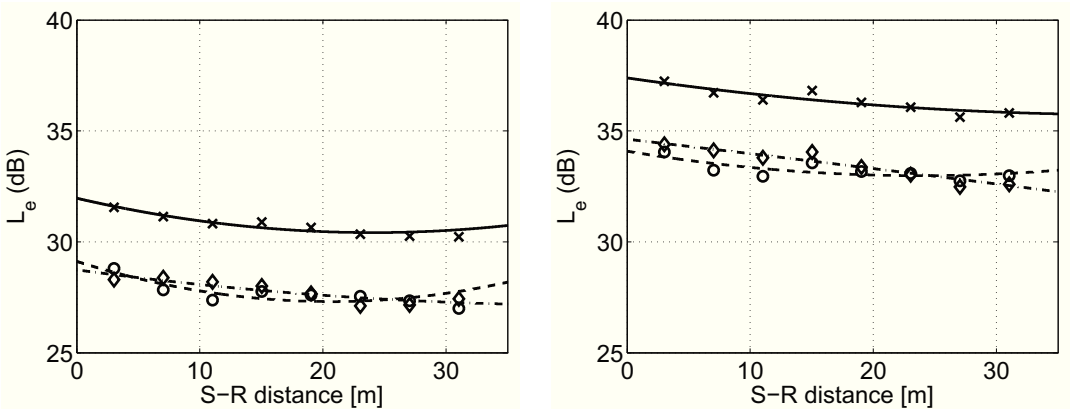

(a) 500 Hz **(b)** 800 Hz

Figure 3.21: Energy density level (L_e) decay inside the scaled long room with flat surfaces, along the line from the source to the end wall at z=1.6 m. Measured values and regression lines for the one-third octave bands of 500 and 800 Hz: total energy density ($\times$ and solid line), potential energy density ($\diamond$ and $-\cdot-$), kinetic energy density ($\circ$ and $--$).

Then, the variation of the reverberation time along the length was analysed in terms of both RT30 and EDT (figure 3.22). As for the energy density level, the observed variation are quite limited, especially for the highest frequencies, where the ratio between RT30 and EDT becomes almost equal to one, meaning that the temporal decay inside of the sound inside the room is rather linear.

All these evidences lead to the conclusion that, inside the long room with flat boundaries, the sound field is close to diffuse, characterized by a uniform energy density throughout the room[2]. In order to asses the diffusiveness of the field, a further check was carried on, applying the Davy's criterion on the measured RT30; for this analysis all the measurement positions were considered. The comparison between theoretical and measured variances of the data is reported in table 3.5, confirming that for all the investigated frequency bands the sound field can be considered as diffuse.

Then, the distribution of the active part of the sound intensity inside the room was considered. In figure 3.23 the spatial decay of the intensity level is represented as a function of the distance from the source, showing a decrease along the length of the room. This result is in accordance with the analysis of the intensity inside reverberant field presented in ref. [56]. In fact, as the room was excited by a random noise (with no correlation in phase), the intensity related to the direct part of the field becomes predominant and leads to a decrease of the total intensity level [29]. Anyway, the measured decrease is always milder than the 6 dB decrease for doubling of distance expected for the direct intensity level: this behaviour can in fact be observed only inside an ideally diffuse sound field [74].

These results can be better understood by analysing also the variations of the sound intensity components. The component along the x-axis (i.e., the component

[2]In a diffuse sound field the kinetic energy density has the same level as the potential energy density (see for example ref. [47]): therefore the agreement between the theoretical behaviour and the measurements can be considered as a confirmation of the validity of the amplitude calibration.

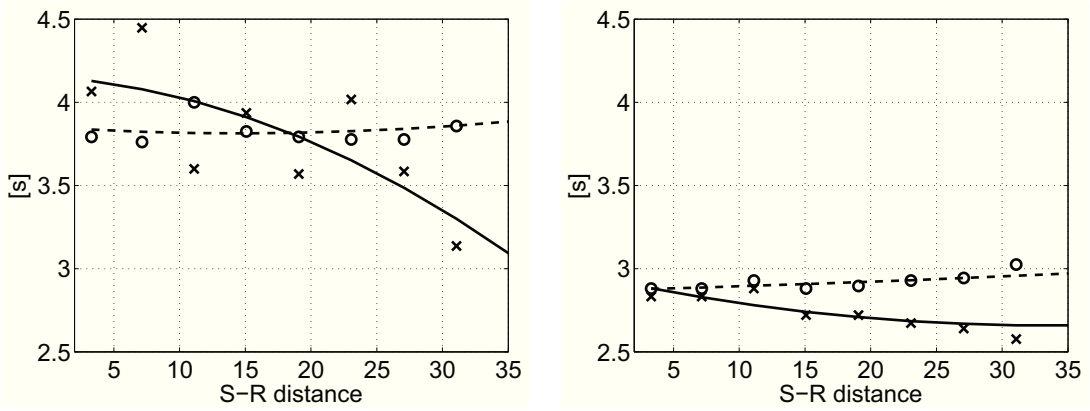

(a) 500 Hz **(b)** 1000 Hz

Figure 3.22: Reverberation time inside the scaled long room with flat surfaces as a function of the source-receiver distance. Measured values and regression lines for the one-third octave bands of 500 and 800 Hz: EDT ($\times$ and solid line), RT30 ($\circ$ and $--$).

Frequency band (FS) Hz	**Theoretical std. deviation** %	**Measured std. deviation** %
160	7.96	7.31
200	6.17	4.59
250	5.30	4.13
315	4.88	4.43
400	4.63	2.66
500	4.51	3.41
630	4.36	2.56
800	4.12	2.63
1000	3.85	2.71

Table 3.5: Application of the Davy's criterion to the RT30 measurements inside the scaled long room with flat surfaces; all the receiver positions were considered in the analysis. According to the criterion, the sound field can be considered as diffuse when the measured standard deviation is lower than the theoretical one.

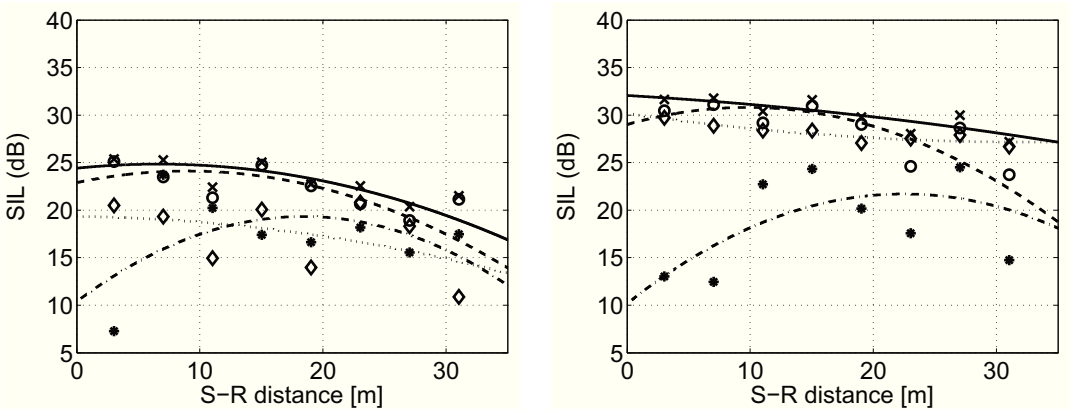

(a) 500 Hz **(b)** 800 Hz

Figure 3.23: Sound intensity level (SIL) decay inside the scaled long room with flat surfaces along the line from the source to the end wall at z=1.6 m. Measured values and regression lines for the one-third octave bands of 500 and 800 Hz: total intensity ($\times$ and solid line), intensity along the x-axis ($\circ$ and $--$), intensity along the y-axis ($*$ and $-\cdot-$), intensity along the z-axis ($\diamond$ and $\cdots$).

in the direction of the longest dimension of the room) is always slightly predominant over the other two; the y and z components, on the other hand show a less recognizable trend and depending on the considered frequency give a different contribute to the global level.

The representation of the normalized intensity vectors distribution over the horizontal plane is shown in figure 3.24. It can be seen that while the energy flow presents a prevailing orientation along the x-axis it is not completely monodimensional, as local, random deviations from the principal direction are always present. These deviations are even more pronounced in the region further from the source (where the sound field is influenced by the reflections on the end wall) and close to the walls of the room. Hence, it can be concluded that inside the long room with flat surfaces the energy flow is mainly oriented along the x-axis but local, random variations, maybe enhanced also by small irregularities in the scale model set up, are also present accounting for the significant values of the two I_y and I_z components.

Evidences of the diffusiveness of the sound field can also be obtained from the comparison between the active and the reactive part of the intensity. In figure 3.25 these quantities are represented over the investigated frequency bands, with reference to the receiver position n° 12, located 18 m (FS) far from the source (figure 3.19). The magnitude of active and reactive intensity is almost the same for all the frequencies (with differences between the two quantities smaller than 3 dB) and generally lower than the normalized energy density $c\,w(\omega)$, fulfilling the condition established in ref. [56] for a diffuse sound field:

$$|\boldsymbol{J}(\omega_0, \Delta\omega)| \approx |\boldsymbol{I}(\omega_0, \Delta\omega)| << c\,w(\omega_0, \Delta\omega), \tag{3.9}$$

where the notation $(\omega_0, \Delta\omega)$ indicates that the quantities are associated with a frequency band. It is worth noting that this relation is valid for a reverberant

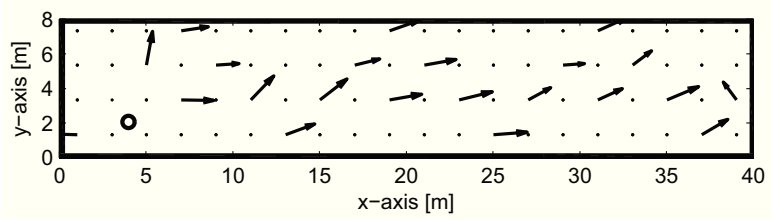

(a) 500 Hz

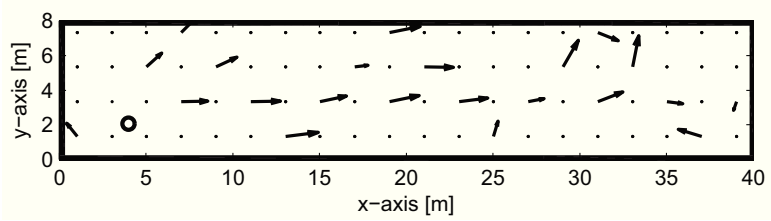

(b) 800 Hz

Figure 3.24: Normalized intensity vectors measured inside the scaled long room with flat surfaces (upper view); results over the horizontal plane at z=1.6 m.

"diffuse" sound field created by a single source and not for a "true" diffuse sound field, homogeneous and isotropic, created by a number of distant, uncorrelated sources, where the reactive intensity is negligible.

Let's recall here the definition of active and reactive components of the sound intensity [42, 54, 56]. In a time-stationary sound field, the instantaneous intensity can be divide in two parts:

- an *active* component, with a non null value and corresponding to the local net flow of sound energy;
- a *reactive* component, with a time-average value equal to zero, corresponding to local oscillatory transport of energy; it describes the non-propagating part of the energy, flowing back and forth around a position.

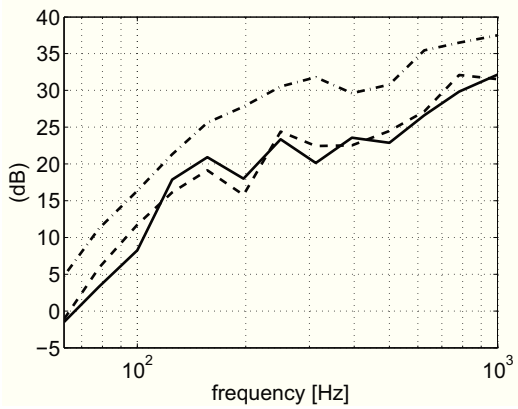

Figure 3.25: Measurements inside the scaled long room with flat boundaries at the position n°12 (as defined in figure 3.19) in 1/3 octave bands: normalized energy density level (-·-), active intensity level (–) and reactive intensity level (- -).

The two quantities are associated with the components of particle velocity which are respectively in phase and in quadrature with the acoustic pressure. According to ref. [56]:

$$I_r = \frac{1}{2}\,\mathrm{Re}\left[pu_r^*\right], \tag{3.10}$$

$$J_r = \frac{1}{2}\,\mathrm{Im}\left[pu_r^*\right], \tag{3.11}$$

where the symbol * denotes the complex conjugate of a complex quantity.

The active and reactive intensities could be related to similar components of propagating and non-propagating energy density. For example, Morse and Ingard [75] define the amount of "radiant sound energy density" near point sources. This energy radiating with the speed of sound and moving outward from the source, is expressed as:

$$e_p(\boldsymbol{r},t) = \frac{|\boldsymbol{I}(\boldsymbol{r},t)|}{c}. \tag{3.12}$$

The remaining part of the total sound energy in the near field is called "reactive energy" and it is obtained as:

$$e_{np}(\boldsymbol{r},t) = w(\boldsymbol{r},t) - \frac{|\boldsymbol{I}(\boldsymbol{r},t)|}{c}. \tag{3.13}$$

As pointed out in ref. [56], equation (3.12) might be used as a definition of the active sound energy density, relating this quantity to the active intensity. On the contrary, a similar simple relationship between reactive energy density and reactive sound intensity can not be established. Mann *et al.* [76] divide instead the particle velocity in a pure tone sound field into a part which is in phase with the sound pressure and a part which is quadrature. An brief review of the different definitions of active and reactive energy density can be found in ref. [56].

In this study the approach proposed in ref. [75] was adopted and an analysis of the sound field inside the scaled long room in terms of relative distribution between propagating and non-propagating energy was performed. The analysis was carried out separately for the three directions, expressing the total energy density along a direction as the sum of the corresponding kinetic and potential components. In figure 3.26 the difference between the calculated energy levels is represented, showing that for all the investigated directions the non-propagating part of the energy is always bigger than the propagating one. That means that only a small part of the total available energy flows inside the room, while the rest is "trapped" and flows back and forth around a position. This observation is especially true for the y and z axes along which the non propagating energy prevails, leading to the local effects observed in the intensity distribution.

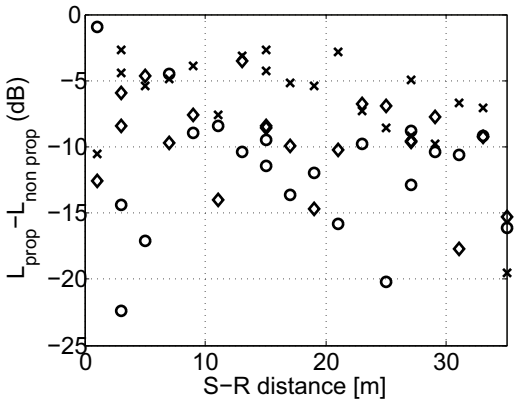

Figure 3.26: Difference between the levels of propagating and non-propagating energy density as a function of the distance from the source inside the long room with flat surfaces; results for the quantities measured along the x-axis (×), y-axis (○), z-axis (◇) for the frequency of 500 Hz.

3.3.3.2 Long room with scattering surfaces

Then, the characteristics of the sound field inside the long room with scattering boundaries were investigated.

The Schroeder frequency was calculated starting from the RT30 averaged value and found to be equal to almost 67 Hz; in this case the RT30 averaged over all the measurement positions is equal to 1.44 ± 0.47 s. Anyway, in accordance with the analysis of the sound field inside the room with flat surfaces, only the frequency bands from 250 to 1000 Hz will be considered.

In this configuration the temporal decay of the signal at each receiver position is affected by both the scattering and absorption properties of the room surfaces, that lead to a non-diffuse sound field. In fact, as represented in figure 3.27, in this case the energy density decreases continuously along the length of the room, especially for the highest frequency bands (see also *Appendix A.2*). Again the kinetic and potential components of the energy density are found to be coincident. The reverberation time, on the other hand shows an increasing trend with the length (figure 3.28) for both RT30 and EDT; moreover, for some of the investigated frequencies the EDT shows a concave behaviour, reaching a maximum value and then slowly decreasing close to the end of the room.

In order to understand if really the spatial decay of the energy was originated by a non-diffuse sound field and not by the presence of the surfaces absorption, the Davy's criterion was applied again to the measured RT30 values. The results are reported in table 3.6 for all the considered frequency bands, showing that at the lowest frequencies (up to 400 Hz), where the effect of the scattering from the boundaries is still limited, the sound field can be again considered close to diffuse. At higher frequencies a non-diffuse behaviour prevails.

The spatial decay of the intensity is represented in figure 3.29 showing that both total sound intensity and its components greatly decrease along the length. In this configuration the prevalence of the x component is less evident than in the configuration with flat boundaries, and limited to the regions closest to the sound

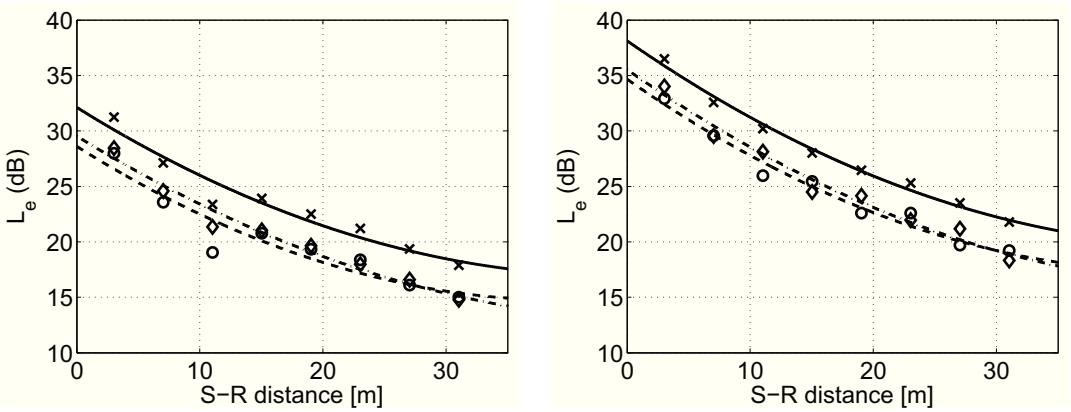

(a) 500 Hz **(b)** 800 Hz

Figure 3.27: Energy density level (L_e) decay inside the scaled long room with scattering surfaces, along the line from the source to the end wall at z=1.6 m. Measured values and regression lines for the one-third octave bands of 500 and 800 Hz: total energy density ($\times$ and solid line), potential energy density ($\diamond$ and $- - -$), kinetic energy density ($\circ$ and $- \cdot -$).

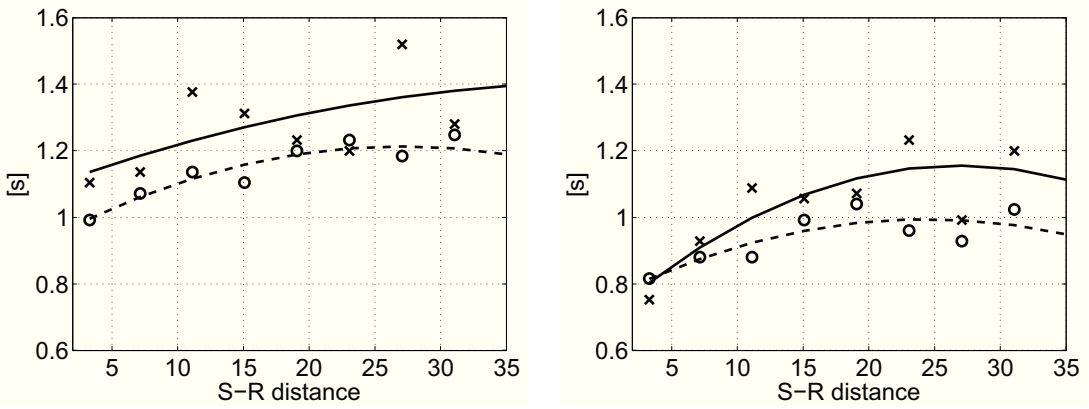

(a) 500 Hz **(b)** 800 Hz

Figure 3.28: Reverberation time inside the scaled long room with scattering surfaces as a function of the distance from the source. Measured values and regression lines for the one-third octave bands of 500 and 800 Hz: EDT ($\times$ and solid line), RT30 ($\circ$ and $--$).

source; in the other parts of the long room also the contribution of the intensity along the y axis becomes important. The intensity level along the z axis is always significantly smaller of the other two components, except for the positions closer to the end wall.

The spatial distribution of the intensity over the horizontal plane is depicted in figure 3.31, confirming the previous remarks: close to the sound source the energy flow is mainly oriented along the longest dimension of the room. Then, the flow becomes less oriented and the intensity vectors starts to be "attracted" from the lateral wall in y=0. On the whole the energy flow inside the room with scattering boundaries is therefore less oriented than that inside the same room with flat boundaries.

Frequency band (FS) Hz	**Theoretical std. deviation** %	**Measured std. deviation** %
160 Hz	12.27 %	9.77 %
200 Hz	11.29 %	6.47 %
250 Hz	10.07 %	6.25 %
315 Hz	9.57 %	8.90 %
400 Hz	8.75 %	8.82 %
500 Hz	8.31 %	8.97 %
630 Hz	7.88 %	8.16 %
800 Hz	7.29 %	7.67 %
1000 Hz	6.68 %	8.38 %

Table 3.6: Application of the Davy's criterion to the RT30 measurements inside the scaled long room with scattering surfaces; all the receiver positions were considered in the analysis. According to the criterion, the sound field can be considered as diffuse when the measured standard deviation is lower than the theoretical one.

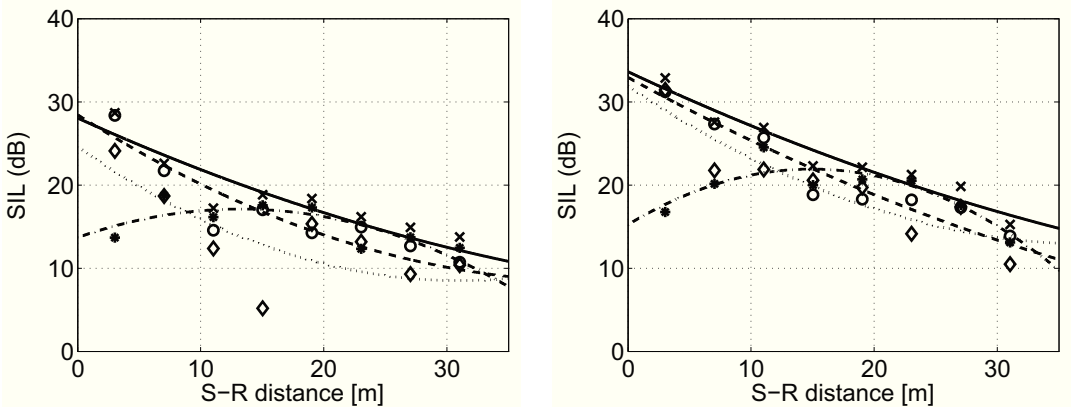

(a) 500 Hz **(b)** 800 Hz

Figure 3.29: Sound intensity level (SIL) decay inside the scaled long room with scattering surfaces along the line from the source to the end wall at z=1.6 m. Measured values and regression lines for the one-third octave bands of 500 and 800 Hz: total intensity ($\times$ and solid line), intensity along the x-axis ($\circ$ and $--$), intensity along the y-axis ($*$ and $-\cdot-$), intensity along the z-axis ($\diamond$ and $\cdots$).

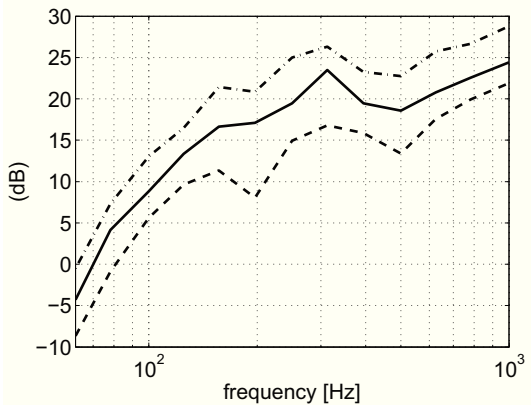

Figure 3.30: Measurements inside the scaled long room with scattering boundaries at the position n°12 (as defined in figure 3.19) in 1/3 octave bands: normalized energy density level (--), active intensity level (–) and reactive intensity level (- -).

The analysis of the active and reactive components of the sound intensity (as represented in figure 3.30) show that the sound field is mainly active, as $|\boldsymbol{I}(\omega_0, \Delta\omega)| > |\boldsymbol{J}(\omega_0, \Delta\omega)|$, with differences bigger than 4 dB, over all the considered frequency bands.

Again, also for this configuration the analysis of the relative contributions of the propagating and non propagating part of the energy density was carried out. The results are shown in figure 3.32 for the frequency of 500 Hz: it can be seen that also inside this room the non propagating component is predominant, leading to local re-circulations of sound energy density and affecting the punctual direction of the intensity vector. Anyway, this predominance appears to be less pronounced than inside the room with flat surfaces, especially for the x and y components.

3.3.3.3 A comparison with two numerical models

The acoustic quantities measured inside the scaled models were then compared with the results provided by two numerical models, with reference to the spatial decay of the energy density.

The first model chosen for the comparison was the revised theory, whose basic features have been already outlined in § 2.3.2. For the comparison, the sound pressure level inside the room was calculated as:

$$SPL(\boldsymbol{r}) = L_W + 10 \log \left(\frac{W}{4\pi r^2} + 25 \frac{T}{V} \exp \left(-0.04 \frac{r}{T} \right) \right). \tag{3.14}$$

where T is the reverberation time inside the enclosure, derived from the spatially averaged RT30 values measured inside the scale models.

The second comparison was performed with a numerical model, based on a hybrid calculation method [77]: depending on the order of reflection the software models in fact the reflections with a mixture of image source method and ray-tracing or with a pure ray-tracing method. The acoustics properties assigned to the room surfaces were chosen in accordance with the results of the measurements

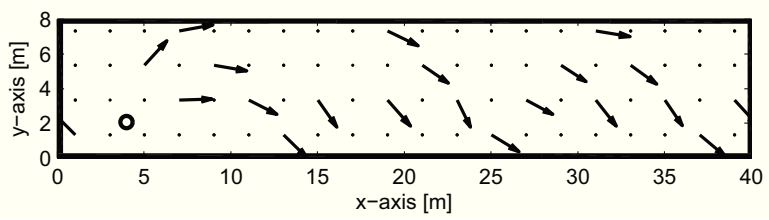

(a) 500 Hz

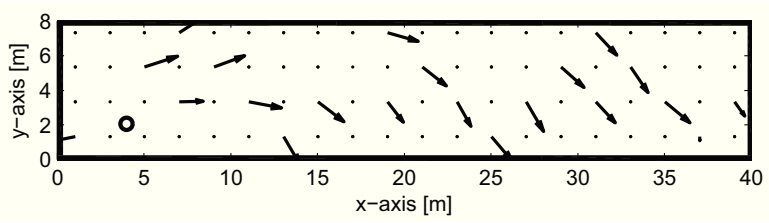

(b) 800 Hz

Figure 3.31: Normalized intensity vectors measured inside the scaled long room with scattering surfaces (upper view); results over the horizontal plane at z=1.6 m.

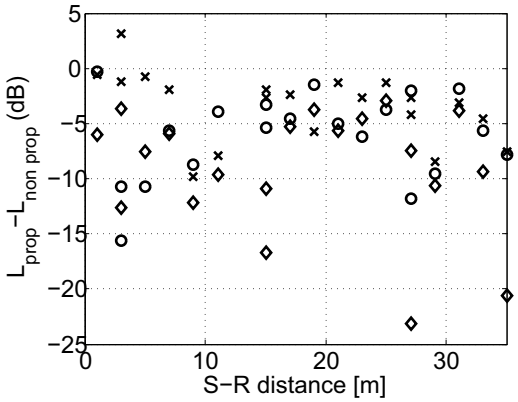

Figure 3.32: Difference between the levels of propagating and non-propagating energy density as a function of the distance from the source inside the long room with scattering boundaries; results for the quantities measured along the x-axis (×), y-axis (○), z-axis (◇) for the frequency of 500 Hz.

inside the scaled reverberation chamber and presented in § 3.3.1. For the simulations were employed 1000 rays and a transition order equal to 2, meaning that the first and the second orders of reflection were modelled using the image source method.

The comparison between the three sets of data, referred to the octave band of 500 Hz, is reported in figure 3.33. Inside the long room with flat boundaries, a good agreement between the three sets of data is found, with differences between each other smaller than 0.5 dB.

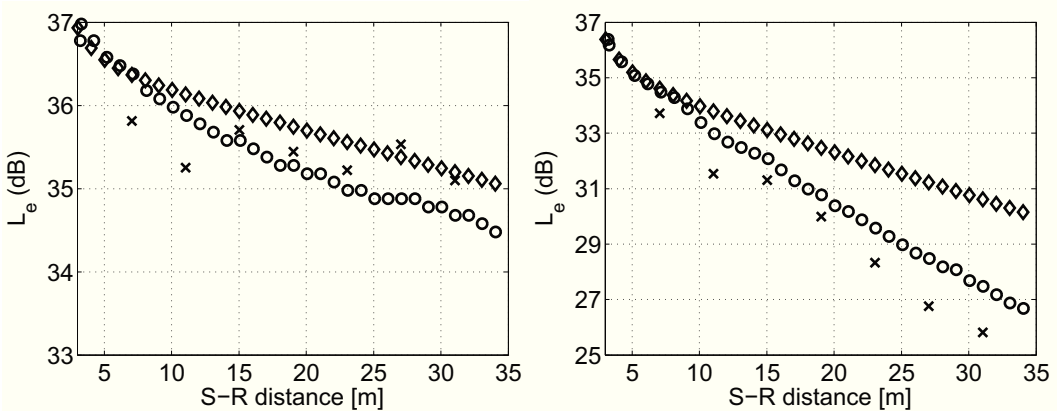

(a) Flat surfaces **(b)** Scattering surfaces

Figure 3.33: Comparison of the energy density level L_e spatial decay along a line from the source to the end wall. Results obtained, for the frequency band of 500 Hz, with measures inside the scale model ($\times$), revised theory equations ($\diamond$), ray-tracing software ($\circ$).

On the other hand, inside the room with scattering boundaries the measured values are in agreement only with the ray-tracing model: the difference is almost constant over the length and equal to 1 dB. The results predicted with the revised theory differ from the measured ones starting from 15 m from the source, where the observed difference is bigger than 1 dB; close to the end wall, the discrepancy reaches 4 dB.

The comparison of the experimental data with the numerical ones confirms the conclusions drawn in the previous Sections. In fact, inside the room with flat boundaries the agreement between measures and revised theory, which correctly predicts the sound decay inside semi-reverberant fields, supports the idea of a diffuse sound field inside this kind of experimental configuration. In the same way, the difference between measures and revised theory inside the long room with scattering boundaries confirms the non-diffuseness of the sound field. The agreement observed between measured data and ray-tracing results is an evidence of the accuracy of the experimental data.

3.4 Conclusions

The target of this first experimental part of the research was to obtain reliable data, to completely describe the sound field inside long rooms with different types

of superficial finishing.

To do so, two main aspects were considered and investigated.

First, the calibration of the intensity probe employed in the measurements was performed: a set of digital filters was derived from measurements inside a sound field of spherical waves, for the calibration of the acquired pressure and velocity signals from 1.5 up to 18 kHz. The use of digital filters allowed to acquire data with high signal-to-noise ratios.

Then, the characterization with energetic and intensimetric quantities of the measured sound fields was carefully accomplished, providing the starting point for the diffusion coefficient estimate inside the two rooms.

For the long room with flat boundaries the analysis of the sound field leaded to the following remarks:

- Inside the room the sound field is close to diffuse: the energy density is uniform throughout the space with equal potential and kinetic components; the reverberation time is constant for all the receiver positions. The analysis of the spatial variance of the measured RT30 with the Davy's criterion confirmed that the sound field can be considered diffuse for all the investigated frequency bands.

- The sound intensity inside the room decreases faintly with the distance from the source; the magnitude of the active and reactive components is comparable for the investigated positions: the sound field inside the room is therefore "no more active than reactive" [54, 56].

- The distribution over the plane of the intensity vectors shows the presence of an overall energy flow along the length of the room but also the effect of local random deviations over the horizontal plane, due to the presence of a great quantity of non-propagated energy inside the room.

On the other hand, inside the long room with scattering boundaries the analysis of the sound field leaded to the following remarks:

- According to the analysis of the sound field with the Davy's criterion, at low frequencies (up to 400 Hz) the sound field is close to diffuse while, at higher frequencies prevails a non-diffuse behaviour. At these frequencies, the energy density decays along the length of the room and the reverberation time increases continuously.

- The sound intensity continuously decreases along the length of the room with a slope greater than that observed inside the room with flat boundaries; in this case the sound field is mainly active.

- The representation of the intensity vectors shows that in this case the energy flow is mainly bi-dimensional over the horizontal plane, with a great contribution of the y-component of the intensity leading to a systematic orientation of the vectors toward a lateral surface of the model. Inside the room, even though the non-propagating component of the energy density prevails,

a greater fraction of energy propagates inside the room with respect to the previous case.

The differences observed between the two configurations will therefore differently affect the relationship between energy density gradient and intensity, allowing to experimentally investigate the dependence of the diffusion coefficient on the characteristics of the sound field.

Chapter 4

Experimental evaluation of the diffusion coefficient inside long rooms

4.1 Introduction

The measurements performed inside the scaled long rooms were finally employed for the experimental investigation of the diffusion gradient equation.

In this Chapter the experimental estimate of the diffusion coefficient is therefore presented and its dependence on the acoustic properties of the room surfaces is discussed, according to the basic features of the investigated sound fields highlighted in *Chapter 3*. The results are moreover compared with the numerical estimates of the diffusion coefficient obtained by using a particle-tracing software, as presented in *Chapter 2*.

The experimental evaluation of the diffusion coefficient was carried out by employing two different methodologies.

The first approach was based on the direct measurement of the acoustic quantities involved in the diffusion process and employed the data acquired at the neighbouring receiver points placed around each "main" receiver position.

The second approach, on the other hand, relied on two hypothesis on the expected variation of D_{meas} inside long rooms, derived from the preliminary numerical investigation: linear increase of the coefficient with the distance from the source and dependence of the coefficient only on the x-component of the sound field. In the same Section also the comparison between the measured data and the results of numerical simulations is discussed, to assess the reliability of the simulation code in predicting the sound intensity inside enclosures.

As will be outlined in the final Section of the Chapter, the two experimental methods lead to similar results and allow to clarify the relationship between energy density and sound intensity inside long rooms as well as the possibility of applying the room-acoustics diffusion theory to long rooms with partially diffusely and non-diffusely reflecting boundaries.

4.2 Evaluation of the local diffusion coefficient

For the experimental estimate of the diffusion coefficient inside the scaled long rooms a methodology based only on the performed measurements was firstly employed.

The basic acoustic quantities involved in the diffusion gradient equation (1.17), that is sound intensity and energy density, were directly measured at each receiver position and employed in the estimate of the measured diffusion coefficient, expressed as:

$$D_{meas}(\boldsymbol{r}) = -\frac{|\boldsymbol{I}(\boldsymbol{r})|}{|\nabla w(\boldsymbol{r})|}. \tag{4.1}$$

As from the characterization of the sound field inside the scale models appeared that the energy flow is not purely mono-dimensional but varies in the space, the estimate was carried out taking into account the variation of the acoustic quantities along the three axes.

Therefore the energy density gradient was calculated starting from the measurements in the six additional points placed around each receiver position, as:

$$|\nabla w(\boldsymbol{r})| = \sqrt{(\nabla_x w(\boldsymbol{r}))^2 + (\nabla_y w(\boldsymbol{r}))^2 + (\nabla_z w(\boldsymbol{r}))^2}. \tag{4.2}$$

$\nabla_x w(\boldsymbol{r})$, $\nabla_y w(\boldsymbol{r})$ and $\nabla_z w(\boldsymbol{r})$ are the energy density gradient components obtained with a finite approximation of the data acquired by moving the probe in two opposite locations along each axis; the distance between each couple of points was equal to 1cm (model scale). The sound intensity was instead simply obtained starting from the I_x, I_y, I_z components measured at each central receiver position.

The estimate procedure followed four main steps:

1. calculation of the energy density gradient at each central receiver position, according to equation (4.2);

2. calculation of the intensity vector at each central position;

3. projection of the energy density gradient along the intensity direction;

4. estimate of the local value of the diffusion coefficient, applying equation (4.1).

The third step was required in order to remove the experimental errors intrinsic to the measurement procedure, that could lead to small (and unpredictable) deviations of the vectors from their main direction. The correction was also accomplished by discarding the values of the diffusion coefficient estimated when the angle between $\nabla w(\boldsymbol{r})$ and $\boldsymbol{I}(\boldsymbol{r})$ was too high; the limit threshold was set to 15° and leaded to the rejection of almost the 15% of the measurement points.

The results of the analysis are shown in figure 4.1, with reference to the frequencies of 500 and 800 Hz; all the measurement points over the horizontal plane were considered in the analysis with the aim of understanding the presence of a systematic variation of the experimental diffusion coefficient inside the room.

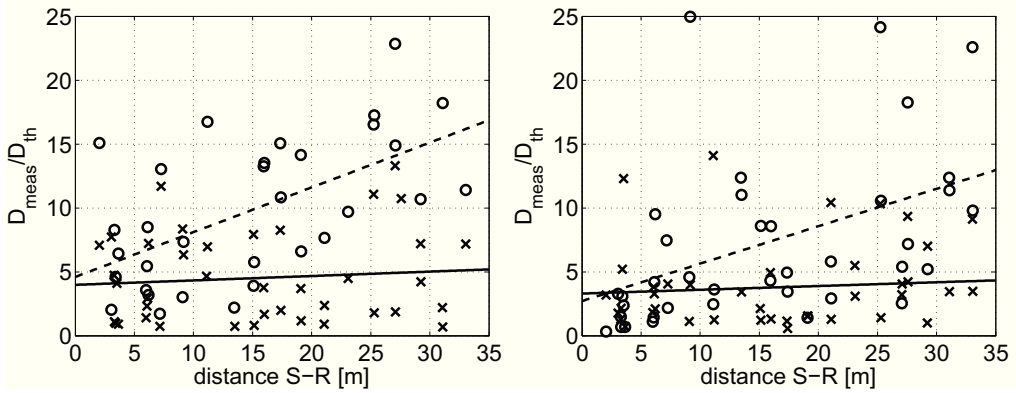

(a) 500 Hz **(b)** 800 Hz

Figure 4.1: Ratio between the measured D_{meas} and the theoretical D_{th} diffusion coefficients inside the scaled long rooms for the frequency bands of 500 and 800 Hz. Results for the room with flat boundaries ($\circ$ and $--$) and the room with scattering boundaries ($\times$, and solid line).

The data show the dispersion typical of the experimental measurements but, nevertheless, both a clear trend of variation of the coefficient with the distance and a distinction between the two investigated sound fields can be observed.

Inside the room with flat boundaries, the diffusion coefficient show an increasing trend with the distance from the source, and the values are generally higher than those obtained inside the room with scattering surfaces. In this configuration, where the sound field is mainly non-diffuse according to the criteria proposed in *Chapter 3*, the measured diffusion coefficient increases again inside the room, but with very limited slopes. In both cases, the experimental diffusion coefficient is greater than the theoretical one, which always represents the smallest value observed in the measured data.

4.3 Particle-tracing simulations of the investigated scaled long rooms

With the aim of comparing the measured values of the diffusion coefficient with the numerical estimates provided by the particle-tracing code, simulations of the two experimental set ups were carried out.

The numerical model of a $2.5 \times 0.5 \times 0.25$ m^3 long room was created, with an omnidirectional sound source located close to the end wall, emitting a constant sound power level. As during the measurement phase, a measure with the *p-u* probe of L_W of the source was not performed, the sound power level was arbitrary chosen for the numerical simulations. This, even though not represented a main issue in the comparison of the results, still required the formulation of an a-priori hypothesis on the correct matching of the results, which will be discussed in the following.

The absorption and scattering coefficients of the surfaces were chosen in accordance to the values derived from the measurements inside the scaled reverberation

Frequency	Model 1		Model 2	
	α	s	α	s
125	0.061	0.010	0.083	0.034
160	0.038	0.010	0.089	0.027
200	0.056	0.010	0.136	0.056
250	0.031	0.010	0.136	0.136
315	0.046	0.010	0.148	0.248
400	0.049	0.010	0.172	0.281
500	0.061	0.010	0.201	0.386
630	0.058	0.025	0.226	0.464
800	0.060	0.027	0.245	0.518
1000	0.046	0.020	0.260	0.582

Table 4.1: Absorption and scattering coefficients employed inside the numerical models; in the table Model 1 refers to the long room with flat surfaces whereas Model 2 refers to the long room with scattering boundaries.

chamber (§ 3.3.1).

In the model of the long room with flat boundaries, where all the surfaces are characterized by the same finishing, the measured absorption coefficients were directly employed, whereas the scattering coefficients lower than 0.01 were discarded and substituted with the limit value of 0.01.

On the other hand, inside the room with scattering surfaces, two further assumptions on the acoustic properties of the boundaries were formulated:

1. On the surfaces where the scattering patches were located, the acoustic properties of the flat and scattering finishes were summed. In fact, given the geometry of the scattering patches (which do not cover continuously the surface), it was supposed that also the varnished finishing upon which the patch was located could contribute to the total properties of the surface.

2. A surface average of the scattering and absorption coefficients was performed, in order to avoid the presence of numerical errors in the numerical results.

The absorption and scattering coefficients employed for the numerical simulations are reported in table 4.1.

Inside the models, particle tracing simulations were carried out with $N = 5 \times 10^6$ particles and a time step $\Delta t = 0.002$ s. The results were obtained for the same source and receiver positions employed in the experimental set up (see § 3.3.2); moreover the grid of receivers was thickened for obtaining a regular step of 1 m (full scale) between the measurement points.

4.3.1 Comparison of the numerical and experimental results

In this Section the results of the numerical simulations are compared with the acoustic parameters measured inside the scale model.

Firstly the reverberation time was considered, comparing predicted and measured values of RT30, whose values are expected to be related to the physical properties of the enclosure [78]. The comparisons are shown in figure 4.2 and figure 4.3 for the line of receivers at z=1.6 m and y=3.33 m.

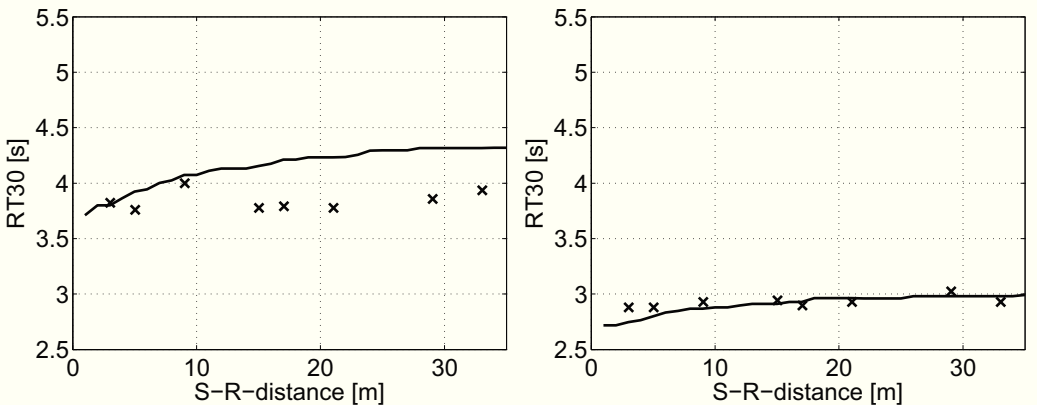

(a) 500 Hz **(b)** 800 Hz

Figure 4.2: RT30 inside the long room with flat boundaires as a function of the distance from the source. Comparison between the measured (×) and the numerically simulated (solid line) values.

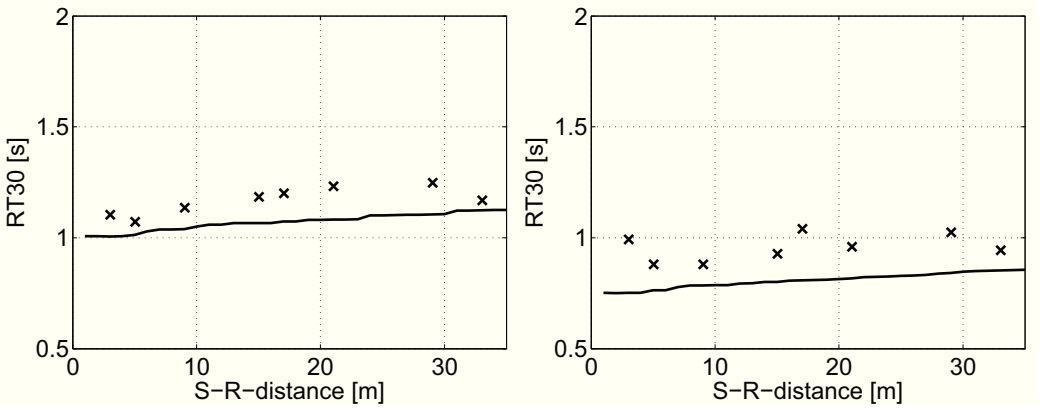

(a) 500 Hz **(b)** 800 Hz

Figure 4.3: RT30 inside the long room with scattering boundaires as a function of the distance from the source. Comparison between the measured (×) and the numerically simulated (solid line) values.

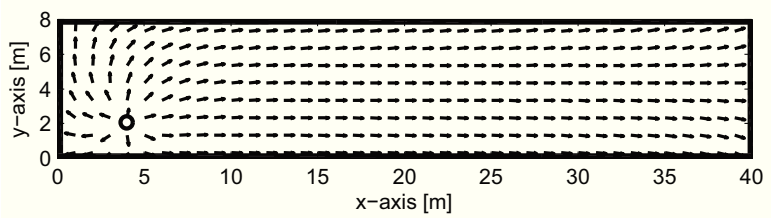

Figure 4.4: Spatial distribution of the normalized intensity vectors obtained from the particle-tracing simulations of the long room with flat boundaries; results over the z=1.6 m plane and the frequency of 800 Hz.

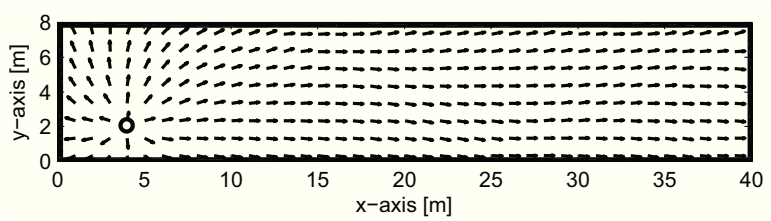

Figure 4.5: Spatial distribution of the normalized intensity vectors obtained from the particle-tracing simulations of the long room with scattering boundaries; results over the z=1.6 m plane and the frequency of 800 Hz.

The obtained trend of variation are quite similar for the two models, with maximum differences that, for the considered 500 and 800 Hz frequency bands, reach the 15 % of the measured values. If the comparison is extended to the whole range of analysed frequencies, it can be see that the agreements is satisfactory (smaller than 20%) only starting from 500 Hz for the room with flat surfaces and 400 Hz for the room with scattering surfaces. The differences are related to the uncertainties in the estimation of the absorption and scattering coefficients that become important especially at low frequency and inside the room with flat surfaces (where the considered coefficients are quite small and affected by uncertainties comparable with their value).

Then, the distribution of the intensity vectors over the horizontal plane was analysed; the results, referred to the surface at z=1.6 m and the frequency of 800 Hz, are shown in figure 4.4 and figure 4.5.

It can be seen that the numerical model predicts an energy flow solely oriented along the main dimension of the room; the intensity vectors deviate from the principal direction of propagation only close to the source (influenced by the presence of the direct field) and close to the edges at the end of the room that (weakly) attract the energy flow. The numerical code predicts a purely mono-dimensional behaviour of the sound field, without the local, random deviations observed inside the scale model, due to the small irregularities in the model set up and the energy re-circulation phenomena, which characterize the real sound fields. Close to the lateral walls the intensity vectors show almost the same orientation observed in the central positions, not affected by the presence of absorbing or reflecting surfaces. Finally, the predicted intensity distribution is almost the same for both investigated models, without differences related to the different reflection laws of the surfaces.

All these remarks yield to the conclusion that the particle-tracing model can not properly predict the intensity distribution inside long rooms, or at least, it can properly predict only the component along the x-axis, which is certainly the predominant component but not the only one affecting in the sound field (as shown in *Chapter 3*). Hence, with the aim of validating the numerical results, they were compared with the only x-component of the acoustic quantities measured inside the scale models.

As the sound power of the source was unknown, it was chosen to rescale the experimental results seeking the best fit between measured and simulated energy density; the obtained rescaling factor was then applied to the measured sound intensity. The choice of employing energy density instead of intensity for the comparison, was originated by the supposed greater reliability of the particle-tracing software in the calculation of the former parameter (see § 2.2).

The best fit between measured and simulated energy density was obtained following a two-step procedure, carried out for the linear values of the data:

1. calculation of a regression curve that could provide a reliable description of the energy density decay along the line from the source to the end wall

2. calculation of the rescaling factor that provide the best fit between simulated data and regression curves of the experimental values, employing a least mean square procedure.

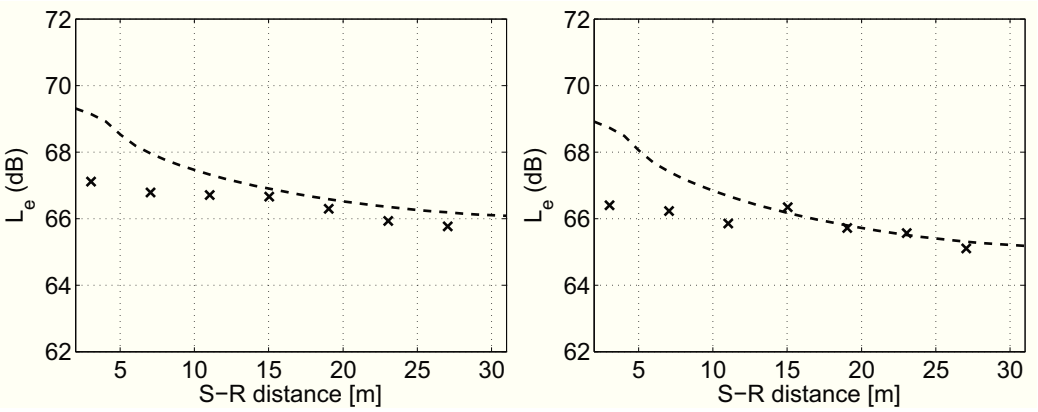

(a) 500 Hz **(b)** 800 Hz

Figure 4.6: Energy density level (L_e) decay along a line from the source to the end wall of the long room with flat boundaries, for the frequency bands of 500 and 800 Hz: measured ($\times$) and simulated data ($--$).

The comparison between measured and simulated energy density inside the rooms is represented in figure 4.6 and figure 4.7, showing a satisfactory agreement for both configurations. Inside the long room with scattering boundaries the whole spatial decrease of the energy density is correctly modelled, with differences lower than 1 dB. On the other hand, inside the room with flat boundaries, the numerical model properly predicts the spatial energy decay only in the far field of the room

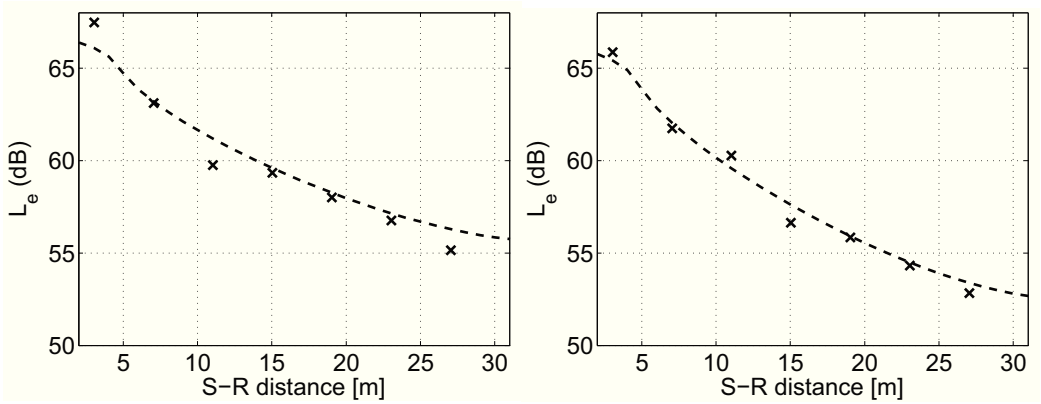

(a) 500 Hz **(b)** 800 Hz

Figure 4.7: Energy density level (L_e) decay along a line from the source to the end wall of the long room with scattering boundaries, for the frequency bands of 500 and 800 Hz: measured ($\times$) and simulated data ($--$).

(starting from 10 m from the source), whereas close to the source, differences of almost 3 dB can be observed.

Finally, the measured and numerically predicted sound intensity decays were compared, as represented in figure 4.8 and figure 4.9. In this case, the best agreement is found for the room with flat boundaries, where the spatial decay is correctly predicted. Conversely, inside the room with scattering boundaries, bigger differences can be observed between the two set of data, with a systematic underestimate of the measured data and the prediction of a slightly different spatial decay trend.

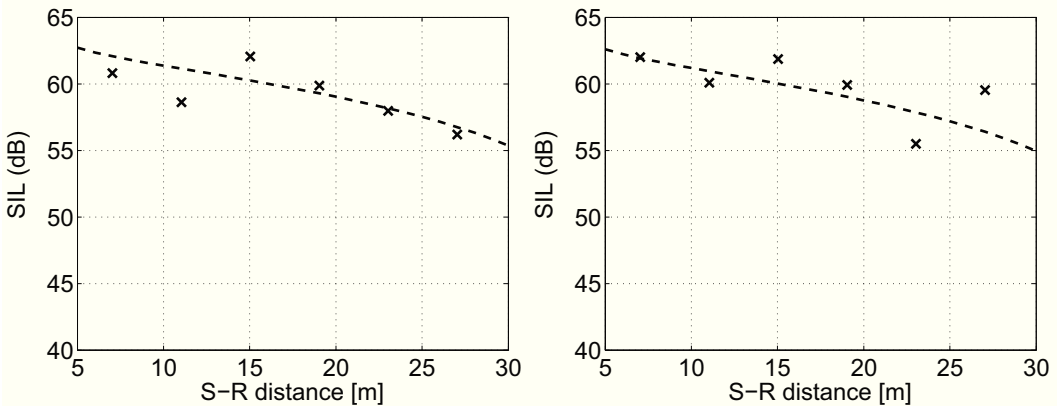

(a) 500 Hz **(b)** 800 Hz

Figure 4.8: Sound intensity level (SIL) decay along a line from the source to the end wall of the long room with flat boundaries, for the frequency bands of 500 and 800 Hz: measured data ($\times$) and simulated data ($--$).

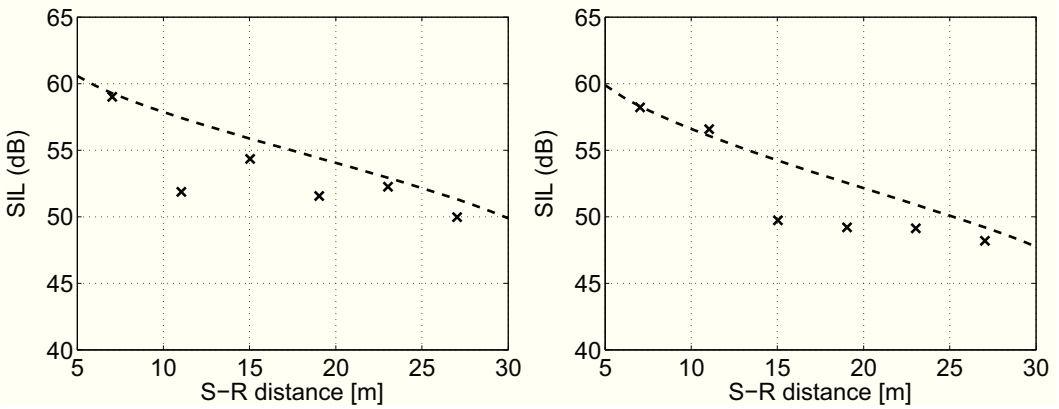

(a) 500 Hz **(b)** 800 Hz

Figure 4.9: Sound intensity level (SIL) decay along a line from the source to the end wall of the long room with scattering boundaries, for the frequency bands of 500 and 800 Hz: measured data ($\times$) and simulated data ($--$).

4.3.2 Semi-empirical estimate of the diffusion coefficient

The particle-tracing simulations allowed to numerically estimate, according to equation (2.14), the diffusion coefficient inside the investigated long rooms. As expected, D_{est} increases linearly with the distance from the source and depends on the fraction of specular reflections present inside the room: an increase in the scattering coefficient, yields indeed to a bigger slope of the distance-D_{est} curve (figure 4.10).

To perform a comparison between these numerical estimates and the measured values of the diffusion coefficient, a new estimate procedure was introduced. In fact, the D_{meas} values derived with the method presented in § 4.2 could not be directly employed in the comparison, being obtained in the hypothesis of variations of the acoustic quantities along the three axes. This alternative methodology, which can be defined as semi-empirical, takes instead into account only the component of the acoustic quantities along the x-axis, which is the only part of the sound field directly comparable with the numerical simulations. Moreover, an additional hypothesis on the trend of variation of the diffusion coefficient with the distance from the source was introduced, derived from the results of the numerical simulations: D_{meas} is therefore supposed to vary linearly with the distance from the source, following the general law $D_{meas} = D_{th} \cdot (\hat{a} + \hat{b}r)$.

The semi-empirical estimate procedure, carried out considering the linear values of the acoustic quantities, follows three main steps:

1. Starting from the measured values of the sound energy density, a regression law $\hat{w}(\boldsymbol{r}) = f(r)$ was calculated, to describe the spatial decay of the parameter along the line from the source to the end wall. For each frequency a best fit procedure allowed to obtain the coefficients of the regression curves, expressed as a power law ($\hat{w}(\boldsymbol{r}) = \hat{A}\, r^{(\hat{B})} + \hat{C}$) for the room with flat boundaries and as an exponential law ($\hat{w}(\boldsymbol{r}) = \hat{A} \exp(\hat{B}\, r) + \hat{C} \exp(\hat{D}\, r)$) for the room with scattering boundaries. Different regression laws were chosen for the two

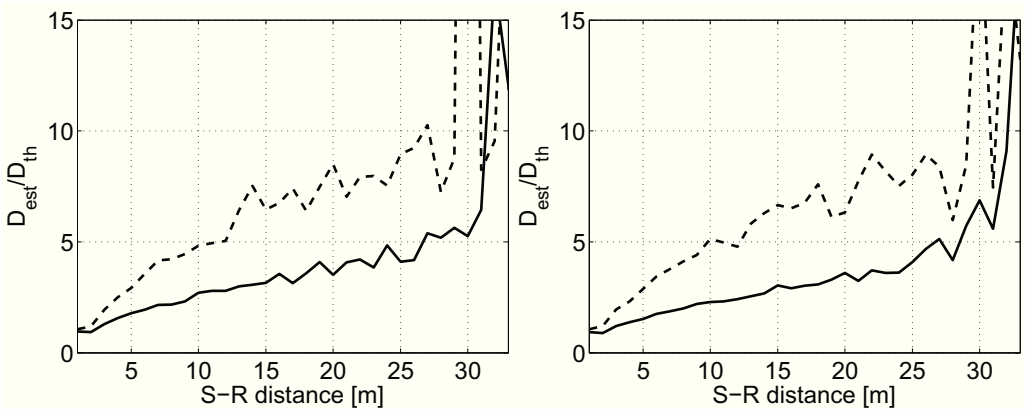

(a) 500 Hz **(b)** 800 Hz

Figure 4.10: Ratio between the estimated D_{est} and theoretical D_{th} diffusion coefficients obtained from particle-tracing simulations for the frequency bands of 500 and 800 Hz; results for the long room with flat ($--$) and scattering (solid line) boundaries.

configuration, confirming the difference in the two investigated sound field; in both cases the law maximizing the correlation coefficient for the majority of the frequency bands, was employed [79].

2. A theoretical regression curve was calculated, for describing the spatial decay of the sound intensity, according to the diffusion gradient equation and the hypothesis of a linear variation of the diffusion coefficient. The obtained regression law can therefore be expressed as: $\hat{I}(\boldsymbol{r}) = -D_{th}(\hat{a}+\hat{b}r)f'(r)$, where the values of $\hat{a}$ and $\hat{b}$ are the only unknown quantities and $f'(r)$ expresses the spatial derivative of the regression curves obtained at step 1.

3. The quantities $\hat{a}$ and $\hat{b}$ were then estimated with a least mean square procedure, comparing the theoretical regression curve with the $I_x(\boldsymbol{r})$ values measured inside the scale model. In particular, the solution of the estimate problem was obtained employing an empirical trial method, that is graphically investigating the quadratic error $E(\hat{a}, \hat{b})$ over a defined range of variation of the estimate coefficients $\hat{a}$ (intercept) and $\hat{b}$ (slope). The quadratic error is calculated as:

$$E(\hat{a}, \hat{b}) = \sum_{i=1}^{N_p} (I_x(\boldsymbol{r}_i) - \hat{I}(\boldsymbol{x}_i))^2, \tag{4.3}$$

where N_p is the number of considered receivers.

An example of the distribution of $1/E(\hat{a}, \hat{b})$ is displayed in figure 4.11 with reference to the long room with scattering boundaries at the frequency of 800 Hz. It can be seen that the inverse of the quadratic error shows a local maximum, centred around the values $(\hat{a}, \hat{b}) = (0.98, 0.05)$ that will be therefore considered as the optimal estimate for intercept and slope of the linear curve.

It is worthy to notice that the choice of the regression law employed for describing the energy density spatial decay (and consequently the sound intensity

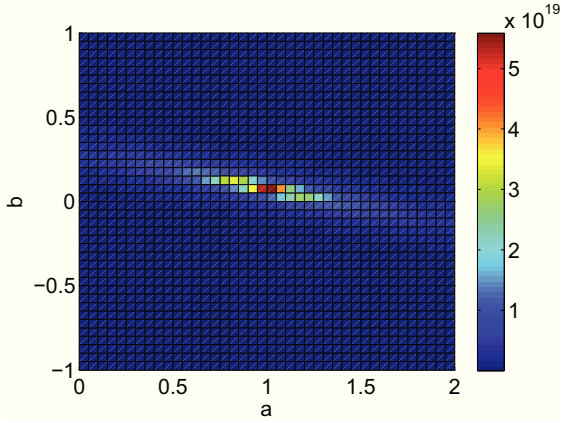

Figure 4.11: Distribution of the inverse of the quadratic error $1/E(\hat{a}, \hat{b})$ as a function of the coefficient $\hat{a}$ and $\hat{b}$, with reference to the long room with scattering boundaries at 800 Hz. The presence of a local maxiumum identifies the couple of optimal ($\hat{a}$,$\hat{b}$) values.

spatial decay) greatly affects the estimate of the parameters $\hat{a}$ and $\hat{b}$. For example if an exponential law is employed for describing the spatial decay inside the room with flat surfaces (regardless of the maximization of the correlation coefficient), it becomes impossible to identify a local minimum in the graphical representation of the quadratic error.

The values of $\hat{a}$ and $\hat{b}$ that satisfy the least mean square criterion are reported in table 4.2 for the two configurations and different frequencies, whereas in figure 4.12 and figure 4.13 a graphical comparison between the numerically estimated and measured diffusion coefficients is presented.

It can be seen that inside the long room with scattering boundaries the estimated diffusion coefficient shows a weakly increasing trend, varying along the distance from D_{th} to $3\,D_{th}$. The numerically predicted coefficient shows instead a bigger variation over the length, with a slope which is almost twice as the measured one.

On the other hand, inside the room with flat boundaries the measured diffusion coefficient increases greatly with the distance from the source, varying from $4\,D_{th}$ up to $28\,D_{th}$. The simulated coefficient D_{est} is instead characterized by both a smaller initial value (close to D_{th}) and a smaller slope, with variations limited between D_{th} and $10\,D_{th}$. The estimated coefficient increases with a linear trend up to 20 m from the source; close to the end of the room the values settle on a constant value.

4.4 Discussion

The first approach employed for the estimate of D_{meas} relies only on the measurements performed inside the scale models: a direct evaluation of the energy density gradient was accomplished, employing the six sets of primary data gathered around each central receiver position.

The uncertainties in the acquisition of the data were taken into account by

Frequency band	**Model 1**		**Model 2**	
[Hz]	$\hat{a}$	$\hat{b}$	$\hat{a}$	$\hat{b}$
500	3.49	0.70	0.94	0.05
630	2.16	0.57	1.32	0.08
800	2.56	0.77	0.98	0.05
1000	1.04	0.42	1.12	0.02

Table 4.2: Intercept $\hat{a}$ and slope $\hat{b}$ of the linear curve describing the variation of D_{meas} with the distance from the source; values estimated with a least-mean square procedure for the line of receivers at z=1.6 m. In the table Model 1 refers to the set up with flat surfaces whereas Model 2 refers to that with scattering boundaries.

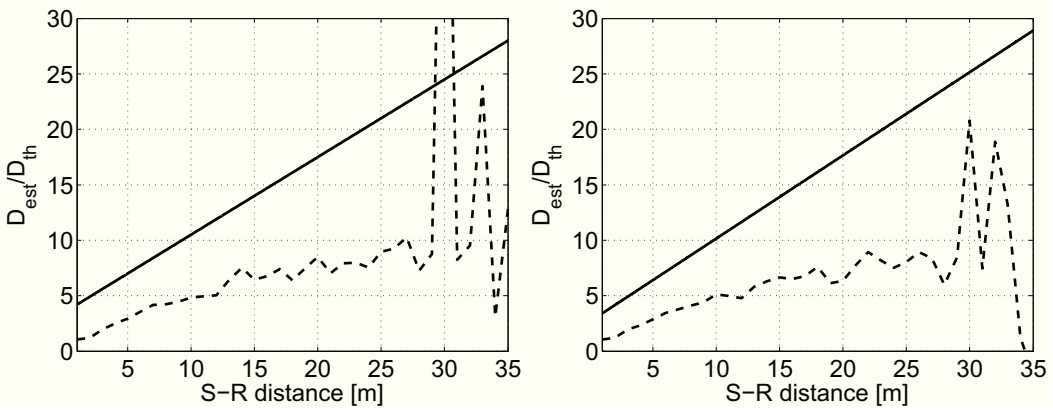

(a) 500 Hz **(b)** 800 Hz

Figure 4.12: Ratio between the estimated (or the measured) and the theoretical D_{th} diffusion coefficient inside the long room with flat boundaries for the frequency bands of 500 and 800 Hz: numerical estimate of D_{est} $(--)$, semi-empirical estimate of D_{meas} (solid line).

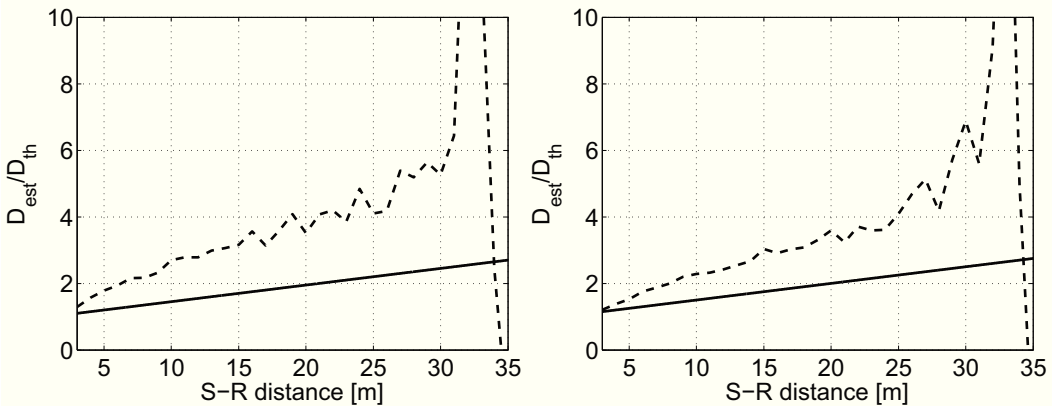

(a) 500 Hz **(b)** 800 Hz

Figure 4.13: Ratio between the estimated (or measured) and the theoretical D_{th} diffusion coefficient inside the long room with scattering boundaries for the frequency bands of 500 and 800 Hz: numerical estimate of D_{est} $(--)$, semi-empirical estimate of D_{meas} (solid line).

discarding the receiver positions where the angle between $\nabla w(\boldsymbol{r})$ and $\boldsymbol{I}(\boldsymbol{r})$ was bigger than the threshold value of 15°. The limited amount of discarded values ensures the reliability of the acquired data: the differences observed between the energy density values measured at the neighbouring points are not merely due to experimental errors but to real variations of the acoustic quantities.

The employed approach describes the sound field only by means of punctual measurements. Several studies in literature deal, on the other hand, with statistical representations of the acoustic quantities, locally averaging the measured parameters over an elementary volume, with dimensions defined by the investigated wavelength. Representing the sound field, and thus the diffusion coefficient, by means of a similar approach, would have required to repeat the acquisition of the seven sets of primary data several times inside the same elementary volume, in order to calculate a local average of sound intensity and energy density gradient. This kind of average can not obviously be performed inside the employed scale model, where the dimensions and the relative positioning of the holes in the ceiling were specifically designed as a good compromise between the necessity of performing measurements at small distance and the possibility of completely characterize the sound field inside a model of big dimensions. However, the obtained results show that the punctual description of the acoustic quantities can carefully describe the characteristics of the sound field in terms of energy density gradient, discriminating the two investigated configurations and allowing to understand their distinctive features.

The second methodology was mainly carried out to compare simulated and measured results, in order to validate the predictions obtained with the particle-tracing software. The main issue in this comparison is the unsuitability of the numerical tool to provide a reliable description of the sound intensity distribution inside the enclosure: the software predicts in fact a purely mono-dimensional energy flow, not affected by the presence of the room boundaries neither by the reflection law of the surfaces. Hence, the direction of the intensity vectors, at least in the region close to the boundaries, can not be considered correct, as the contributions of the other components of the sound intensity, along the y and z axes, are completely discarded. Anyway, if the comparison is limited to the only x-component of the measured acoustic quantities, the particle-tracing software provides results in fair agreement with the measured acoustic quantities in terms of RT30, energy density and sound intensity.

Finally, a comparison between the two methodologies employed for the estimate of the measured diffusion coefficient can be performed. Obviously, as the two methods take into account different components of the sound field, the obtained results are not perfectly coincident; anyway, a general agreement can be observed in the results: both methods predict in fact the same general trend of variation, highlighting the same basic features marking the diffusion coefficient values inside the two considered sound fields.

The following discussion will be therefore focused on the results obtained with the semi-empirical methodology; the measured diffusion coefficients are shown, for the frequency bands between 500 and 1000 Hz, in figure 4.14.

The diffusion coefficients measured inside the two long rooms always differ from

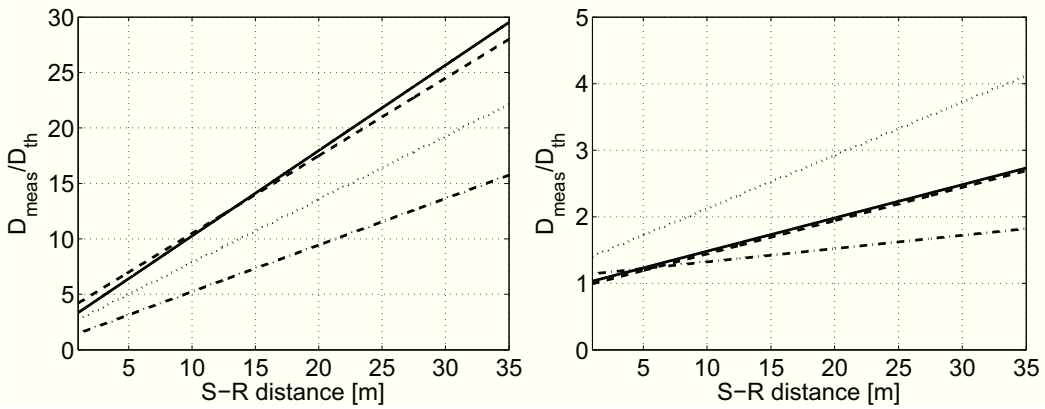

(a) Flat boundaries **(b)** Scattering boundaries

Figure 4.14: Ratio between the measured D_{meas} and the theoretical D_{th} diffusion coefficient inside the two scaled long rooms. Results obtained with the semi-empirical methodology for the one-third octave frequency bands: 500 Hz ($--$), 630 Hz ($\cdots$), 800 Hz (solid line), 1000 Hz ($-\cdot-$)

the theoretical, constant value showing two distinctive features:

- values always bigger than D_{th};
- increase of the measured coefficient along the length of the room.

These effects can be related to the presence of specular reflections inside the long room: increasing the scattering coefficient of the room surfaces (for instance moving from the room with flat boundaries to the room with scattering boundaries) leads to a decrease of both slope and initial value of the distance-D_{meas} curve. A similar effect can be observed moving, within the same configuration, from the coefficients obtained at low frequency to those obtained at high frequency.

The presence of values always bigger than D_{th} can be explained by taking into account the spatial variation of the acoustic quantities as a function of the scattering coefficient of the boundaries: increasing the amount of specular reflections inside long rooms leads in fact to a lower spatial attenuation of both energy density and sound intensity. Therefore, the ratio of the two acoustic quantities, that expresses the local value of the diffusion coefficient, will be higher inside long room characterized by low scattering coefficients. Increasing the amount of diffuse reflections inside the room, will lead to value progressively smaller and close to D_{th}. Only in the limiting case of long room with completely diffusely boundaries (s=1), where the biggest spatial attenuation of the acoustic parameters is expected, the local value of the ratio between intensity and energy density will reach its lowest value, equal to the theoretical constant.

The increase of the measured diffusion coefficient along the length of the room can be, on the other hand, related to the amount of non-propagating energy inside the enclosure. The characterization of the acoustic sound fields presented in § 3.3.3 shows in fact that inside both enclosures the prevailing part of the energy density does not flow inside the room but merely re-circulates around a given position or it is steady. This non-propagating part of the energy, that increases with the distance

from the source and is always bigger inside the long room with flat boundaries, could therefore be interpreted as a "resistance" to the energy flow. Its presence obviously affects the energy density gradient values, that, inside the long room with flat boundaries or in the regions further from the source will describe not only the flow of the energy inside the room but also all the non-propagating effects, that disguise the real differences that occurs at the receiver positions. Therefore constant values of the diffusion coefficient will be observed only when the effect of the non-propagating part of the energy is small, for instance inside the long room with scattering boundaries at high frequencies.

Let's now consider the possibility that the diffusion gradient equation can properly express only the relationship between the intensity and the gradient of the propagating part of the energy density, that is the only component really flowing inside the room. If the propagating energy is expressed as $e_p(\boldsymbol{r}) = |\boldsymbol{I}(\boldsymbol{r})|/c$, then the diffusion gradient equation becomes:

$$\boldsymbol{I}(\boldsymbol{r}) = -D \nabla \left(\frac{|\boldsymbol{I}(\boldsymbol{r})|}{c} \right). \tag{4.4}$$

It is clear from equation (4.4) that the diffusion coefficient will be a constant only if the intensity inside a room can be expressed through an exponential function. The condition is met for example in a three-dimensional sound field that could be described according to the revised theory [48], where the intensity at each position of the room is expressed as:

$$\boldsymbol{I}(\boldsymbol{r}) = \frac{W}{V} \frac{\exp(-\gamma r)}{\gamma}, \tag{4.5}$$

where $\gamma = -\ln(1-\bar{\alpha})/\lambda$ and λ is the mean free path of the room.

An attempt to verify this kind of approach was therefore performed, estimating the diffusion coefficient inside the long room with flat boundaries, where the sound field can be adequately described with the expressions of the revised theory (§ 3.3.3.3). The analysis was carried out following the same approach described in § 4.2 and the energy density gradient was calculated taking into account only the propagating part of the energy. The results are shown in figure 4.15 for the frequency of 500 Hz and represent a first confirmation of the hypothesis made, being the diffusion coefficient D characterized by an almost constant trend centred around $0.7 \cdot D_{th}$.

4.5 Conclusions

The main aim of the experimental part of this study was to assess the relationship between energy density gradient and sound intensity inside long rooms, by means of an experimental estimate of the diffusion coefficient value.

Two different methodologies were employed for the analysis: the first method was based on a direct measure of the two acoustic quantities whereas the second one was a semi-empirical approach, based on the hypothesis of a linear variation of the diffusion coefficient with the length of the room. Even though the two

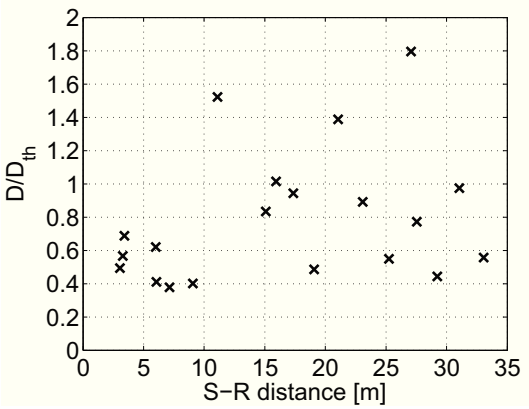

Figure 4.15: Ratio between the measured D and the theoretical D_{th} diffusion coefficient inside the long room with flat boundaries, for the frequency of 500 Hz. D values calculated taking into account only the propagating component of the energy density.

methods can not be directly compared, as they model different part of the sound field, the predicted diffusion coefficients show similar trend of variations and the same distinctive features that allowed to discriminate the two investigated long rooms.

In particular, the analysis leaded to the two following principal remarks:

- inside the long room with flat surface, characterized by the prevailing presence of specular reflections, the diffusion coefficient is bigger than the theoretical value, due to the low spatial attenuation of the acoustic quantities; the coefficient increases sharply with the distance from the source, influenced by the increasing presence of non-propagating energy density inside the room;

- inside the long room with scattering boundaries, the presence of mixed (specular and diffuse) reflections lead to a diffusion coefficient slightly bigger than D_{th}; the theoretical value can in fact be reached only when the all the reflection inside the room are purely diffuse.

Finally, the comparison between measured and simulated acoustic quantities provided an experimental validation of the particle-tracing code, especially focused on the prediction of the sound intensity. The results show that only the predominant component of the sound field, that is the x-component, is properly simulated with the numerical code; anyway, if the comparison is limited to this part of the sound field, a fair agreement can be observed between measured and simulated data.

Conclusions

The aim of this research was to investigate the room-acoustics diffusion theory, establishing its conditions for validity. In particular the analysis was focused on the diffusion gradient equation, that is the equation at the basis of the theoretical formulation of the model, relating energy density gradient and sound intensity through a proportional relationship. The equation was investigated by means of numerical simulations and measurements inside a scale model, setting out to understand when the assumed relation is fulfilled inside the enclosures.

This kind of study has never been undertaken before, as the expression of the diffusion coefficient was directly derived from the formulation of the diffusion equation applied to the propagation of elementary particles; comparisons with numerical results have only been performed. Anyway, as the diffusion coefficient represents the central parameter of the diffusion model, a systematic investigation of its expression is believed to represent a main requirement in order to validate the model.

This study was also extended to enclosures characterized by mixed (specular and diffuse) reflections, in order to understand if the sound field inside them could be described through a diffusion process. Rooms with different shapes and acoustic properties of the boundaries were therefore considered in the analysis.

The numerical part of the research was performed using a particle-tracing code that allowed a direct and independent calculation of the acoustic quantities involved in the diffusion gradient equation: the numerical estimated energy density and sound intensity were then employed for retrieving a local, numerical estimate of the diffusion coefficient.

During this part of the research, an analytical correction for the solution of the diffusion equation was also derived, necessary for correctly describing the reverberant part of sound field in the region within two mean free paths from the sound source, where the diffusion model does not return valid results. The numerical estimate of the diffusion coefficient was firstly performed inside proportionate rooms: in this case the solution of the diffusion equation was proved to be almost independent on the diffusion coefficient value. Anyway the agreement between the acoustic quantities derived from the diffusion model and the results of the numerical model assessed the reliability of the diffusion gradient equation for the reverberant part of the sound field. The case of long rooms was then considered, showing that the diffusion coefficient is not a constant inside the rooms but increases with the distance from the source; the variation of the coefficient with the shape of the room and the acoustic properties of the boundaries was systematically evaluated, assessing

the dependence of D_{est} on the scattering coefficient of the boundaries.

The results obtained during the first, numerical analysis helped in outlining the basic features of the problem that were then further investigated by means of experimental measurements.

The experimental analysis of the diffusion gradient equation was accomplished inside the scale model of a long room. Measurements of sound pressure and particle velocity were performed with a three-dimensional p-u probe; a set of digital filters was specifically derived, for the calibration of the probe and the correction of the acquired raw data. A local experimental estimate of the diffusion coefficient was calculated, proving definitely that inside long rooms, the diffusion coefficient does not coincide with the constant theoretical value but increases along the length of the room, influenced by the presence of the predominant, non-propagating part of the energy density. Similarly, the dependence of the diffusion coefficient on the scattering coefficient of the boundaries was investigated, proving that an increasing amount of specular reflections inside the room leads also to an increase in the diffusion coefficient value.

Therefore this research allowed to assess the relationship between energy density and sound intensity inside long rooms and provided an experimental, direct analysis of the physical phenomena theoretically predicted by the room-acoustics diffusion model. The obtained results proved the necessity of further investigation to assess the validity of the model inside enclosures with non-proportionate geometries. Moreover a modification of the analytical formulation of the room-acoustics diffusion equation is believed to be necessary for taking into account spatial variations of the diffusion coefficient inside the enclosures and better representing the real phenomena.

Appendix A

Acoustic parameters inside the scaled long room

In this Appendix the results of the analysis of the sound field inside the two investigated scaled long rooms are reported, for the one-third octave frequency bands between 160 and 1000 Hz (frequency expressed as the full-size equivalent FS). The characterization of the two sound fields is discussed in detail in § 3.3.3.

The acoustic parameters are presented firstly for the long room with flat boundaries (*Appendix A.1*) and then for the same room with scattering boundaries (*Appendix A.2*) organized as follows:

1. energy density level L_e;
2. reverberation time (RT30 and EDT);
3. sound intensity level SIL;
4. normalized intensity vectors distribution over the horizontal plane.

A.1 Long room with flat boundaires

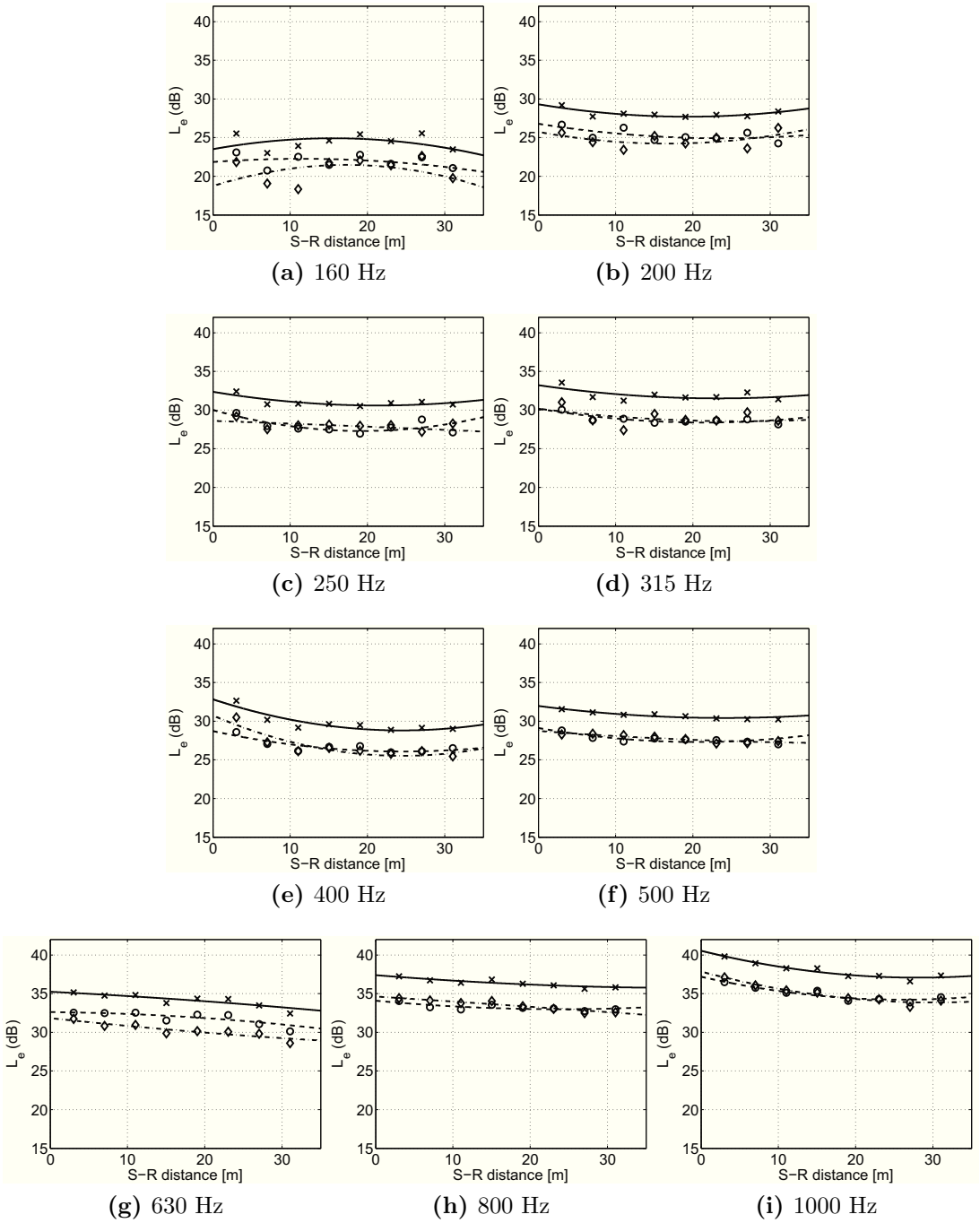

(a) 160 Hz **(b)** 200 Hz

(c) 250 Hz **(d)** 315 Hz

(e) 400 Hz **(f)** 500 Hz

(g) 630 Hz **(h)** 800 Hz **(i)** 1000 Hz

Figure A.1: Energy density level (L_e) decay inside the scaled long room with flat surfaces, along the line from the source to the end wall at z=1.6 m. Measured values and regression lines: total energy density ($\times$ and solid line), potential energy density ($\diamond$ and $-\cdot-$), kinetic energy density ($\circ$ and $--$).

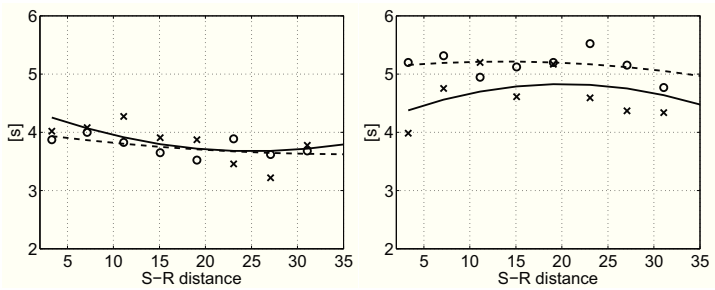

(a) 160 Hz **(b)** 200 Hz

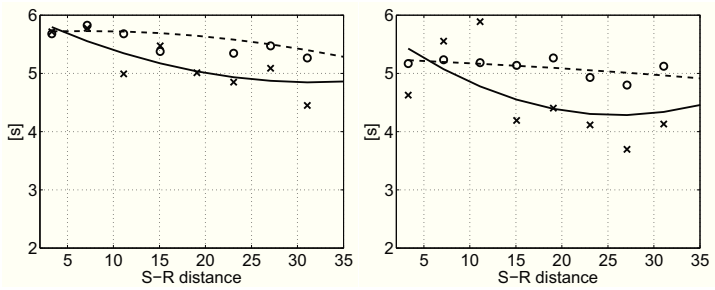

(c) 250 Hz **(d)** 315 Hz

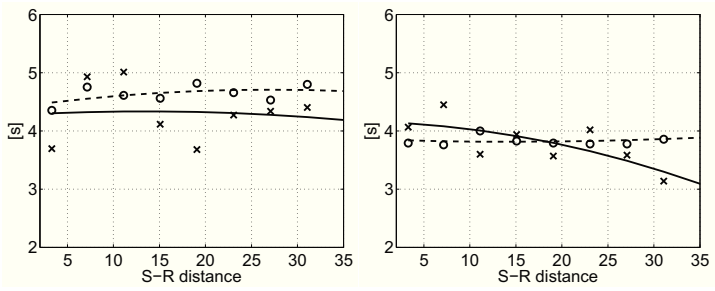

(e) 400 Hz **(f)** 500 Hz

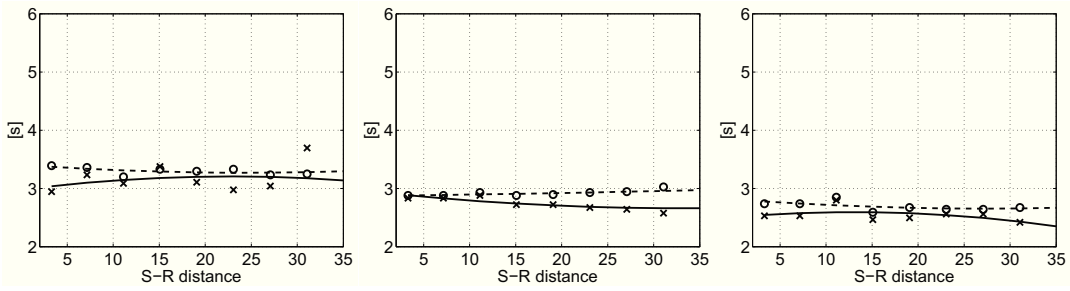

(g) 630 Hz **(h)** 800 Hz **(i)** 1000 Hz

Figure A.2: Reverberation time inside the scaled long room with flat surfaces. Measured values and regression lines: EDT ($\times$ and solid line), RT30 ($\circ$ and $--$).

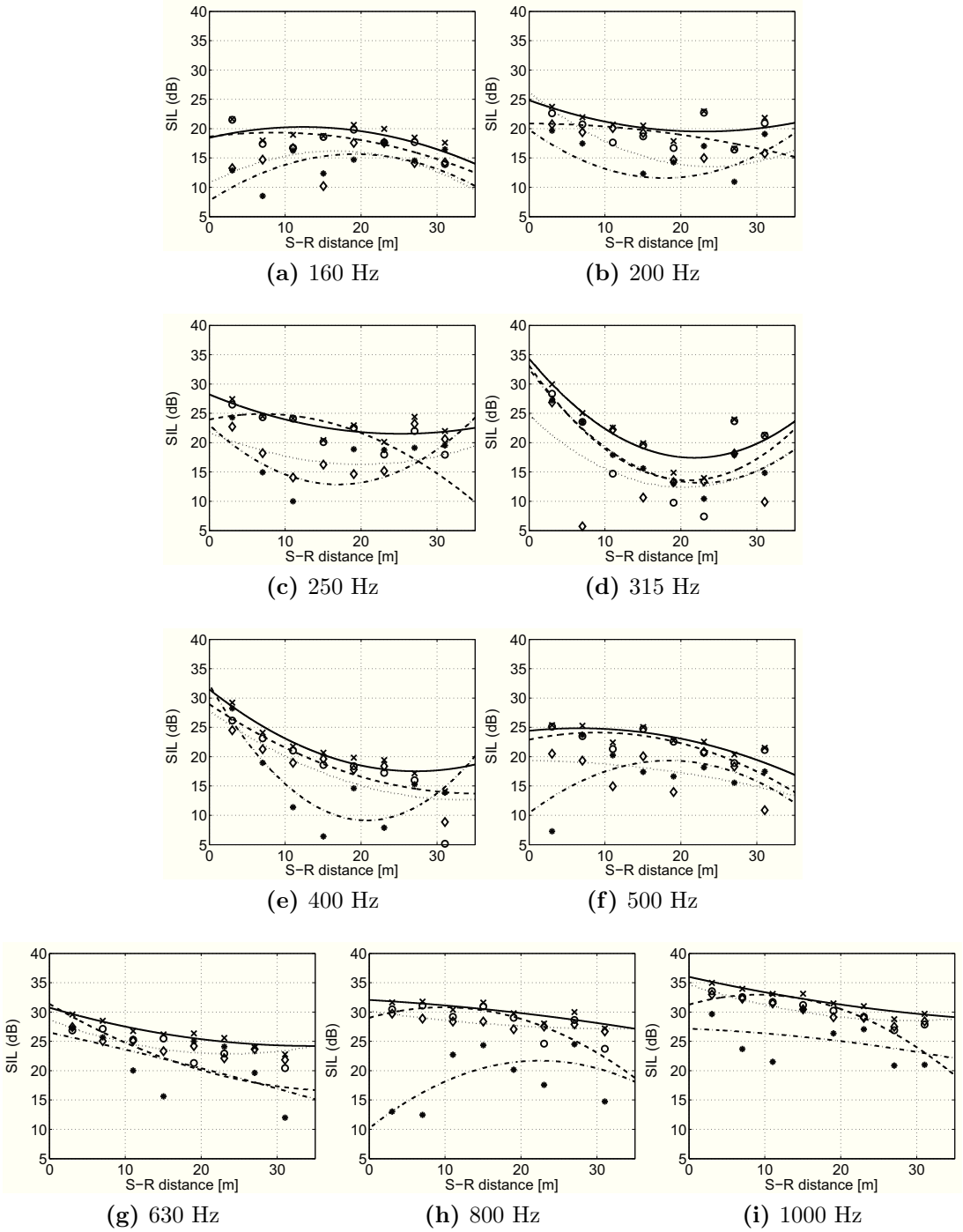

(a) 160 Hz **(b)** 200 Hz

(c) 250 Hz **(d)** 315 Hz

(e) 400 Hz **(f)** 500 Hz

(g) 630 Hz **(h)** 800 Hz **(i)** 1000 Hz

Figure A.3: Sound intensity level (SIL) decay inside the scaled long room with flat surfaces along the line from the source to the end wall at z=1.6 m. Measured values and regression lines: total intensity ($\times$ and solid line), intensity along the x-axis ($\circ$ and $--$), intensity along the y-axis ($*$ and $-\cdot-$), intensity along the z-axis ($\diamond$ and $\cdots$).

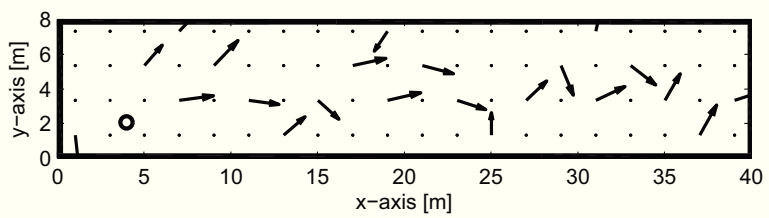

(a) 160 Hz

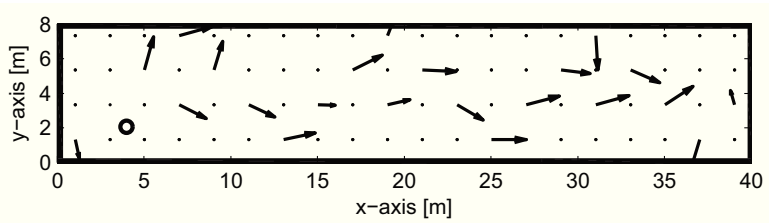

(b) 200 Hz

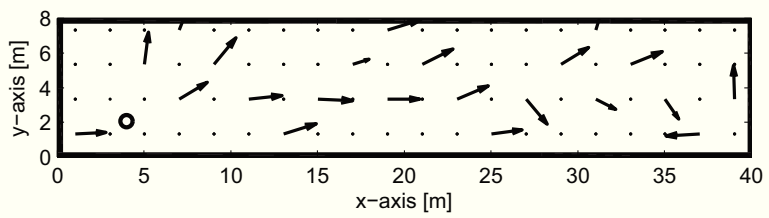

(c) 250 Hz

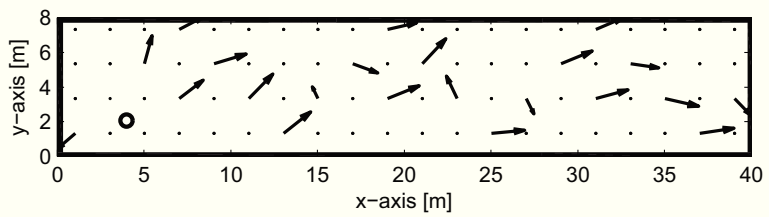

(d) 315 Hz

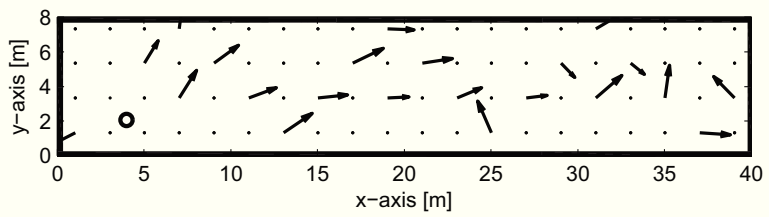

(e) 400 Hz

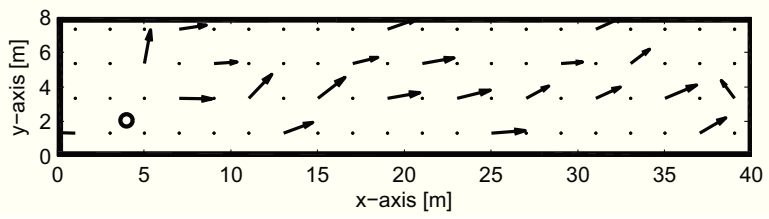

(f) 500 Hz

Figure A.4: Normalized intensity vectors inside the scaled long room with flat surfaces; results over the horizontal plane at z=1.6 m for the frequency bands from 160 to 500 Hz.

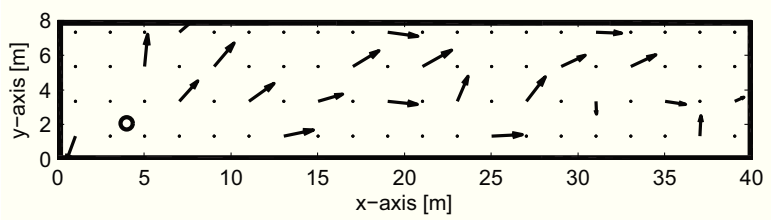

(a) 630 Hz

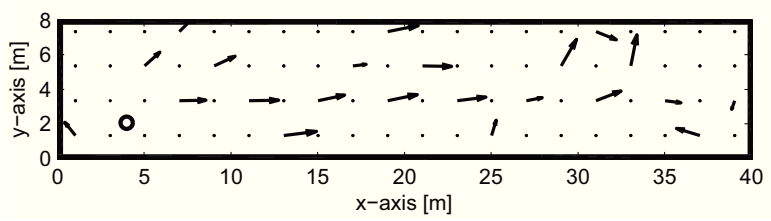

(b) 800 Hz

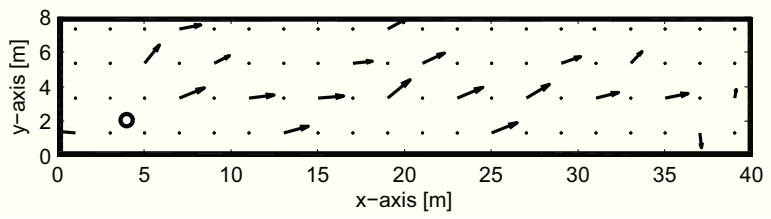

(c) 1000 Hz

Figure A.5: Normalized intensity vectors inside the scaled long room with flat surfaces; results over the horizontal plane at z=1.6 m for the frequency bands from 630 to 1000 Hz

A.2 Long room with scattering boundaries

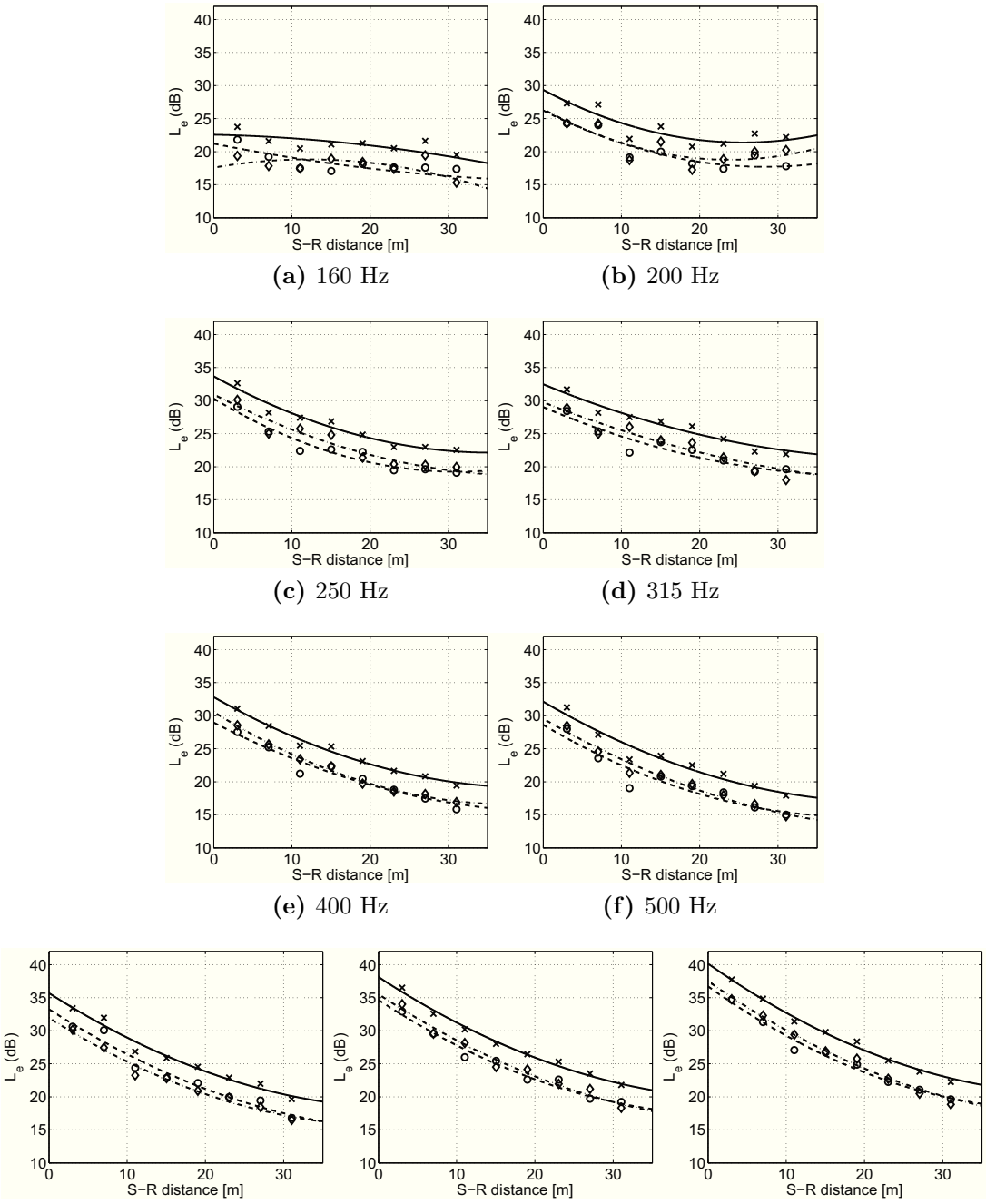

(a) 160 Hz **(b)** 200 Hz

(c) 250 Hz **(d)** 315 Hz

(e) 400 Hz **(f)** 500 Hz

(g) 630 Hz **(h)** 800 Hz **(i)** 1000 Hz

Figure A.6: Energy density level (L_e) decay inside the scaled long room with scattering surfaces, along the line from the source to the end wall at z=1.6 m. Measured values and regression lines: total energy density ($\times$ and solid line), potential energy density ($\diamond$ and $-\cdot-$), kinetic energy density ($\circ$ and $--$).

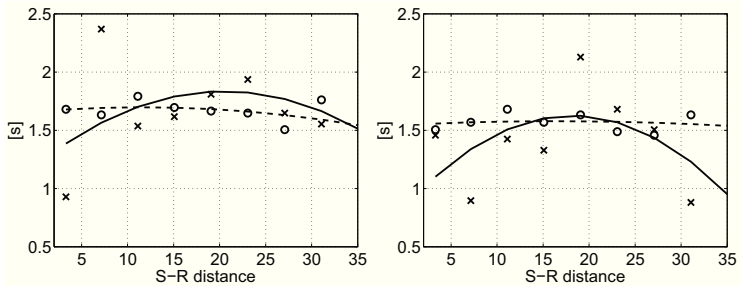

(a) 160 Hz **(b)** 200 Hz

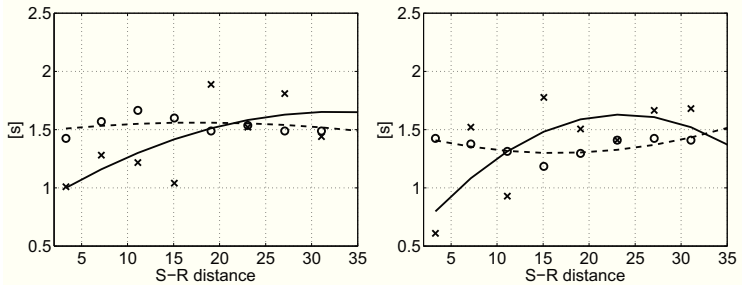

(c) 250 Hz **(d)** 315 Hz

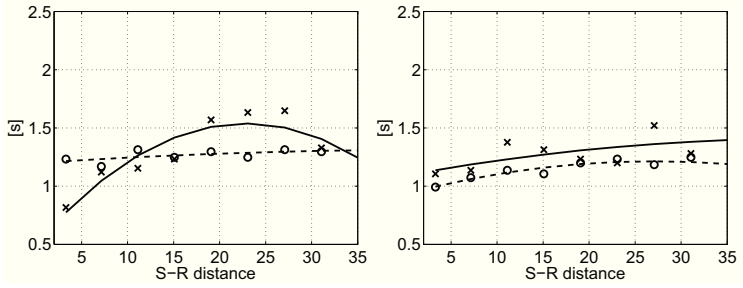

(e) 400 Hz **(f)** 500 Hz

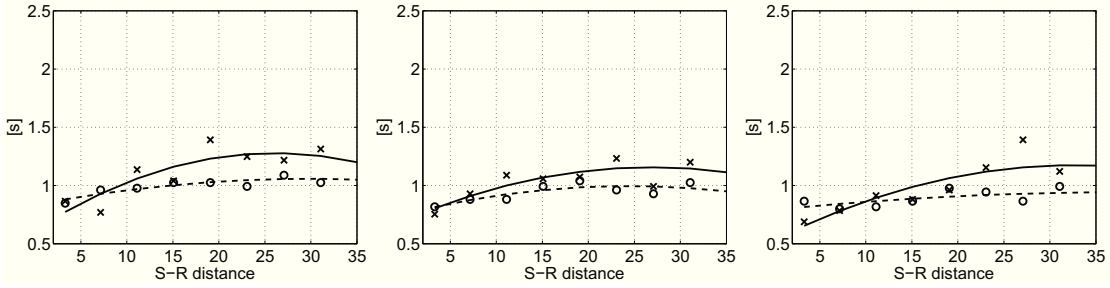

(g) 630 Hz **(h)** 800 Hz **(i)** 1000 Hz

Figure A.7: Reverberation time inside the scaled long room with scattering surfaces. Measured values and regression lines: EDT (× and solid line), RT30 (∘ and −−).

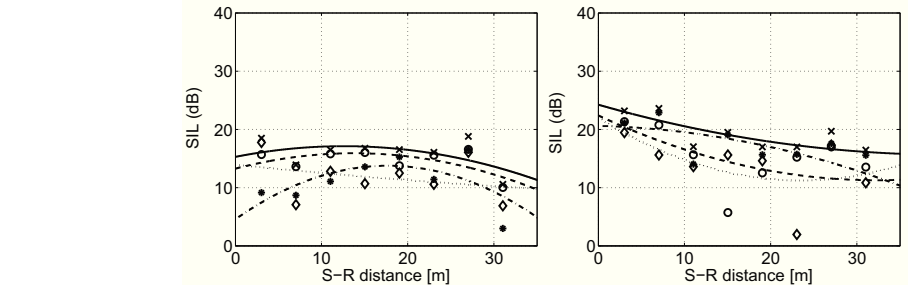

(a) 160 Hz **(b)** 200 Hz

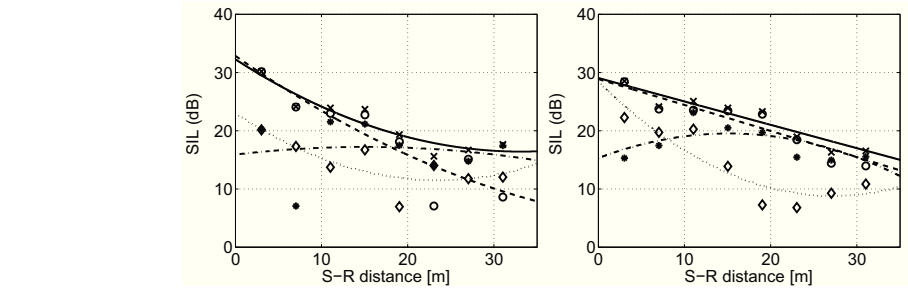

(c) 250 Hz **(d)** 315 Hz

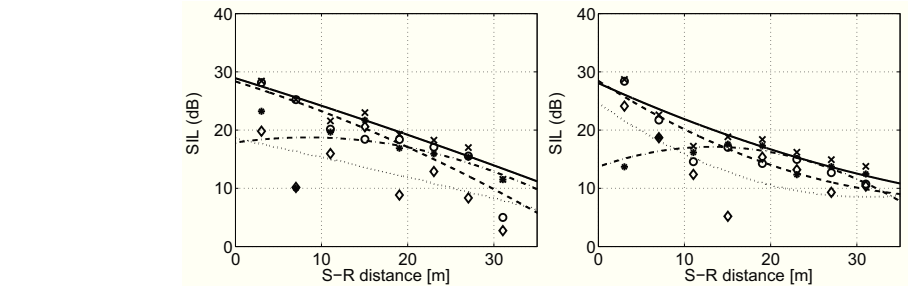

(e) 400 Hz **(f)** 500 Hz

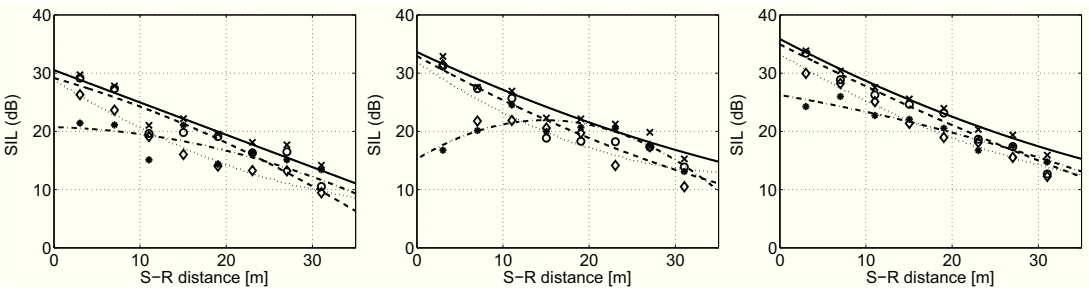

(g) 630 Hz **(h)** 800 Hz **(i)** 1000 Hz

Figure A.8: Sound intensity level (SIL) decay inside the scaled long room with scattering surfaces along the line from the source to the end wall at z=1.6 m. Measured values and regression lines: total intensity ($\times$ and solid line), intensity along the x-axis ($\circ$ and $--$), intensity along the y-axis ($*$ and $-\cdot-$), intensity along the z-axis ($\diamond$ and $\cdots$).

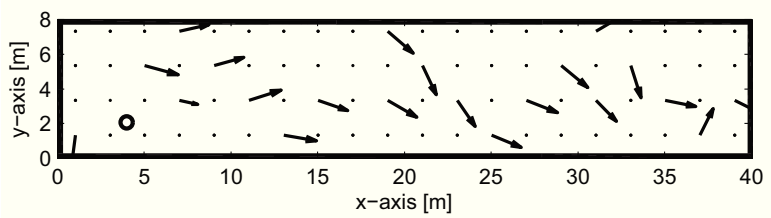

(a) 160 Hz

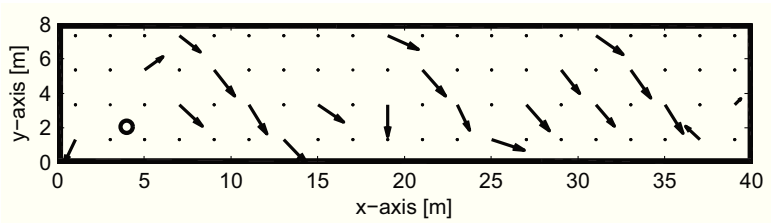

(b) 200 Hz

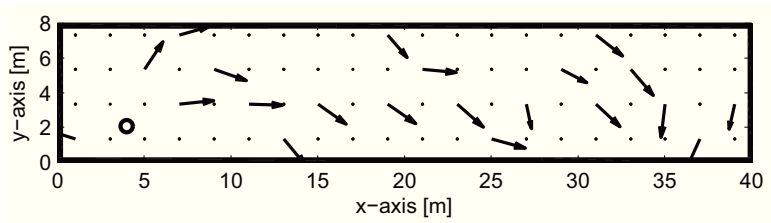

(c) 250 Hz

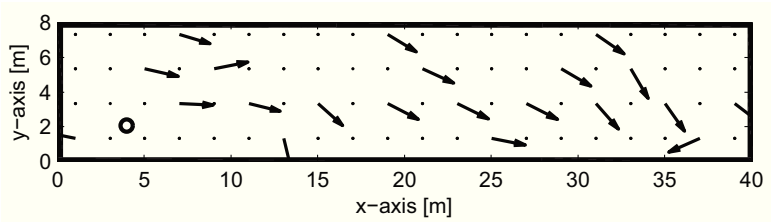

(d) 315 Hz

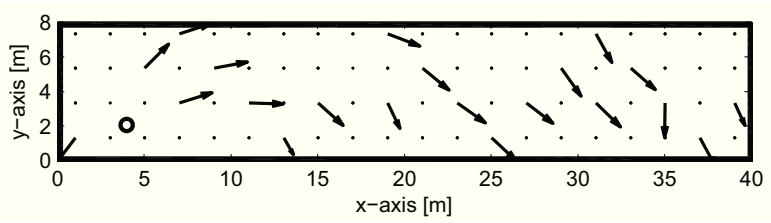

(e) 400 Hz

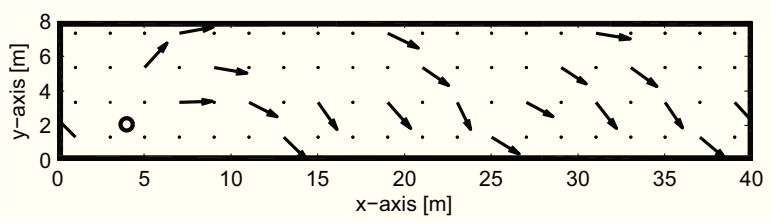

(f) 500 Hz

Figure A.9: Normalized intensity vectors inside the scaled long room with scattering surfaces; results over the horizontal plane at z=1.6 m for the frequency bands from 160 to 500 Hz.

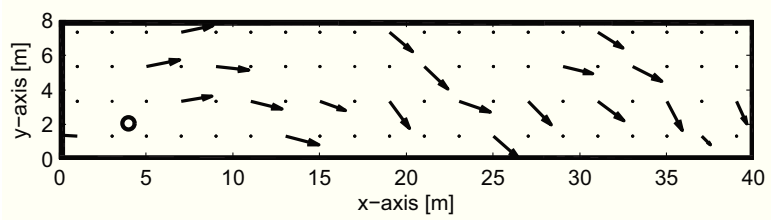

(a) 630 Hz

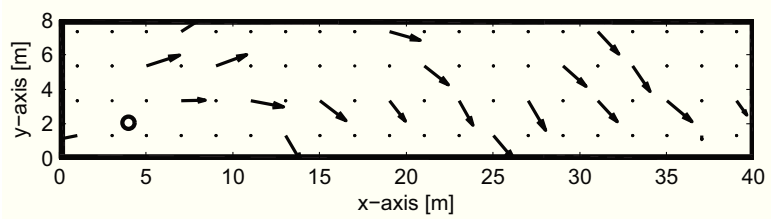

(b) 800 Hz

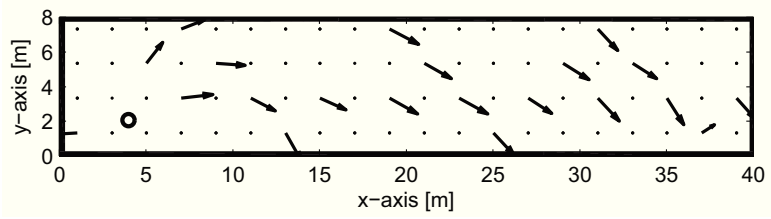

(c) 1000 Hz

Figure A.10: Normalized intensity vectors inside the scaled long room with scattering surfaces; results over the horizontal plane at z=1.6 m for the frequency bands from 630 to 1000 Hz

Appendix B

Experimental diffusion coefficients

In this Appendix the results concerning the experimental estimate of the diffusion coefficient discussed in *Chapter 4* are presented, with reference to all the investigated frequency bands.

Firstly, in *Appendix B.1* the results of the experimental estimates based on the direct measurements performed inside the models are reported. Then, in *Appendix B.2* the comparison between the measured parameters and the numerical simulations (in terms of RT30, energy density spatial decay and sound intensity decay) is detailed.

B.1 Local estimate of the diffusion coefficient

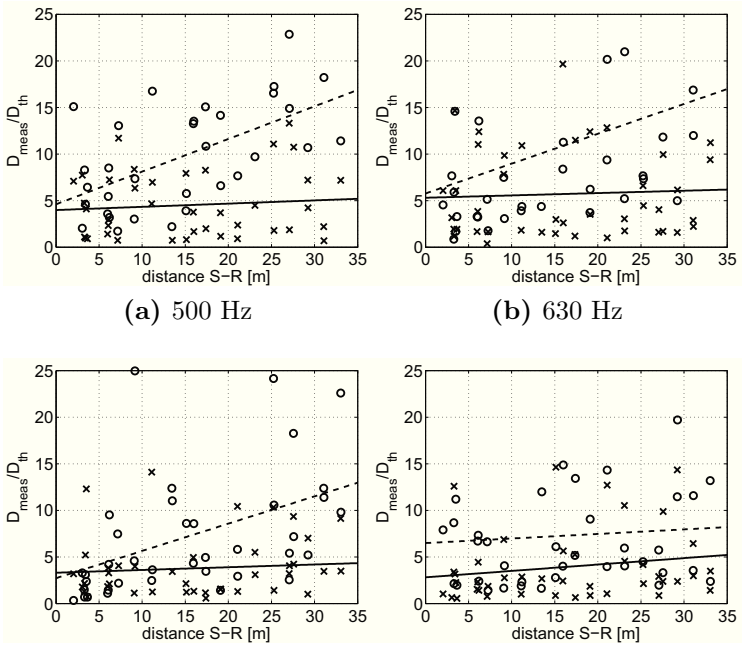

(a) 500 Hz **(b)** 630 Hz

(c) 800 Hz **(d)** 1000 Hz

Figure B.1: Ratio between the measured D_{meas} and the theoretical D_{th} diffusion coefficients as a function of the distance from the source inside the scaled long rooms. Results for the model with flat boundaries ($\circ$ and $--$) and the model with scattering boundaries ($\times$ and solid line).

B.2 Comparison between numerical simulations and measured values

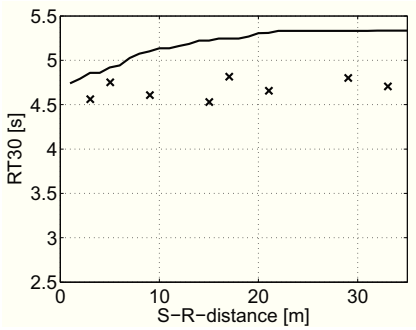

(a) 400 Hz

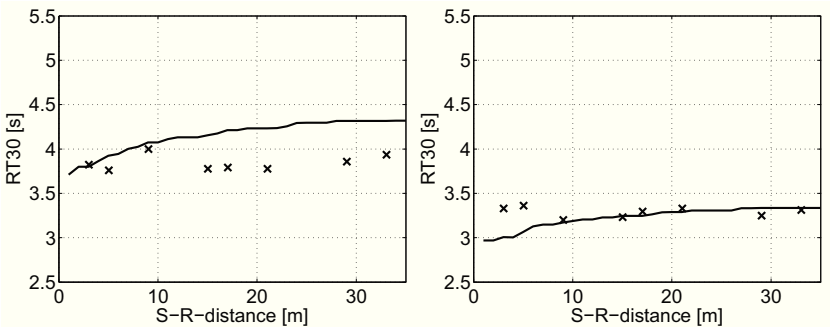

(b) 500 Hz **(c)** 630 Hz

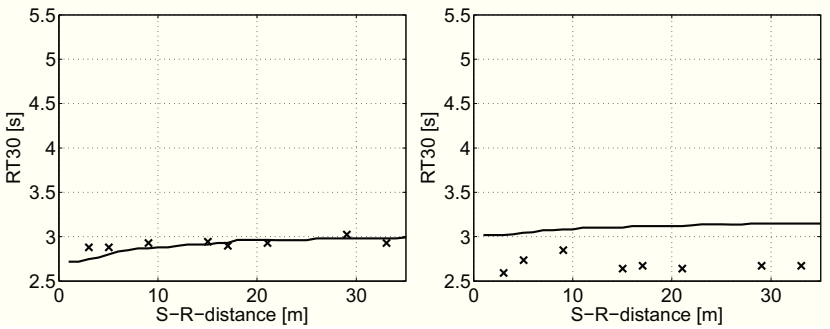

(d) 800 Hz **(e)** 1000 Hz

Figure B.2: RT30 inside the long room with flat boundaries as a function of the distance from the source. Comparison between the measured (×) and the numerically simulated (solid line) values.

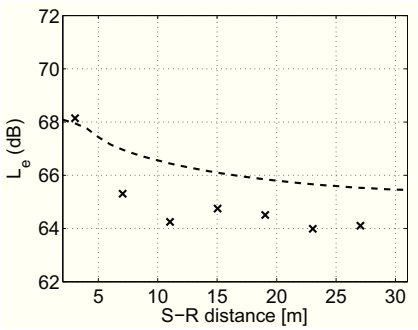

(a) 400 Hz

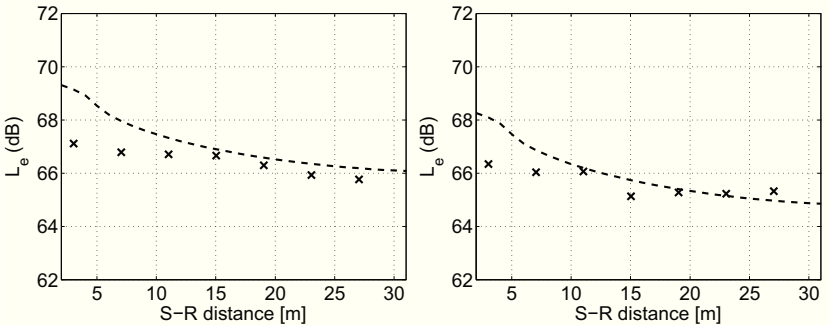

(b) 500 Hz **(c)** 630 Hz

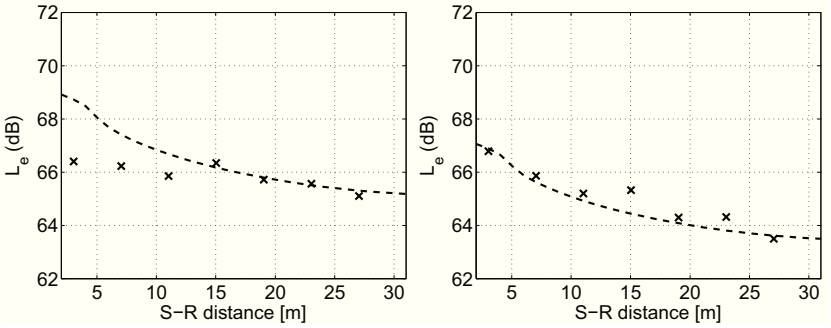

(d) 800 Hz **(e)** 1000 Hz

Figure B.3: Energy density level (L_e) decay along a line from the source to the end wall of the long room with flat boundaires: measured data ($\times$) and simulated data ($--$).

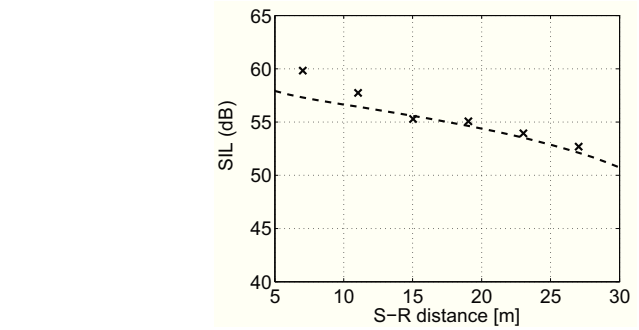

(a) 400 Hz

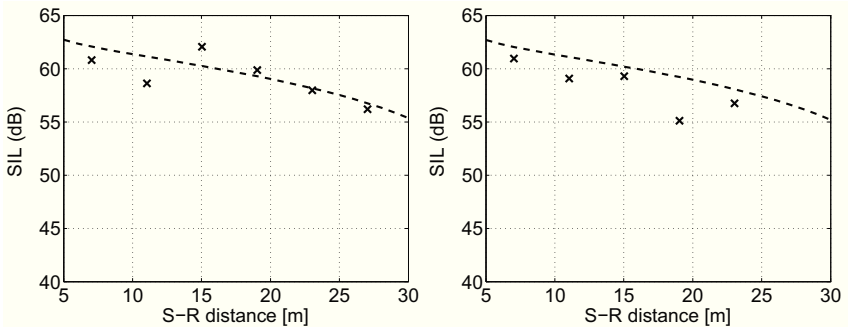

(b) 500 Hz **(c)** 630 Hz

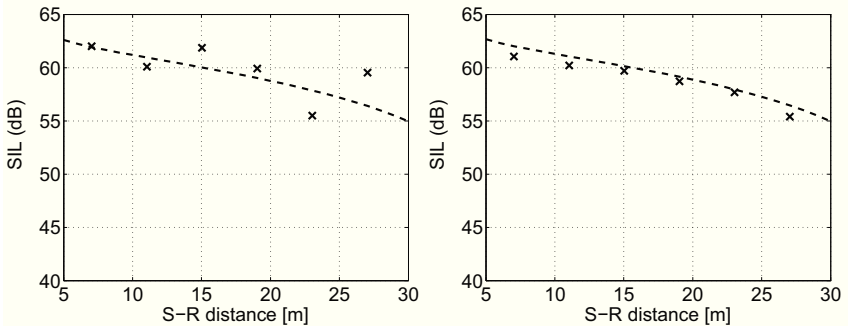

(d) 800 Hz **(e)** 1000 Hz

Figure B.4: Intensity level (SIL) decay along a line from the source to the end wall of the long room with flat boundaires: measured data (×) and simulated data (−−).

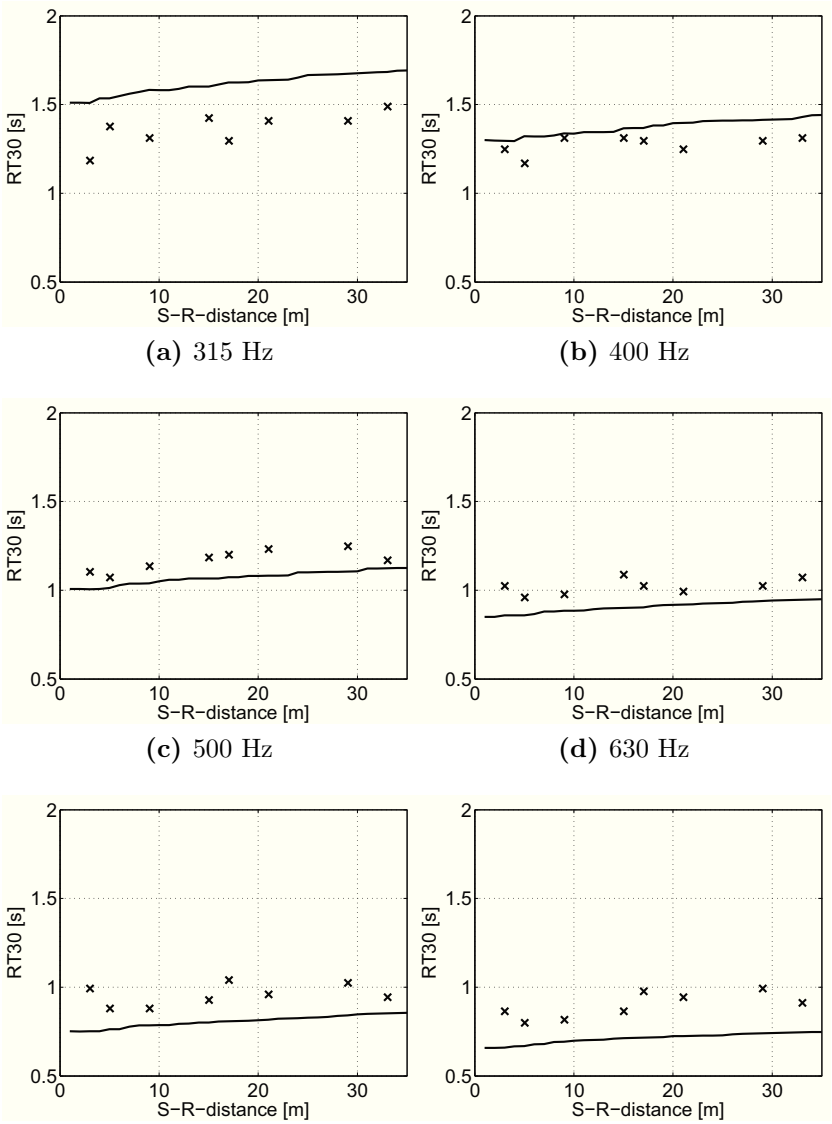

(a) 315 Hz **(b)** 400 Hz

(c) 500 Hz **(d)** 630 Hz

(e) 800 Hz **(f)** 1000 Hz

Figure B.5: RT30 inside the long room with scattering boundaires as a function of the distance from the source. Comparison between the measured (×) and the numerically simulated (solid line) values.

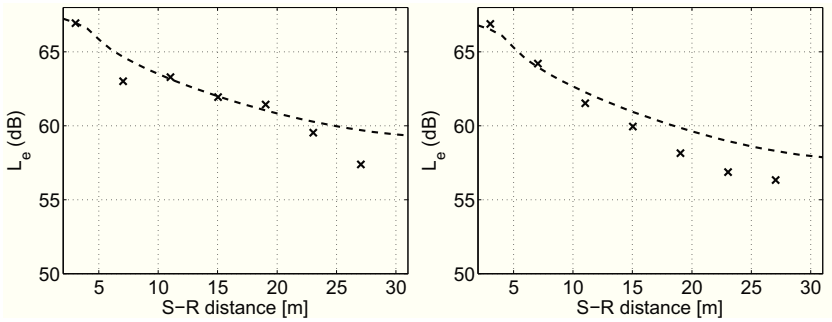

(a) 315 Hz **(b)** 400 Hz

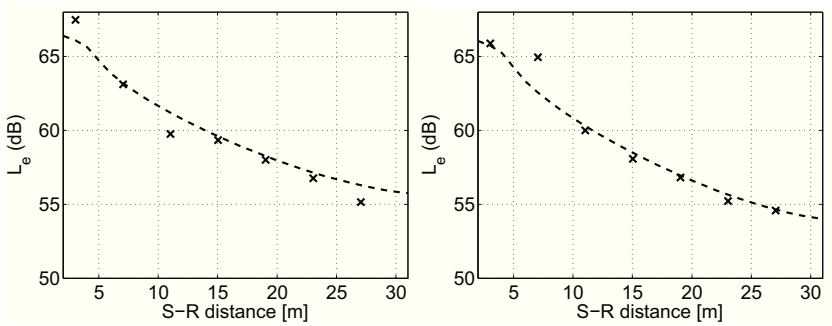

(c) 500 Hz **(d)** 630 Hz

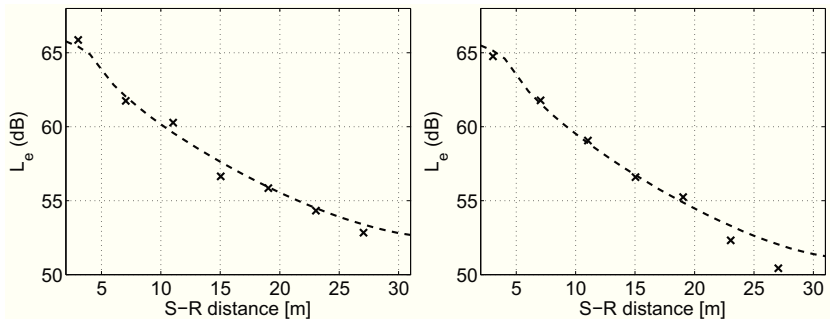

(e) 800 Hz **(f)** 1000 Hz

Figure B.6: Energy density level (L_e) decay along a line from the source to the end wall of the long room with scattering boundaires: measured data ($\times$) and simulated data ($--$).

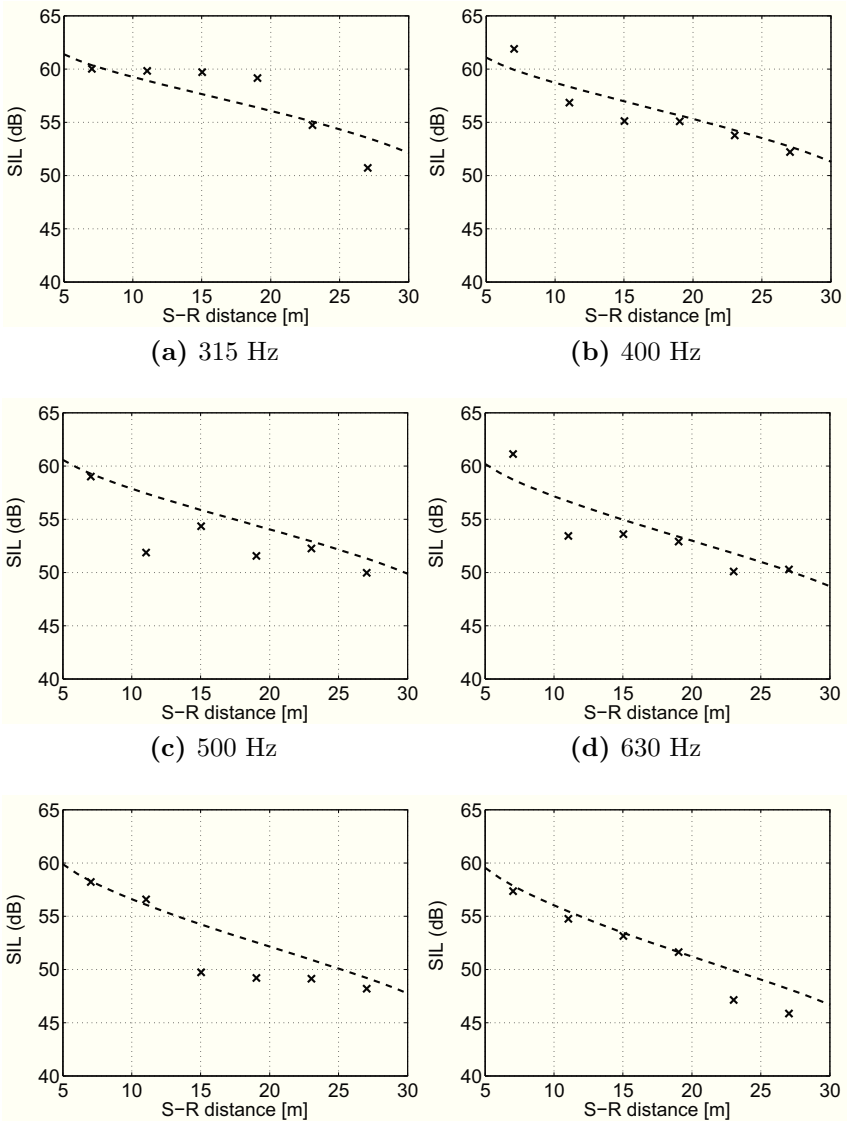

(a) 315 Hz **(b)** 400 Hz

(c) 500 Hz **(d)** 630 Hz

(e) 800 Hz **(f)** 1000 Hz

Figure B.7: Intensity level (SIL) decay along a line from the source to the end wall of the long room with scattering boundaires: measured data (×) and simulated data (−−).

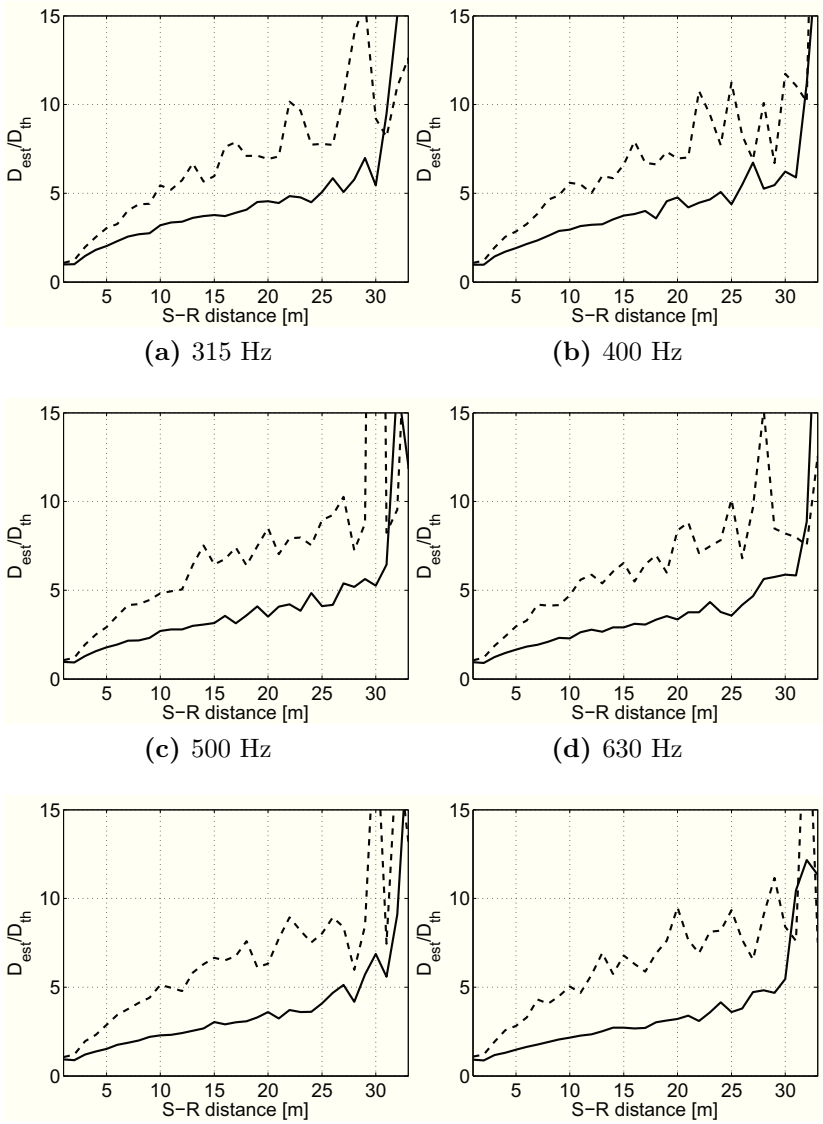

(a) 315 Hz **(b)** 400 Hz

(c) 500 Hz **(d)** 630 Hz

(e) 800 Hz **(f)** 1000 Hz

Figure B.8: Ratio between the estimated D_{est} and the theoretical D_{th} diffusion coefficients obtained from particle-tracing simulations; results for the long room with flat ($--$) and scattering (solid line) boundaries.

Bibliography

[1] J. Picaut, L. Simon, and J.D. Polack. "A mathematical model of diffuse sound field based on a diffusion equation". *Acust. Acta Acust.* 83 (1997), pp. 614–621.

[2] A. Billon et al. "Modeling the sound transmission between rooms coupled through partition walls by using a diffusion model". *J. Acoust. Soc. Am.* 123 (2008), pp. 4261–71.

[3] N. Xiang, Y. Jing, and A.C. Bockman. "Investigation of acoustically coupled enclosures using a diffusion-equation model". *J. Acoust. Soc. Am.* 126 (2009), pp. 1187–1198.

[4] F. Ollendorff. "Statistical room-acoustics as a problem of diffusion (a proposal)". *Acustica* 21 (1969), pp. 236–245.

[5] F. Ollendorff. "Diffusionstheorie des schallfeldes im straßentunnel". *Acustica* 34 (1976), pp. 311–315.

[6] J. Picaut, L. Simon, and J.D. Polack. "Sound field in long rooms with diffusely reflecting boundaries". *Appl. Acoust.* 56 (1999), pp. 217–240.

[7] V. Valeau, J. Picaut, and M. Hodgson. "On the use of a diffusion equation for room-acoustic prediction". *J. Acoust. Soc. Am.* 119 (2006), pp. 1504–1513.

[8] A. Billon et al. "On the use of a diffusion model for acoustically coupled rooms". *J. Acoust. Soc. Am.* 120 (2006), pp. 2043–2054.

[9] Y. Jing and N. Xiang. "Visualizations of sound energy across coupled rooms using a diffusion equation model (L)". *J. Acoust. Soc. Am.* 124 (2008), pp. 360–365.

[10] V. Valeau, M. Hodgson, and J. Picaut. "A diffusion-based analogy for the prediction of sound fields in fitted rooms". *Acust. Acta Acust.* 93 (2007), pp. 94–105.

[11] A. Billon, J. Picaut, and A. Sakout. "Prediction of the reverberation time in high absorbent room using a modified-diffusion model". *Appl. Acoust.* 69 (2008), pp. 68–74.

[12] Y. Jing and N. Xiang. "A modified diffusion equation for room-acoustic predication". *J. Acoust. Soc. Am.* 121 (2007), pp. 3284–3287.

[13] A. Billon et al. "Introducing atmospheric attenuation within a diffusion model for room-acoustic predictions (L)". *J. Acoust. Soc. Am.* 123 (2008), pp. 4040–4043.

[14] C. Foy. “Simulation de l’acoustique intérieure d’un bâtiment par la résolution numérique d’une équation de diffusion: introduction de la diffusivité aux parois”. PhD thesis. Université de La Rochelle (France), 2007.

[15] C. Foy et al. “An empirical diffusion model for acoustic prediction in rooms with mixed diffuse and specular reflections”. *Acust. Acta Acust.* 95 (2009), pp. 97–105.

[16] W.B. Joyce. “Sabine’s reverberation time and ergodic auditorium”. *J. Acoust. Soc. Am.* 58 (1975), pp. 643–655.

[17] H. Kuttruff. *Room acoustics*. 4th ed., Spon Press, London, 1999.

[18] F.J. Fahy and J. Walker. *Fundamental of Noise and Vibrations*. Spon, London, 1998.

[19] J. Picaut. *Modélisation des champs ”diffus” en acoustique architecturale et urbaine par un processus de diffusion de l’énergie sonore*. Habilitation à diriger des recherches. Académie de Nantes - Faculté des sciences de l’Université du Maine (France), 2006.

[20] T. Le Pollès et al. “Sound-field modeling in architectural acoustics by a transport theory: Application to street canyons”. *Physical Review E* 72 (2005), pp. 1–17.

[21] P. Morse and H. Feshbach. *Methods of theoretical physics*. McGraw-Hill, New York, 1953.

[22] C.W. Kosten. “The mean free path in room acoustics”. *Acustica* 10 (1960), pp. 245–250.

[23] T. Le Pollès, J. Picaut, and M. Bérengier. “Sound field modeling in a street canyon with partially diffusely reflecting boundaries by the transport theory”. *J. Acoust. Soc. Am.* 116 (2004), pp. 2969–2983.

[24] Y. Jing, E.W. Larsen, and N. Xiang. “One-dimensional transport equation models for sound energy propagation in long spaces : theory”. *J. Acoust. Soc. Am.* 127 (2010), pp. 2312–2322.

[25] Y. Jing and N. Xiang. “One-dimensional transport equation models for sound energy propagation in long spaces: simulations and experiments”. *J. Acoust. Soc. Am.* 127 (2010), pp. 2323–2331.

[26] N. Prodi. “On the theory of sound transfer in rigid-frame porous materials”. *Acust. Acta Acust.* 95 (2009), pp. 306–313.

[27] M. Djimadoum and J.L. Guyader. “Vibratory prediction with an equation of diffusion”. *Acust. Acta Acust.* 3 (1995), pp. 11–24.

[28] Y. Jing and N. Xiang. “On boundary conditions for the diffusion equation in room-acoustic prediction: Theory, simulations, and experiments”. *J. Acoust. Soc. Am.* 123 (2008), pp. 145–153.

[29] B.G. van Zyl, F. Anderson, and P.J. Erasmus. “Sound intensity in diffuse sound fields”. *J. Acoust. Soc. Am.* 78 (1985), pp. 587–589.

[30] J. Escolano, J.M. Navarro, and J.J. Lopez. "On the limitation of a diffusion equation model for acoustic predictions of rooms with homogeneous dimensions (L)". *J. Acoust. Soc. Am.* 128 (2010), pp. 1586–1589.

[31] R.V. Waterhouse. "Statistical properties of reverberant sound fields". *J. Acoust. Soc. Am.* 43 (1967), pp. 1436–1444.

[32] D. Lubman. "Fluctuations of sound with position in a reverberant room". *J. Acoust. Soc. Am.* 44 (1968), pp. 1491–1502.

[33] A.D. Pierce. *Acoustics: an introduction to its physical principles and applications*. Acoustical Society of America, New York, 1981.

[34] J. Pujolle. "Les differentes définitions du libre parcours moyen du son dans une salle". *Revue d'Acoustique* 36 (1976), pp. 44–50.

[35] U. Stephenson. "An acoustic computer simulation technique for calculating parameters relevant to subjective acoustical impression in concert hall". *Acustica* 59 (1985), pp. 1–20.

[36] U. Stephenson. "Comparison of the mirror image source method and the sound particle simulation method". *Appl. Acoust.* 29 (1990), pp. 35–72.

[37] J. Picaut. "Numerical application of the concept of sound particles to modeling sound fields in architectural acoustics". *Bulletin des Laboratoires des Ponts et Chaussées* (2005), pp. 59–88.

[38] J. Picaut and D. Scouarnec. "Using acoustic diffusors to reduce noise in urban areas". *Acust. Acta Acust.* 95 (2009), pp. 653–668.

[39] J. Picaut and N. Fortin. *Manuel de référence du code SPPS*. Laboratoire Central des Ponts et Chaussées, 2009.

[40] W.H. Press et al. *Numerical recipes in FORTRAN 77. The art of scientific computing*. Cambridge University Press, 1992.

[41] *TetGen*. URL: `http://wias-berlin.de/software/tetgen`.

[42] F.J. Fahy. *Sound intensity*. 2nd ed., E & FN Spon, London, 1995.

[43] M. Hodgson. "When is diffuse-field theory applicable?" *Appl. Acoust.* 49 (1996), pp. 197–207.

[44] F. Jacobsen. *The sound field in a reverberation room*. Tech. rep. Acoustic Technology, Department of Electrical Engineering (Technical University of Denmark), Note no 31261, 2008.

[45] S. Chiles and M. Barron. "Sound level distribution and scatter in proportionate spaces". *J. Acoust. Soc. Am.* 116 (2004), pp. 1585–1595.

[46] F. Jacobsen and A.R. Molares. "The ensemble variance of pure-tone measurements in reverberation rooms". *J. Acoust. Soc. Am.* 127 (2009), pp. 233–237.

[47] F. Jacobsen and A.R. Molares. "Ensemble statistics of active and reactive sound intensity in reverberation rooms". *J. Acoust. Soc. Am.* 129 (2011), pp. 211–218.

[48] M. Barron and L.J. Lee. "Energy relations in concert auditoriums". *J. Acoust. Soc. Am.* 84.2 (1988), pp. 618–628.

[49] W.B. Joyce. "Exact effect of surface roughness on the reverberation time of a uniformly absorbing spherical enclosure". *J. Acoust. Soc. Am.* 64 (1978), pp. 1429–1436.

[50] M.M. Carroll and C.F. Chien. "Decay of reverberant sound in a spherical enclosure". *J. Acoust. Soc. Am.* 62 (1977), pp. 1442–1446.

[51] R.V. Waterhouse. "Interference patterns in reverberant sound fields". *J. Acoust. Soc. Am.* 27 (1955), pp. 247–258.

[52] J. Kang. "The unsuitability of the classic room acoustical theory in long enclosures". *Architectural Science Review* 39 (1996), pp. 89–94.

[53] J. Kang. *Acoustics in long spaces: theory and design guide*. Thomas Telford Publishing, London, 2002.

[54] F. Jacobsen. "Active and reactive sound intensity in a reverberant sound field". *J. Acoust. Soc. Am.* 143 (1990), pp. 231–240.

[55] M. Hodgson. "Evidence of diffuse surface reflections in rooms". *J. Acoust. Soc. Am.* 89 (1991), pp. 765–771.

[56] F. Jacobsen. "Active and reactive, coherent and incoherent sound fields". *J. Sound. Vib.* 130 (1989), pp. 493–507.

[57] F. Jacobsen and A.R. Molares. "Statistical properties of kinetic and total energy densities in reverberant spaces". *J. Acoust. Soc. Am.* 127 (2010), pp. 2332–2337.

[58] F. Jacobsen and H.E. de Bree. "A comparison of two different sound intensity measurement principles". *J. Acoust. Soc. Am.* 118 (2005), pp. 1510–1517.

[59] H.E. de Bree et al. "The μ-flown: a novel device for measuring acoustic flows". *Sensors and Actuators A* 54 (1996), pp. 552–557.

[60] H.E. de Bree. "The Microflown, an acoustic particle velocity sensor". *Acoust. Aust.* 31 (2003), pp. 91–94.

[61] H.E. de Bree. "An overview of Microflown Technologies". *Acust. Acta Acust.* 89 (2003), pp. 163–172.

[62] *Microflown*. URL: `http://www.microflown.com`.

[63] V.B. Svetovoy and I.A. Winter. "Model of the μ-flown microphone". *Sensors and Actuators* 86 (2000), pp. 171–181.

[64] F. Jacobsen and V. Jaud. "A note on the calibration of pressure-velocity sound intensity probes". *J. Acoust. Soc. Am.* 120 (2006), pp. 830–837.

[65] T.G.H. Basten and H.E. de Bree. "Full bandwidth calibration procedure fro acoustic probes containing a pressure and particle velocity sensor". *J. Acoust. Soc. Am.* 127 (2010), pp. 264–270.

[66] D. Stanzial, G. Sacchi, and G. Schiffrer. "Calibration of pressure-velocity probes using a progressive plane wave reference field and comparison with nominal calibration filters". *J. Acoust. Soc. Am.* 129 (2011), pp. 3745–3755.

[67] J.S. Bendat and A.G. Pierson. *Random data. Analysis and measurement procedures*. 3rd ed., Wiley, New York, 2000.

[68] R.B. Randall. *Frequency analysis*. 3rd ed., Bruel & Kjaer, Naerum (DK), 1987.

[69] *ISO 9613-1: Acoustics - Attenuation of sound during propagation outdoors - Part 1: Calculation of the absorption of sound by the atmosphere*. International Organization for Standardization, Genève. 1993.

[70] *ISO 354: Acoustics - Measurements of sound absorption in a reverberation room*. International Organization for Standardization, Genève. 2003.

[71] *ISO 17497-1: Acoustics - Sound scattering properties of surfaces - Part 1: Measurement of the random-incidence scattering coefficient in a reverberation room*. International Organization for Standardization, Genève. 2004.

[72] J.L. Davy, I.P. Dunn, and P. Dubout. "The variance of decay rates in reverberation room". *Acustica* 43 (1979), pp. 12–25.

[73] J.L. Davy. "The variance of impulse decays". *Acustica* 44 (1980), pp. 51–56.

[74] G. Del Galdo et al. "The diffuse sound field in energetic analysis". *J. Acoust. Soc. Am.* 131 (2012), pp. 2141–2151.

[75] P. Morse and K.U. Ingard. *Theoretical acoustics*. McGraw-Hill, New York, 1968.

[76] J.A. Mann III, J. Tichy, and A.J. Romano. "Instantaneous and time-averaged energy transfer in acoustic fields". *J. Acoust. Soc. Am.* 82 (1987), pp. 17–30.

[77] *ODEON Room acoustics modelling software*. URL: `http://www.bksv.com/Products/RoomAcousticsSoftware/ODEON.aspx`.

[78] *ISO 3382-1: Measurements of reverberation time - Part1: Performance spaces*. International Organization for Standardization, Genève. 2009.

[79] D.S. Moore et al. *The practice of business statistics. Using data for decisions*. W.H. Freeman and Company, New York, 2003.